



UNIVERSIDADE FEDERAL DE SANTA CATARINA
CENTRO TECNOLÓGICO
PROGRAMA DE PÓS-GRADUAÇÃO EM ENGENHARIA QUÍMICA

Marina de Souza Melchiors

**Development of nanostructured polymeric systems based on Ring-Opening
Polymerization (ROP) and Reversible Addition-Fragmentation Chain-Transfer (RAFT)
polymerization**

Florianópolis

2021

Marina de Souza Melchior

**Development of nanostructured polymeric systems based on Ring-Opening
Polymerization (ROP) and Reversible Addition-Fragmentation Chain-Transfer (RAFT)
polymerization**

Tese de Doutorado submetida ao Programa de
Engenharia Química da Universidade Federal de
Santa Catarina para a obtenção do título de Doutor
em Engenharia Química

Orientadora: Prof^a. Dr^a. Claudia Sayer.

Coorientador: Prof^a. Dr^a Débora de Oliveira e Prof.
Dr. Pedro Henrique Hermes de Araújo

Florianópolis

2021

Ficha de identificação da obra elaborada pelo autor,
através do Programa de Geração Automática da Biblioteca Universitária da UFSC.

Melchiors, Marina de Souza
Development of Nanostructured Polymeric Systems Based
on Ring-Opening Polymerization (ROP) and Reversible
Addition-Fragmentation Chain-Transfer (RAFT)
Polymerization / Marina de Souza Melchiors ; orientador,
Claudia Sayer, coorientador, Débora de Oliveira,
coorientador, Pedro Henrique Hermes de Araújo, 2021.
140 p.

Tese (doutorado) - Universidade Federal de Santa
Catarina, Centro Tecnológico, Programa de Pós-Graduação em
Engenharia Química, Florianópolis, 2021.

Inclui referências.

1. Engenharia Química. 2. Limoneno, Óxido de Limoneno. 3.
Epoxidação mediada por enzima. 4. Polimerização por Abertura
de Anel. 5. Polimerização mediada por Transferência
Reversível de Cadeia por Adição-Fragmentação. I. Sayer,
Claudia. II. de Oliveira, Débora. III. Hermes de Araújo,
Pedro Henrique IV. Universidade Federal de Santa Catarina.
Programa de Pós-Graduação em Engenharia Química. V. Título.

Marina de Souza Melchiors

**Development of nanostructured polymeric systems based on Ring-Opening
Polymerization (ROP) and Reversible Addition-Fragmentation Chain-Transfer (RAFT)
polymerization**

O presente trabalho em nível de doutorado foi avaliado e aprovado por banca examinadora
composta pelos seguintes membros

Prof.^a Claudia Sayer, Dr.^a

Universidade Federal de Santa Catarina

Prof.^a Fernanda Vitória Leimann, Dr.^a

Universidade Tecnológica Federal do Paraná

Prof. Marcelo Luis Mignoni, Dr.

Universidade Regional Integrada do Alto Uruguai e das Missões

Prof.^a Ana Paula Serafini Immich Bueno, Dr.^a

Universidade Federal de Santa Catarina

Certificamos que esta é a **versão original e final** do trabalho de conclusão que foi julgado
adequado para obtenção do título de doutor em Engenharia Química pelo Programa de Pós-
Graduação em Engenharia Química.

Prof.^a Dr.^a Débora de Oliveira

Coordenação do Programa de Pós-Graduação

Prof.^a Dr.^a Claudia Sayer

Orientadora

Florianópolis, 09 de julho de 2021.

AGRADECIMENTOS

Não podia deixar de iniciar meus agradecimentos por aqueles que são minha base e meus maiores incentivadores, meus pais, Ana e Lotário, obrigada por todo apoio e por toda dedicação que sempre me proporcionaram na realização de todas minhas conquistas. Aos meus irmãos, Michele e Mathias, por toda a paciência e pelo apoio em todas as minhas decisões. À minha tia e madrinha Fabiana que sempre me incentivou e vibra sempre pelo meu sucesso, obrigada por apoiar em todas minhas decisões. Amo todos vocês.

Aos meus orientadores Dr.^a Claudia Sayer, Dr.^a Débora de Oliveira e Dr. Pedro Araújo pelas oportunidades e pela parceria, fundamental para o desenvolvimento deste trabalho. Ao professor Dr. Bruno Carciofi por me inserir no universo dos terpenos. À Prof. Dr.^a. Katarina Landfester do Max-Planck-Institut für Polymerforschung (MPIP - Mainz - Alemanha) por ter aberto as portas no seu grupo de pesquisa na Alemanha e ter me dado a oportunidade de conhecer um novo mundo na pesquisa. Ao Dr. Calum Ferguson e Dr. Lucas Caire, por todos os ensinamentos e paciência em um ano de Max-Planck, sou muito grata por todo apoio e incentivos. A todos os membros do Grupo Landfester, Vielen Dank! Thank you!

Ao meu amor, Bruno, meu parceiro desde sempre nessa jornada, por todo afeto e companheirismo em todos esses anos, por sempre me ouvir e me aconselhar. Sou eternamente grata por todo carinho e dedicação. Amo você.

Aos meus amigos do Laboratório de Controle e Processos de Polimerização (LCP), vou levar vocês no meu coração, em especial à Shanda, Dani, Luiz Paulo, Rafa e Thayne, muito obrigada por sempre me apoiar e por todo carinho.

À Universidade Federal de Santa Catarina e ao Programa de Pós-Graduação em Engenharia Química por todos os recursos disponibilizados. Ao Laboratório Central de Microscopia Eletrônica da Universidade Federal de Santa Catarina (LCME/UFSC) pelas análises de microscopia eletrônica de transmissão. Ao Laboratório Central de Biologia Molecular e Estrutural (CEBIME) pelas análises de MALDI-TOF. À Coordenação de Aperfeiçoamento de Pessoal de Nível Superior (CAPES) e ao Conselho Nacional de Desenvolvimento Científico e Tecnológico (CNPq) pelo apoio financeiro no Brasil e no exterior.

A todos que passaram pela minha vida nessa grande jornada e sempre torceram pelo meu sucesso.

Muito Obrigada!

Nothing in life is to be feared, it is only to be understood. Now is the time to understand more,
so that we may fear less.

Marie Curie

RESUMO

O desenvolvimento de processos mais sustentáveis e a obtenção de materiais nanoestruturados tem despertado cada vez mais a atenção da sociedade. Neste contexto, esta tese teve como objetivo o estudo da síntese do óxido de limoneno, de origem renovável, via um processo enzimático, e sua utilização para obtenção de poliésteres e nanopartículas poliméricas. Adicionalmente, com o intuito de explorar novos métodos de obtenção de nanoestruturas poliméricas em condições de reação brandas, reações de polimerização mediadas por transferência reversível de cadeia por adição-fragmentação (RAFT) e transferência reversível de cadeia por adição-fragmentação por transferência de elétrons fotoinduzida (PET-RAFT) foram realizadas. Para atingir estas metas, este trabalho foi dividido em três etapas. Inicialmente, o óxido de limoneno foi sintetizado pela primeira vez por meio de reações de epoxidação do R-(+)-limoneno mediada pela enzima *Candida antarctica* lipase fração B (NS 88011) imobilizada em um novo suporte com material de baixo custo. Parâmetros que afetam essa reação foram estudados. As sínteses foram realizadas em reatores tipo tanque agitado operados em modo batelada alimentada. Os dois biocatalisadores utilizados, NS 88011 e Novozym 435, utilizada para comparação com a NS88011, levaram a resultados semelhantes, o que faz da NS 88011 uma alternativa promissora e de baixo custo para as reações de epoxidação mediadas por lipase. O uso de biocatalisadores atóxicos, como enzimas imobilizadas, tem se tornado uma opção vantajosa. O maior rendimento na síntese de óxido de limoneno foi de $74,92 \pm 1,12\%$ após 40 min de reação. Além disso, ambos, NS 88011 e Novozym 435, puderam ser usados por até três ciclos. Portanto, a lipase NS 88011 apresentou um desempenho bom e viável nas reações de epoxidação do R-(+)-limoneno e, após a purificação, levou a um produto final com pureza $>95\%$. A segunda etapa do trabalho consistiu na síntese de copolímeros de óxido de limoneno, via mecanismo de polimerização catiônica por abertura de anel (ROP), empregando diferentes anidridos cíclicos, anidrido ftálico ou anidrido maleico catalisada pelo líquido iônico heptacloro-bis-ferrato de 1-n-butil-3-n-metilimidazólio ($\text{BMI} \cdot \text{Fe}_2\text{Cl}_7$). Foram alcançadas conversões em torno de 80% de óxido de limoneno, massa molar média numérica acima de 1000 g mol^{-1} e ligações duplas pendentes que permitem a modificação posterior de sua estrutura. Em relação à sua aplicação, como nanodispositivos para sistemas biológicos, nanopartículas (NPs) de poli(anidrido ftálico-co-óxido de limoneno) (PAFOL) também foram produzidas e reticuladas com tetratiol via reação tiol-eno. NPs-PAFOL reticuladas com um diâmetro médio ponderado em número de 56 nm, morfologia esférica e boa estabilidade coloidal foram obtidos. Essas NPs foram testadas quanto à compatibilidade sanguínea e viabilidade celular, apresentando potencial para aplicações biomédicas. Na terceira etapa do trabalho, reações de polimerização mediadas por RAFT e PET-RAFT foram estudadas por serem estratégias eficientes para produção de nanoestruturas com diferentes tamanhos e formatos em meio aquoso em condições brandas. Efeitos de parâmetros de reação por iniciação térmica e fotoiniciação foram analisados, empregando diferentes monômeros, fotocatalisadores e agentes RAFT. Essa etapa forneceu novas perspectivas para o mecanismo de autoagregação induzida pela polimerização (PISA) via RAFT em meio aquoso. Nano-objetos em forma de esferas, vermes e vesículas foram obtidos nas reações de fotopolimerização. A polimerização mediada por luz visível pode ser considerada uma técnica emergente que permite a preparação de polímeros bem definidos em condições moderadas e de forma ecológica, constituindo uma alternativa sustentável frente à polimerização térmica tradicional.

Palavras-chave: Reação de epoxidação. Biocatálise. Limoneno. NS 88011. Polimerização por Abertura de Anel. Poliéster. Líquido iônico. RAFT-PISA. PET-RAFT. Nanoestruturas.

RESUMO EXPANDIDO

Introdução

Polímeros provenientes de fontes naturais são materiais intrinsecamente mais sustentáveis, que apresentam grande interesse para diversos setores de nossa sociedade devido à grande variedade de propriedades, que estes materiais podem apresentar. Entre os diferentes polímeros provenientes de recursos renováveis, pode-se destacar poliésteres, tais como o poli(ácido láctico) (PLA), poli(succinato de butileno) (PBS), que já são alternativas promissoras para substituição de plásticos oriundo de fontes não renováveis. No entanto, diversos outros poliésteres também podem ser obtidos a partir de recursos renováveis devido à grande variedade de compostos oriundos de biomassa, que são passíveis de polimerização. Os poliésteres apresentam como característica principal a presença de ligações éster ao longo da cadeia principal. Estes grupamentos químicos são passíveis de hidrólise, permitindo a degradação do polímero em condições adequadas, e vários apresentam elevada biocompatibilidade (POMERANSKY; KHRIPLOVICH, 1999; VERT, 2005; NEJAD et al., 2013; HILLMYER; TOLMAN, 2014). As reações de esterificação ocorrem usualmente entre um ácido carboxílico e um álcool com a formação de água como subproduto. No entanto, esta é uma reação reversível, e a presença de água retarda e pode até mesmo impedir o prosseguimento da reação. Já a reação entre um epóxido e um anidrido, forma a ligação éster, sem formar o subproduto indesejado (NEJAD et al., 2013). Dentre os monômeros provenientes de fontes renováveis para síntese dessa classe de polímero, os epóxidos são ótimos candidatos, pois já são utilizados como intermediários vitais em um grande número de processos químicos (WARWEL et al., 2001; ADHVARYU; ERHAN, 2002; BENANIBA; BELHANECHÉ-BENSEMRA; GELBARD, 2003; WILBON; CHU; TANG, 2013; ISNARD et al., 2017). Além disto, existem diversos anidridos oriundos de fontes renováveis que são explorados comercialmente e que são passíveis de serem utilizados para a obtenção de poliésteres (ISNARD et al., 2017). Estes poliésteres de origem renovável são excelentes candidatos para a produção de nanopartículas (NPs) visando aplicações biomédicas por muitas vezes apresentarem elevada biocompatibilidade e biodegradabilidade, a depender da composição do poliéster. Atualmente, os métodos mais comuns de obtenção de nanopartículas de poliéster dispersos em água envolvem a utilização de polímeros previamente sintetizados, já que a reação de esterificação não prossegue na presença de água. Portanto, estes métodos ficam restritos a miniemulsificação/evaporação de solvente ou difusão de solvente (MUSYANOVYCH; LANDFESTER, 2014; MENDOZA-MUÑOZ; ALCALÁ-ALCALÁ; QUINTANAR-GUERRERO, 2016).

A formação de nanopartículas poliméricas durante a síntese do polímero permite uma maior flexibilidade em relação ao método de obtenção. Neste ponto, processos de polimerização em miniemulsão se destacam, pois diferentes mecanismos de polimerização, tais como polimerização em etapas ou cadeia, podem ser utilizados. No entanto, as partículas obtidas são usualmente esféricas, por ser esta morfologia a que apresenta menor razão área/volume diminuindo com isto a tensão interfacial entre as fases contínua e dispersa. No entanto, outra abordagem pode ser empregada para obtenção de diferentes morfologias. Nanoestruturas como esferas, vermes ou vesículas podem ser preparadas diretamente na água, empregando avanços recentes de automontagem induzida por polimerização (PISA) via transferência reversível de cadeia de adição-fragmentação (RAFT). A iniciação térmica é a estratégia mais usada para PISA em meio aquoso resultando em vários nano-objetos de copolímero de bloco. No entanto, a alta temperatura de reação restringe a preparação de nanoestruturas biorelacionadas. Desse modo, a introdução da polimerização via radicais livres mediada por luz visível no processo PISA é uma técnica emergente que permite a preparação de polímeros bem definidos em condições moderadas.

O presente trabalho foi dividido em três etapas distintas, primeiro o óxido de limoneno foi sintetizado via epoxidação mediada por enzima utilizando um biocatalisador imobilizado em um material de baixo custo, e parâmetros que afetam essa reação foram estudados em detalhes. Na segunda etapa, a copolimerização do óxido de limoneno com anidridos cíclicos foi realizada via polimerização catiônica por abertura de anel (ROP) em solução catalisada pelo líquido iônico heptacloro-bis-ferrato de 1-n-butil-3-n-metilimidazólio ($\text{BMI} \cdot \text{Fe}_2\text{Cl}_7$). Visando futuras aplicações, o material sintetizado foi utilizado para obtenção de nanopartículas, reticuladas e não reticuladas, por meio de reações tiol-eno, seguida por estudos de citotoxicidade. Na terceira etapa, o processo PISA via RAFT mediado por termo e foto polimerização foi explorado a fim de produzir materiais nanoestruturados em meio aquoso.

Objetivo

O trabalho propõe a síntese e estudo de novas estratégias para a produção de materiais poliméricos nanoestruturados. Esforços foram feitos no sentido de compreender a automontagem induzida por polimerização via transferência reversível da cadeia por adição-fragmentação (RAFT), bem como a polimerização por abertura de anel (ROP) do óxido de limoneno e anidridos derivados de fontes renováveis. A reação de epoxidação do limoneno mediada por lipase imobilizada foi estudada tendo como foco o desenvolvimento de processos mais sustentáveis.

Metodologia

A reação de epoxidação foi realizada na configuração batelada alimentada usando 20 mL de tolueno como solvente. As reações foram realizadas adicionando 40, 70 e 250 mM de ácido octanóico; 40, 70 e 100 mM de limoneno; 100, 250 e 500 mM de H_2O_2 (solução aquosa a 35%); e 1, 5, 10 e 20% do biocatalisador NS 88011 em relação à quantidade total de substratos (ácido octanóico e H_2O_2 (solução aquosa a 35%)). Um biocatalisador comercial, Novozym 435, também foi usado nas melhores condições de reação (rendimento máximo obtido) para comparar com os resultados obtidos com NS 88011. Estudos de reuso das enzimas imobilizadas foram realizados ao longo de três ciclos para a mesma configuração de reação. Alíquotas de 500 μL da fase orgânica foram retiradas em diferentes intervalos de tempo e adequadamente diluídas para quantificação por Cromatografia Gasosa (GC).

As reações de polimerização via ROP foram realizadas à 110 °C sob agitação magnética (450 rpm) e atmosfera de nitrogênio. Líquido iônico (LI), anidrido maleico (AM) ou anidrido ftálico (AF) foram pesados diretamente no frasco Schlenk, usando razões molares de LI: OL: AM ou AF de 1: 100: 100. O tolueno destilado constituindo 50% em peso do meio de reação foi adicionado ao frasco de Schlenk. As polimerizações foram conduzidas por 300 min. Um dos materiais sintetizados, (poli(anidro ftálico-*co*-óxido de limoneno)(PAFOL)), foi utilizado para o preparo de nanopartículas (NPs), não reticuladas e reticuladas via reação tiol-eno. As NPs foram preparadas de acordo com o método de miniemulsão/evaporação de solvente, a fase orgânica foi obtida pela mistura do PAFOL pré-sintetizado (400 mg) e clorofórmio como solvente (4 g). A fase aquosa, constituída por água (14 g) e surfactante SDS (0,2% p/p), foi adicionada à fase orgânica e a mistura foi agitada durante 10 min. Posteriormente, a emulsão grosseira foi sonicada por 2 min (pulso de 10 s on, pulso de 10 s off) com uma amplitude de 60%. Após a sonicação, a miniemulsão foi deixada em um banho termostático com uma temperatura de 40 °C até a evaporação completa do solvente. As NPs foram reticuladas por meio de reações de tiol-eno entre as ligações duplas pendentes na cadeia do polímero e o pentaeritritol tetraquis (3-mercaptopropionato) (PETMP). A dispersão purificada contendo NPs de PAFOL foi colocada em um frasco contendo PETMP e fotoiniciador 2,2-dimetoxi-2-

fenilacetofenona (DMPA), sob atmosfera de nitrogênio. A reação foi conduzida sob luz ultravioleta (365 nm; 1,53 mW cm⁻²) por 4 h com agitação magnética contínua. Estudos de citotoxicidade foram realizados em termos de viabilidade celular com células de fibroblastos de camundongo (NIH3T3) e hemólise utilizando sangue humano (eritrócitos), seguindo protocolos descritos na literatura.

Por fim, protocolos típicos adaptados foram utilizados para sínteses de copolímeros de bloco, poli(monometacrilato de glicerol)-*b*-poli(2-hidroxipropil metacrilato) (PGMA₃₀-*b*-PHPMA_n) e poli(monometacrilato de glicerol)-*b*-poli(metacrilato de benzila) (PGMA₃₀-*b*-PBzMA_n), via RAFT-PISA: PGMA_n macro-CTA previamente sintetizado e purificado (0,200 g) foi adicionado a um frasco de 40 mL equipado com um septo, seguido por monômero 2-hidroxipropil metacrilato (HPMA) ou metacrilato de benzila (BzMA) com um grau alvo de polimerização (DP) de 50 a 400 e água (quantidades variáveis para resultar em conteúdo de sólidos variando entre 2,5 e 15% p/p). Iniciador, ACVA ou AIPD, foi então adicionado (razão molar CTA/Iniciador = 1,0) e a solução foi purgada com N₂ por 10 min. O frasco foi selado e imerso em um banho regulado a 70 °C para ACVA ou 45 °C para AIPD. O meio de reação foi agitado magneticamente até completa conversão do monômero e a polimerização foi subsequentemente extinta por exposição ao ar.

Para polimerizações via transferência reversível de cadeia por adição-fragmentação por transferência de elétrons fotoinduzida (PET-RAFT), procedimentos típicos adaptados da literatura foram utilizados para sintetizar copolímeros de bloco PGMA_n-*b*-PHPMA_n e PGMA_n-*b*-PBzMA_n ([M]:[macro-CTA]: [fotocatalisador]:[TEA]=100 a 600: 1: 0,01: 0 a 1) e teor de sólidos de 10% p/p foi estabelecido como segue: PGMA, HPMA ou BzMA, fotocatalisador (1% p/p em relação ao macro-CTA) e TEA foram dissolvidos em água deionizada em um frasco de vidro. O frasco de vidro foi selado com um septo de borracha e purgado com nitrogênio por 10 min. O frasco foi então irradiado com luz LED azul (0,16 W cm⁻², λ 460 nm) à temperatura ambiente até completar a conversão do monômero, a reação foi extinta por exposição ao ar e armazenada no escuro. As conversões de monômero tanto para termo e quanto para fotopolimerização foram determinadas por ¹H NMR e as distribuições de peso molecular foram analisadas por GPC. Alíquotas de polímero foram retiradas e diluídas com água até uma concentração apropriada para análise de DLS.

Resultados e Discussão

Na epoxidação mediada por lipase (Capítulo 3), os dois biocatalisadores utilizados, NS 88011 e Novozym 435, levaram a resultados semelhantes, o que faz da NS 88011 uma alternativa promissora e de baixo custo para as reações de epoxidação mediadas por lipase. O maior rendimento na síntese de óxido de limoneno foi de 74,92 ± 1,12% após 40 min de reação. Além disso, ambos, NS 88011 e o Novozym 435, puderam ser usados por até três ciclos. Portanto, a lipase NS 88011 apresentou um desempenho bom e viável nas reações de epoxidação do limoneno e, após a purificação, levou a um produto com pureza >95%.

Nas reações de síntese dos copolímeros de óxido de limoneno (Capítulo 4), via mecanismo de polimerização catiônica por abertura de anel (ROP), conversões em torno de 80% de óxido de limoneno, massa molar média numérica acima de 1000 g mol⁻¹, estruturas perfeitamente alternadas com duplas ligações pendentes que permitem futuras modificações foram obtidas. As nanopartículas (NPs) reticuladas preparadas com poli(anidrido ftálico-*co*-óxido de limoneno) apresentaram um diâmetro médio ponderado em número de 56 nm, morfologia esférica e boa estabilidade coloidal. Essas NPs apresentaram compatibilidade sanguínea elevada e viabilidade celular levemente reduzida em diferentes concentrações, sugerindo biocompatibilidade do material com potencial para aplicação biomédica.

No Capítulo 5, os diferentes macro-CTAs sintetizados apresentaram evolução linear do peso molecular médio ponderal (M_w) em função da conversão do monômero, com distribuições estreitas de peso molecular ($\mathcal{D} \leq 1,47$), indicando que um bom controle foi alcançado durante a polimerização em solução via RAFT. Copolímeros de blocos foram sintetizados com conversões de monômeros superiores a 90%, peso molecular médio de até $270 \times 10^3 \text{ g mol}^{-1}$ e diferentes nanoestruturas em meio aquoso foram obtidas, tais como esferas, vermes e vesículas. Nas polimerizações via PET-RAFT vários DPs foram direcionados para formação do segundo bloco. A maioria das polimerizações atingiu mais de 90% de conversão, foram observados pesos moleculares elevados, que se tornaram mais proeminentes quanto maior o DP. O sistema com PGMA-*b*-PHPMA funcionou melhor com o PGMA-CCCP em comparação com PGMA-CPADB como macro-CTAs. Uma inspeção visual das dispersões aquosas finais usando PGMA-CPADB como macro-CTA revelou polímero precipitado que afetou o aumento da polidispersidade, o que confirma o baixo controle de polimerização.

Os gráficos cinéticos para PISA em meio aquoso de HPMA a uma concentração de 10% p/p utilizando PGMA₃₀-CCCP como o agente macro-CTA (grau alvo de polimerização (DP) de 100 e 200) exibiu taxa de polimerização do foto-PISA maiores do que a do PISA iniciado termicamente com $\geq 74\%$ de conversão de monômero sendo alcançada em 15 min sob irradiação de luz. Em contraste, 60 min foram necessários para atingir alta conversão de monômero para PISA iniciado termicamente. O comportamento de polimerização rápida do foto-PISA aquoso pode ser atribuído à rápida iniciação do fotocatalisador sob irradiação de luz visível de 460 nm. As imagens de TEM indicaram que a automontagem ocorreu na síntese de PGMA₃₀-*b*-PHPMA₂₀₀ usando NH como fotocatalisador sob irradiação de luz azul. Vesículas foram obtidas apenas em uma concentração de monômero de 10% p/p com um DP de 200.

Em uma abordagem semelhante, utilizando BzMA como um segmento central hidrofóbico, PGMA₃₀-*b*-PBzMA₂₀₀ foi formado via RAFT polimerização em dispersão, resultando em morfologia puramente esféricas. A conversão total foi alcançada com alto peso molecular ($464.835 \text{ g mol}^{-1}$). Após 24 h, suspensões estáveis foram obtidas, o que foi atribuído à lenta polimerização do BzMA favorecendo o rearranjo das nanopartículas e, conseqüentemente, levando à estabilidade coloidal.

Considerações finais

Este trabalho apresenta uma alternativa biotecnológica para produzir óxido de limoneno via reações de epoxidação mediada por uma nova preparação enzimática (lipase obtida a partir de *Candida antarctica*) imobilizada em um material baixo custo (NS 88011). Rendimentos acima de 70% foram alcançados em solventes orgânicos, em baixa concentração de substrato e temperatura moderada. Os resultados revelaram que não há grandes diferenças na reação de epoxidação ao usar diferentes materiais de suporte do biocatalisador como Novozym 435 e NS 88011. Este trabalho mostrou pela primeira vez um relato bem sucedido da produção de óxido de limoneno por reação de epoxidação mediada por NS 88011, apresentando resultados promissores de rendimento do epóxido.

Na copolimerização do óxido de limoneno com anidrido ftálico ou anidrido maleico, os experimentos foram capazes de confirmar a polimerização de abertura de anel catalisada por líquido iônico (LI) BMI·Fe₂Cl₇. Conversões em torno de 80% foram alcançadas em uma razão molar catalisador: óxido de limoneno de 1:100. O polímero resultante apresentou uma estrutura perfeitamente alternada; número de massa molar média acima de 1000 g mol^{-1} e ligações duplas pendentes que permitem a modificação posterior na estrutura do polímero. Em relação à sua aplicação, como nanodispositivos para sistemas biológicos, nanopartículas (NPs) de poli(anidrido ftálico-*co*-óxido de limoneno) (PAFOL) também foram produzidas e reticuladas com tetratiol via reação tiol-eno. As NPs-PAFOL reticuladas com um diâmetro médio

ponderado em número de 56 nm, morfologia esférica e boa estabilidade coloidal foram obtidas. Essas NPs foram testadas quanto à compatibilidade sanguínea e viabilidade celular, apresentando potencial para aplicações biomédicas.

A síntese de nanopartículas diretamente na água é desejável para uma ampla gama de aplicações, como a área biomédica. Nesta tese, os macromônômeros utilizados como agentes de transferência de cadeia, poli(monometacrilato de glicerol) (PGMA) e poli (N, N-dimetilacrilamida (PDMA) (macro-CTAs), foram estendidos em cadeia com uma gama de monômeros via polimerização mediadas por transferência reversível de cadeia por adição-fragmentação (RAFT) para formar copolímeros de blocos. Os copolímeros foram preparados com alto grau de conversão (> 90%) e resultando em nanopartículas no formato de esféricas e vesículas. A análise de cromatografia de permeação em gel (GPC) confirmou que as polimerizações RAFT foram bem controladas.

Com base nos resultados expostos nesta tese, foi possível sintetizar enzimaticamente o óxido de limoneno por um biocatalisador de relativo baixo custo. Além disso, os resultados da copolimerização via ROP e produção de nanopartículas foram promissores, pois aumentam o espectro de aplicação desses polímeros a partir de recursos renováveis, uma vez que não há estudos na literatura envolvendo a formação de nanopartículas com este polímero. Além disso, a polimerização RAFT fornece um ótimo método para produzir nano-objetos em meio aquoso. Aliada a esta estratégia, a polimerização por transferência reversível de cadeia por adição-fragmentação por transferência de elétrons fotoinduzida (PET-RAFT) provou ser uma ferramenta poderosa para sintetizar polímeros em condições ambientalmente amigáveis, requer luz visível de baixa energia e abre portas para a criação de diferentes arquiteturas poliméricas.

ABSTRACT

The development of more sustainable materials derived from renewable resources and nanostructured polymeric systems has increasingly gained attention from society. This work was divided in three steps, initially, limonene oxide was synthesized for the first time via epoxidation reactions of R-(+)-limonene mediated by a new immobilized preparation with low-cost material from *Candida antarctica* lipase fraction B (NS 88011). Parameters affecting this reaction were studied, such as enzyme amount, acyl donor concentration, oxidant concentration, R-(+)-limonene concentration, reaction time, and temperature. The syntheses were performed in agitated tank reactors operated in fed-batch mode. Both used biocatalysts, NS 88011 and Novozym 435, led to similar results, which makes NS 88011 a promising and low-cost alternative for epoxidation reactions mediated by lipase. The use of non-toxic biocatalysts, such as immobilized enzymes, has become an advantageous option. The highest yield in the 1,2-limonene oxide synthesis was $74.92 \pm 1.12\%$ of yield at 40 min. In addition, both NS 88011 and Novozym 435, could be used for up to three cycles. Therefore, NS 88011 lipase had a good and viable performance in the epoxidation reactions of the R-(+)-limonene and after purification led to a final product with purity $>95\%$. The second step of the work consisted in the synthesis of limonene oxide copolymers via ring-opening polymerization mechanism, employing different cyclic anhydrides, phthalic anhydride, or maleic anhydride catalyzed by the ionic liquid 1-n-butyl-3-methylimidazolium heptachlorodiferrate ($\text{BMI}\cdot\text{Fe}_2\text{Cl}_7$). Conversions around 80% were reached with a 1:100 catalyst:limonene oxide molar ratio. The resulting polymers presented a perfectly alternating structure, number-average molar mass over 1000 g mol^{-1} , and pendant double-bonds that allow posterior modification of their structure. Regarding their application, such as nanodevices for biological systems, poly(phthalic anhydride-co-limonene oxide) (PPALO) nanoparticles (NPs) were also produced and cross-linked with tetrathiol via thiol-ene reaction. The cross-linked PPALO-NPs with a number-weighted mean diameter of 56 nm, spherical morphology, and good colloidal stability were obtained. These NPs were tested for blood compatibility and cell viability, presenting the potential for biomedical applications. In the third step, polymerization reactions mediated by reversible addition-fragmentation chain transfer (RAFT) and photoinduced electron/energy transfer reversible addition-fragmentation chain transfer (PET-RAFT) were studied in detail, being efficient strategies to produce nanostructures with different sizes and shapes in aqueous media. The effects of reaction parameters by thermal initiation and photoinitiation were analyzed, using different monomers, photocatalysts, and RAFT agents. This research provided new perspectives for reactions of polymerization induced self-assembly (PISA) via RAFT in aqueous medium. Nano-objects, such as spheres, worms, and vesicles were obtained in the reactions of photopolymerizations. Polymerization mediated by visible light is an emerging technique that allows the preparation of well-defined polymers in moderate conditions, considered ecological and a sustainable alternative to traditional thermal polymerization.

Keywords: Epoxidation reaction. Biocatalysis. Limonene NS 88011. ROP. Polyester. Ionic liquid. RAFT-PISA. PET-RAFT. Nanostructures.

LIST OF FIGURES

Figure 1 – Chemical structure of isoprene (2-methyl-1,3-butadiene).	31
Figure 2 – Structures and classifications of Terpenes	32
Figure 3 – The isomers of limonene	33
Figure 4 – The chemical equations involved in the epoxidation, with preformed peracid (1) and epoxidation methods with <i>in situ</i> formed peracid (2).	38
Figure 5 – Secondary structure diagram of the ‘canonical’ α/β hydrolase fold. The location of the catalytic triad is indicated by black dots. Dashed lines indicate the location of possible insertions. α Helices and β strands are represented by white cylinders and gray arrows, respectively.	41
Figure 6 – Mechanism of lipase-catalyzed perhydrolysis reaction.	42
Figure 7 – Epoxidation of alkenes by lipase-catalyzed perhydrolysis of carboxylic acids.	43
Figure 8 – Schematic presentation of the mass transport of hydrogen peroxide and water in an organic-water biphasic system.	48
Figure 9 – The reaction of carboxylic acids esters with hydrogen peroxide.	49
Figure 10 – Copolymerization of limonene oxide and CO ₂	51
Figure 11 – Copolymerization of limonene cyclic and anhydride oxides.	52
Figure 12 – Elementary steps occurring during epoxide–anhydride ring-opening copolymerizations.	52
Figure 13 – Composition of typical ionic pairs present in ionic liquids.	54
Figure 14 – Examples of cations derived from 1,3-dialkylimidazolium.	55
Figure 15 – Chemical structure of the catalyst BMI·Fe ₂ Cl ₇	56
Figure 16 – Schematic representation of the miniemulsification /solvent evaporation technique	58
Figure 17 - Representation of the RAFT agents and macro-RAFT formation.	60
Figure 18 - Structure of commercially available RAFT agents: CCCP and CPADB.	61
Figure 19 - Basic reaction steps of the Reversible Addition–Fragmentation Chain Transfer (RAFT) processes: initiation, pre-equilibrium, re-initiation, main-equilibrium, and termination.	62
Figure 20 - Block copolymers by sequential RAFT polymerizations overall RAFT process.	63
Figure 21 - Evolution of the self-assembly process as polymerization progresses.	64

Figure 22 - Synthesis of sterically stabilized (PGMA _x -b-PHPMA _y) diblock copolymer nanoparticles via PISA utilizing RAFT aqueous dispersion polymerization	65
Figure 23 - Proposed mechanism for PET-RAFT process. Note: PC: photocatalyst; PET: photoinduced electron transfer.	67
Figure 24 – Schematic structure of epoxidation reaction using immobilized CALB as catalyst (NS 88011).	69
Figure 25 – Influence of temperature in the 1,2-limonene oxide biosynthesis using NS 88011 as catalyst, using 100 mM of R-(+)-limonene, 70 mM of octanoic acid, 500 mM of hydrogen peroxide (35% aqueous solution), and 20% in mass of NS 88011 in solvent toluene. The line connecting the experimental points is a guide for the eye.....	74
Figure 26 – Effect of enzyme loading (% in mass) on: a) yield of 1,2-limonene oxide (mol%), and b) initial reaction rates ($\mu\text{M min}^{-1}$). Conditions: NS 88011 as catalyst, 100 mM of R-(+)-limonene, 70 mM of octanoic acid, 500 mM of hydrogen peroxide (35% aqueous solution), solvent toluene, and 50 °C. The line connecting the experimental points is a guide for the eye.	75
Figure 27 - Yield of 1,2-limonene oxide (%) obtained at varying H ₂ O ₂ concentrations. Conditions: 5% in mass of NS 88011 as catalyst, 40 mM of R-(+)-limonene, 70 mM of octanoic acid, 100 to 500 mM of hydrogen peroxide (35% aqueous solution), solvent toluene, and 50 °C. The line connecting the experimental points is a guide for the eye.	76
Figure 28 – Effect of octanoic acid concentration (mM) on: a) yield 1,2-limonene oxide (%); b) initial reaction rates ($\mu\text{mol min}^{-1} \text{g}^{-1}$). Conditions: 5% in mass of NS 88011 as catalyst, 40 mM of R-(+)-limonene, 40 – 250 mM of octanoic acid, 250 mM of hydrogen peroxide (35% aqueous solution), solvent toluene, and 50 °C. The line connecting the experimental points is a guide for the eye.....	77
Figure 29 – Effect of R-(+)-limonene concentration (mM) on: a) yield 1,2-limonene oxide (%); and b) initial reaction rates ($\mu\text{mol min}^{-1} \text{g}^{-1}$). Conditions: 5% in mass of NS 88011 as catalyst, 40 to 100 mM of R-(+)-limonene, 70 mM of octanoic acid, 500 mM of hydrogen peroxide (35% aqueous solution), solvent toluene, and 50 °C. The line connecting the experimental points is a guide for the eye.	78
Figure 30 – Performance of NS 88011 and Novozym 435 over three cycles in a fed-batch reactor on: a) yield 1,2-limonene oxide (%); and b) initial reaction rates ($\mu\text{mol min}^{-1} \text{g}^{-1}$). Conditions: 5% in mass of enzyme, 40 mM of R-(+)-limonene, 70 mM of octanoic acid,	

250 mM of hydrogen peroxide (35% aqueous solution), solvent toluene, and 50 °C. The line connecting the experimental points is a guide for the eye.....	79
Figure 31 – Chromatogram of the 1,2-limonene oxide in ethyl acetate after purification using column chromatography on silica gel. Peak 1: cis-limonene internal epoxide; Peak 2: trans-limonene internal epoxide.	80
Figure 32 – ¹ H NMR spectrum of the 1,2-limonene oxide in CDCl ₃ after purification using column chromatography on silica gel (n-hexane:ethyl acetate 9:1).....	81
Figure 33 - Synthesis of polyesters from limonene oxide (LO) and phthalic anhydride (PA) or maleic anhydride (MA) using the ionic liquid BMI·Fe ₂ Cl ₇ as catalyst.....	84
Figure 34 - Second heating DSC curves of PPALO (black) and DSC curves of PMALO (red).	89
Figure 35 – MALDI-TOF spectrum of PPALO copolymer synthesized using liquid BMI·Fe ₂ Cl ₇ as catalyst. Reaction conditions: Ratio molar [IL]:[LO]:[anhydride] 1:100:100; Temperature: 110°C; Toluene 50 %wt; Reaction time: 300 min.....	89
Figure 36 – MALDI-TOF spectrum of PMALO copolymer synthesized using liquid BMI·Fe ₂ Cl ₇ as catalyst. Reaction conditions: Ratio molar [IL]:[LO]:[anhydride] 1:100:100; Temperature: 110 °C; Toluene 50 %wt; Reaction time: 300 min.	90
Figure 37 – Analysis of ¹ H NMR spectra of (1) LO-PA and (2) LO-MA in CDCl ₃ , using TMS as the peak reference. Reaction conditions: Ratio molar [IL]:[LO]:[anhydride] 1:100:100; Temperature: 110 °C; Toluene 50 %wt; Reaction time: 300 min.	91
Figure 38 – Analysis of ¹³ C NMR spectra of the LO-PA, using TMS as the peak reference. Reaction conditions: Molar ratios [IL]:[LO]:[anhydride] 1:100:100; Temperature: 110 °C; Toluene 50 %wt; Reaction time: 300 min.	91
Figure 39 – FT-IR spectra of (A) Poly(phthalic anhydride- <i>co</i> -limonene oxide), (B) Limonene oxide, (C) Phthalic anhydride.....	92
Figure 40 – FT-IR spectra of (A) Poly(maleic anhydride- <i>co</i> -limonene oxide), (B) Limonene oxide, (C) Maleic anhydride.....	93
Figure 41 - (a) TEM images of PPALO NPs (b) Details of the shape of the particles with higher magnification and size distribution histogram.....	94
Figure 42 - (a) TEM images of cross-linked PPALO NPs (b) Details of the shape of the particles with higher magnification and size distribution histogram.	94

Figure 43 – Cytotoxicity assay. Cytotoxicity effects of different concentrations of PPALO NPs on mouse embryo fibroblast (NIH3T3) cell exposed 24 h. The cell viability was monitored through MTT assay. ($p > 0.05$) using one-way ANOVA followed by post-test Bonferroni's...	95
Figure 44 - Hemolysis assay. Relative rate of hemolysis of human red blood cells upon incubation with PPALO at $50 \mu\text{g mL}^{-1}$, $100 \mu\text{g mL}^{-1}$ and $200 \mu\text{g mL}^{-1}$. The presence of hemoglobin in the supernatant (red) was observed at 540 nm. Data are mean \pm SD ($n = 3$)...	96
Figure 45 - Photocatalysts used for PET-RAFT polymer synthesis.....	103
Figure 46 - ^1H NMR spectra of glycerol monomethacrylate (GMA, prepared via hydrolysis of glycidyl methacrylate at 10% w/w) and commercial glycidyl methacrylate (GlyMA, Sigma-Aldrich) in D_2O	104
Figure 47 – Evolution of monomer conversion and weight average molecular weight with reaction time during the syntheses of three macro-CTAs, $\text{PGMA}_{30}\text{-CCCP}$ (squares), $\text{PGMA}_{60}\text{-CCCP}$ (circles) and $\text{PGMA}_{30}\text{-CPADB}$ (triangles) at $70 \text{ }^\circ\text{C}$ via RAFT aqueous dispersion polymerization with ACVA as initiator.	105
Figure 48 – Evolution of monomer conversion and weight average molecular weight with reaction time curves during the syntheses of macro-CTA, $\text{PDMA}\text{-CCCP}$ at $70 \text{ }^\circ\text{C}$ via RAFT aqueous dispersion polymerization with ACVA as initiator.	106
Figure 49 - Molecular weight distribution of a $\text{PGMA}_{30}\text{-CCCP}$ macro-CTA and a series of $\text{PGMA}_{30}\text{-b-PHPMA}_y$ diblock copolymers synthesized at 10% w/w solids at $70 \text{ }^\circ\text{C}$. A macro-CTA/ACVA molar ratio of 1.0 was used in all cases.....	108
Figure 50 - TEM images of RAFT-PISA nano-objects of $\text{PGMA}_n\text{-P(HPMA}_n)$ and $\text{PGMA}_{30}\text{-P(BzMA}_{200})$ diblock copolymers synthesized at 10% w/w solids at $70 \text{ }^\circ\text{C}$. A macro-CTA/ACVA molar ratio of 1.0 was used in all cases.....	109
Figure 51 - Evolution of monomer conversion, weight average molecular weight (M_w , left) and polydispersity (D , right) with time during NIPAM block polymerization at $70 \text{ }^\circ\text{C}$ in deionized water with ACVA as initiator, Monomer DP_{200}	110
Figure 52 - Z-average particle size as a function of temperature for $\text{PDMA}_{30}\text{-b-PNIPAM}_{200}$ of $M_w = 31190 \text{ g mol}^{-1}$ obtained from cumulant fits. Concentration 10 mg mL^{-1} . Heating step (red), Cooling step (blue). The lines connecting the experimental points are only guides for the eyes.	111
Figure 53 - Z-average particle size as a function of the number of heating–cooling cycles, between 25 and $40 \text{ }^\circ\text{C}$ for $\text{PDMA}_{30}\text{-b-PNIPAM}_{200}$ of $M_w = 31190 \text{ g mol}^{-1}$ obtained from	

cumulant fits. Concentration 10 mg mL^{-1} . The lines connecting the experimental points are only guides for the eyes.	112
Figure 54 - Evolution of monomer conversion during thermally initiated ($70 \text{ }^\circ\text{C}$) and photoinitiated ($25 \text{ }^\circ\text{C}$) PISA of HPMA in deionized water using PGMA_{30} -CCCP as the macro-RAFT agent at a 10% w/w solids content and the target DP of 100 and 200. Thermally initiated with ACVA, DP 100 (black); Photo-PISA with JB55-61X as photocatalyst, DP 200 (red); CF193 as photocatalyst, DP 200 (blue); NH@SBA15 as photocatalyst, DP 200 (green).	114
Figure 55 - Transmission electron microscopy (TEM) images of the vesicles observed during the synthesis of PGMA_{30} -b- PHPMA_{200} via photocatalytic polymerization. Solvent: water; light source: blue LED light ($\lambda_{\text{max}} = 460 \text{ nm}$, 0.16 mW cm^{-2}); Photocatalyst: NH; reaction time: 24 hours.	115
Figure 56 - Transmission electron microscopy (TEM) images of the nanoparticles observed during the synthesis of PGMA_{30} -b- PBzMA_{200} via photocatalytic polymerization. Solvent: water:ethanol; light source: blue LED light ($\lambda_{\text{max}} = 460 \text{ nm}$, 0.16 mW cm^{-2}); Photocatalyst : NH; reaction time: 24 hours.	116

LIST OF TABLES

Table 1 – Identification and main physical properties of R-(+)-limonene.	34
Table 2 – Identification and main physical properties of the 1,2-limonene oxide.	35
Table 3 – Literature review of the 1,2-limonene oxide synthesis.	36
Table 4 – Literature review of the epoxidation of vegetable oils and alkenes using immobilized lipases.	44
Table 5 – Literature review of the copolymerization of limonene oxide and cyclic anhydrides.	53
Table 6 – Literature review of the polymerizations using the ionic liquid BMI·Fe ₂ Cl ₇	56
Table 7 – Results of ring-opening copolymerization of LO with phthalic or maleic anhydrides using the ionic liquid BMI·Fe ₂ Cl ₇ as catalyst.	88
Table 8 - Aqueous RAFT-PISA polymerizations of different systems thermally initiated upon varying solids contents and monomer types and concentrations (DP).....	107
Table 9 – Aqueous RAFT-PISA polymerizations with PDMA-CCCP as the macro-CTA to mediate polymerization of NIPAM at 70 °C in deionized water using ACVA as initiator and varying NIPAM concentration.	110
Table 10 - PET-RAFT polymerizations catalyzed by different photocatalysts in deionized water irradiated by blue LED varying Macro-CTAs, monomer concentrations (DP) and with or without reducing agent.	113

LIST OF SCHEMES

Scheme 1 - Steps to produce nano-objects via RAFT-PISA polymerization.....	98
Scheme 2 - Syntheses of PGMA macro-CTAs with CCCP (a) and CPADB (b) RAFT agents.	100
Scheme 3 - Synthesis of PDMA macro-CTA with CCCP RAFT agent.	100
Scheme 4 - Syntheses of PGMA ₃₀ -b-HPMA _n and PGMA ₃₀ -b-BzMA _n diblock copolymer nano- objects via thermally initiated PISA in water.....	101
Scheme 5 - Synthesis of the PDMA ₃₀ -b-PNIPAM _n nano-assemblies by RAFT polymerization.	102

SUMMARY

CONCEPTUAL DIAGRAM	24
1 INTRODUCTION	26
1.1 OBJECTIVES	28
2 LITERATURE REVIEW	31
2.1 TERPENES	31
2.1.1 R-(+)-limonene	33
2.1.2 Limonene oxide	35
2.2 EPOXIDATION	37
2.2.1 Epoxidation mediated by lipases	40
2.3 LIMONENE OXIDE POLYMERIZATION	50
2.3.1 Ionic liquids	54
2.4 PREPARATION OF POLYESTER NANOPARTICLES	57
2.5 BLOCK COPOLYMER SYNTHESIS BY RAFT POLYMERIZATION	59
2.5.1 RAFT agents	60
2.5.2 RAFT Polymerization	61
2.5.3 RAFT-PISA Polymerization	63
2.5.3.1 Thermal RAFT-PISA polymerization	65
2.5.3.2 Photo RAFT-PISA polymerization	66
2.6 FINAL CONSIDERATIONS REGARDING THE STATE OF THE ART	68
3 EPOXIDATION OF R-(+)-LIMONENE TO 1,2-LIMONENE OXIDE MEDIATED BY LOW-COST IMMOBILIZED <i>Candida antarctica</i> LIPASE FRACTION B	69
3.1 MATERIAL AND METHODS	70
3.1.1 Enzymes and chemicals	70
3.1.2 Reaction conditions	70
3.1.3 Reuse cycles assay	71
3.2 LIMONENE OXIDE QUANTIFICATION	71

3.3	INITIAL REACTION RATE.....	72
3.4	SCALE-UP AND 1,2-LIMONENE OXIDE PURIFICATION.....	72
3.5	RESULTS AND DISCUSSION	73
3.5.1	Optimization of the enzyme-catalyzed epoxidation conditions.....	73
3.5.1.1	Temperature.....	73
3.5.1.2	Enzyme concentration	74
3.5.1.3	Oxidant concentration	75
3.5.1.4	Octanoic acid concentration	76
3.5.1.5	R-(+)-limonene concentration	77
3.5.2	Successive cycles using NS 88011 lipase.....	78
3.5.3	Scale-up and purification of 1,2-limonene oxide.....	79
3.6	Conclusions	81
4	COPOLYMERIZATION OF LIMONENE OXIDE AND CYCLIC ANHYDRIDES CATALYZED BY IONIC LIQUID BMI·Fe₂Cl₇ AND CYTOTOXICITY STUDIES.....	82
4.1	MATERIAL AND METHODS	83
4.1.1	Chemicals	83
4.1.2	General procedure for ring-opening polymerization using BMI·Fe ₂ Cl ₇	83
4.1.3	Poly(phthalic anhydride- <i>co</i> -limonene oxide) (PPALO) nanoparticles preparation.....	84
4.1.4	Crosslinking of Poly(phthalic anhydride- <i>co</i> -limonene oxide) (PPALO) nanoparticles	85
4.1.5	Characterization.....	85
4.1.5.1	Polymer characterization.....	85
4.1.5.2	Nanoparticles characterization	86
4.1.5.3	<i>In vitro</i> cytotoxicity assay of the cross-linked nanoparticles	87
4.2	RESULTS AND DISCUSSION	88
4.3	CONCLUSION	96
5	DEVELOPMENT OF NANOSTRUCTURED POLYMERIC SYSTEMS BASED ON REVERSIBLE ADDITION-FRAGMENTATION CHAIN-TRANSFER (RAFT) POLYMERIZATION	98

5.1	MATERIAL AND METHODS	99
5.1.1	Chemicals	99
5.1.2	Synthesis and purification of PGMA _n and PDMA _n macro-CTAs	99
5.1.3	Thermally initiated aqueous RAFT dispersion polymerization to form diblock copolymers.....	100
5.1.3.1	Synthesis of PGMA ₃₀ -b-PHPMA _n and PGMA ₃₀ -b-PBzMA _n diblock copolymer nanoparticles.....	100
5.1.3.2	Synthesis of PDMA _n -b-PNIPAM _n diblock copolymer nanoparticles.....	101
5.1.4	Photocatalysis aqueous RAFT dispersion polymerization of diblock copolymer	102
5.1.4.1	Synthesis of PGMA ₃₀ -b-PHPMA _n and PGMA ₃₀ -b-PBzMA _n diblock copolymer nanoparticles.....	102
5.1.5	Characterization.....	103
5.2	RESULTS AND DISCUSSION	104
5.2.1	Synthesis of PGMA _n and PDMA _n macro-CTAs.....	104
5.2.2	Thermally initiated aqueous RAFT dispersion polymerization to form diblock copolymers.....	106
5.2.2.1	Syntheses of PGMA ₃₀ -b-PHPMA _n and PGMA ₃₀ -b-PBzMA _n diblock copolymer nanoparticles.....	106
5.2.2.2	Synthesis of PDMA _n -b-PNIPAM _n diblock copolymer nanoparticles.....	109
5.2.3	PET-RAFT dispersion polymerization to form diblock copolymers.....	112
5.2.3.1	Syntheses of PGMA ₃₀ -b-PHPMA _n and PGMA ₃₀ -b-PBzMA _n diblock copolymer nanostructures.....	112
5.3	CONCLUSION	116
6	FINAL CONCLUSION	117
6.1	FURTHER WORK.....	118
	REFERENCES	119

CONCEPTUAL DIAGRAM

“DEVELOPMENT OF NANOSTRUCTURED POLYMERIC SYSTEMS BASED ON RING-OPENING POLYMERIZATION (ROP) AND REVERSIBLE ADDITION-FRAGMENTATION CHAIN-TRANSFER (RAFT) POLYMERIZATION”

Why?

- ✓ Utilization of renewable resources and different polymerization methods to produce new materials employing new catalysts and free of toxic waste, enables the application in the biomedical area and expands the range of available materials;
- ✓ R-(+)-limonene is a highly abundant raw material for limonene oxide synthesis, and it is a renewable source to produce polymers;
- ✓ The alternative environmentally friendly epoxidation process has prominence in the industrial and academic scenario;
- ✓ RAFT-mediated PISA is a robust and efficient route to produce block copolymer nanostructures of controlled molecular weight, size, and morphology;
- ✓ PET-RAFT technique, with readily available light sources, permits simple, environmentally friendly, and precise control of polymer manufacturing.

Who did?

- ✓ No reports were found in the literature for epoxidation reactions mediated by a new immobilized preparation with low-cost material from *Candida antarctica* fraction B (NS 88011);
- ✓ No reports were found in the literature for copolymerization of limonene oxide and cyclic anhydrides applying the ionic liquid BMI·Fe₂Cl₇ as catalyst;
- ✓ There are no studies in the literature on poly(phthalic anhydride-co-limonene oxide) nanoparticles;
- ✓ RAFT-mediated PISA is widely studied, which confirms the potential of this technique for producing nanostructures;
- ✓ There are few reports available in the literature on copolymerization via PET-RAFT applying heterogeneous photocatalysts.

Hypotheses

- ✓ Can the epoxidation of R-(+)-limonene mediated by a new lipase immobilized in a low-cost material from *Candida antarctica* fraction B (NS 88011) be performed efficiently?
- ✓ Is the copolymerization of limonene oxide and cyclic anhydrides applying the ionic liquid BMI·Fe₂Cl₇ possible?
- ✓ Is the production of poly (phthalic anhydride-co-limonene oxide) nanoparticles possible?
- ✓ Can RAFT combined with PISA be used to produce stable nanostructures using different monomers?
- ✓ Is the polymerization via PET-RAFT applying heterogeneous photocatalysts specific for nano-objects materials production possible?

Methodologies

- ✓ Epoxidation of R-(+)-limonene mediated by a new immobilized preparation with low-cost material from *Candida antarctica* fraction B (NS 88011) in fed-batch reactions;
- ✓ (+)-1,2-Limonene oxide quantification by gas chromatograph;
- ✓ Copolymerization of limonene oxide and cyclic anhydrides via ROP polymerization;
- ✓ Polyester nanoparticles according to the miniemulsification/solvent evaporation method;
- ✓ Classic RAFT-PISA polymerization and PET-RAFT polymerization.

Responses

- ✓ Promote an effective route for 1,2-limonene oxide biotechnological production with a low-cost system;
- ✓ Synthesis of a polyester via ROP polymerization with pendant double bonds using renewable resources and a new catalyst;
- ✓ Preparation of poly(phthalic anhydride-*co*-limonene oxide) nanoparticles with morphology, size, and size distribution suitable for biomedical applications;
- ✓ Preparation of nano-objects via RAFT-PISA and PET-RAFT with well-defined structures, such as spherical, worm or vesicular morphologies, with controllable size and functionality.

1 INTRODUCTION

The demand for alternative processes that meet the principles of “green” chemistry such as, the use of renewable feedstocks, the use of catalysts with more efficient and diverse catalytic reactions, and the increased energy efficiency by reducing reaction temperature (AHLUWALIA; KIDWAI, 2004) has intensified the efforts for the development of more sustainable technologies. From this perspective, the use of monomers derived from renewable resources for the synthesis of polymeric materials has become an important topic in polymer science, such as the ring-opening polymerization of epoxides derived from natural oils (ANDJELKOVIC et al., 2005; LI et al., 2005; SILVESTRE; GANDINI, 2008; KUKHTA; VASILENKO; KOSTJUK, 2011).

Epoxides are an important class of chemicals widely used as raw materials in the paint and polymer industries, as well as vital intermediates in a large number of chemical processes (WARWEL et al., 2001; ADHVARYU; ERHAN, 2002; BENANIBA; BELHANECHÉ-BENSEMRA; GELBARD, 2003; ISNARD et al., 2017). The use of naturally occurring cyclic monoterpenes, such as R-(+)-limonene, is attractive for the synthesis of such epoxides. R-(+)-limonene is extracted from citric oil being a highly abundant raw material (SELL, 1999; CIRIMINNA et al., 2014; FELIPE; BICAS, 2017). About 80% of the oranges produced in Brazil are destined for obtaining juice, and the oil extracted from the peel is a by-product of commercial value. Therefore, the use of this raw material and the desire to make R-(+)-limonene a chemical platform, aiming, for example, applications of limonene oxide in valuable fragrances, food additives, and monomers, makes its use attractive for the industry (FIRDAUS; MEIER, 2013; WINKLER et al., 2015).

The epoxidation of vegetable oils is a well-known reaction with patented applications since 1946 (TERRY; WHEELER, 1949; TARAMASSO et al., 1983; WULFF; WATTIMENA, 1983). It uses acids such as acetic, formic, and sulfuric acids or ion exchange resins as catalysts (BHATTACHARYA, 2011), which cause damage to the environment.

In this way, the search for an alternative environmentally friendly epoxidation process has prominence in the industrial and academic scenario. In this context, the use of non-toxic biocatalysts, such as immobilized enzymes, has become an advantageous option. Among the biocatalysts, lipases are the best candidates to catalyze reactions based on organic media, once they are highly regio- and enantio-selective, versatile, and able to catalyze innumerable organic

syntheses (BJÖRKLING et al., 1992; LEMOULT; RICHARDSON; ROBERTS, 1995; PETKAR et al., 2006).

Based on this, the first step of this work was to synthesize 1,2-limonene oxide via epoxidation reactions mediated by a new immobilized preparation with low-cost material from *Candida antarctica* fraction B (NS 88011), since no studies were found in the literature evaluating the use of this new biocatalyst in this reaction. Therefore, it expands the range of options in the use of these biocatalysts and contributes to the economic viability of the process.

In addition, polymers from natural resources are materials of great interest for various sectors, such as the industrial, biomedical, and academic. The production of bioderived materials with low toxicity, less waste formation during the synthesis, and low production and processing costs are highly desirable (JACOB et al., 2017).

Among the different polymers studied from renewable resources, polyesters represent a promising alternative. Polyester is a ubiquitous class of polymers that can be broadly divided into semi-aromatic and aliphatic polyesters (LONGO; SANFORD; COATES, 2016). Aliphatic polyesters have received attention in recent years as an alternative and potentially sustainable due to their numerous renewable resources to synthesis, easy hydrolytic degradation, and high biocompatibility (POMERANSKY; KHRIPLOVICH, 1999; VERT, 2005; NEJAD et al., 2013; HILLMYER; TOLMAN, 2014). This material is a great candidate to produce nanoparticles (NPs), several different preparation techniques have been published describing the formulation of polyester-based particles. Currently, the most popular methods involving previously synthesized polyester are emulsion/solvent evaporation or diffusion (MUSYANOVYCH; LANDFESTER, 2014; MENDOZA-MUÑOZ; ALCALÁ-ALCALÁ; QUINTANAR-GUERRERO, 2016).

Using a different approach, nanostructures as spheres, worms, or vesicles can be prepared directly in the water taking advantage of the recent advances in polymerization induced self-assembly (PISA) via reversible addition–fragmentation chain transfer (RAFT) for the synthesis of AB diblock copolymers (XU et al., 2015; ZAQUEN et al., 2019; LI; HAN; ZHANG, 2020). Aqueous RAFT-mediated dispersion polymerization is particularly appealing with both economic and environmental considerations. It also facilitates the preparation of bio-related polymer materials (TAN et al., 2017). Thermal initiation is the most used strategy for aqueous PISA to prepare various diblock copolymer nano-objects. However, the high reaction temperature (typically 70 °C) restricts the preparation of bio-related polymer nano-objects. In this way, the introduction of visible light-mediated living radical polymerization in PISA has

recently been explored by several groups (XU et al., 2015; SHANMUGAM; XU; BOYER, 2017; TAN et al., 2017; LI; HAN; ZHANG, 2020). Visible light-mediated living radical polymerization is an emerging technique, which allows the preparation of well-defined polymers under mild conditions. Polymerization regulated by visible light is considered to be eco-friendly and a sustainable alternative to traditional thermal initiated polymerization, along with a variety of attractive features (XU et al., 2015).

In this scenario, combined with the growing search for the development of new polymerization processes using more efficient and diversified catalytic reactions ring-opening polymerization (ROP) and reversible addition-fragmentation chain-transfer (RAFT) polymerization deserve attention. Coupled with this, polymer production for noble applications has become the focus of attention of much research. Thus, nano-objects production is interesting for biomedical applications, for example, leading to the creation of a new materials platform.

1.1 OBJECTIVES

The aim of this thesis is to study novel strategies to produce nanostructured polymeric materials based on the principles of “green” chemistry. Efforts were made towards understanding the polymerization-induced self-assembly via RAFT polymerization as well as, ring-opening polymerization of biobased limonene oxide and anhydrides. The enzymatic catalyzed epoxidation of limonene was investigated as a more sustainable process.

In this way, the specific goals of this work are:

- Evaluate the synthesis of limonene oxide using immobilized lipase as biocatalyst. The epoxidation reaction of limonene may produce isomeric forms of both limonene monoepoxide and diepoxide and the focus of this work is on monoepoxide production.
- Investigate the effect of the process variables (enzyme amount, acyl donor concentration, oxidant concentration, R-(+)-limonene concentration, reaction time, and temperature) on the epoxide yield, as well as the study of limonene conversion over time.
- Study the recycling of the biocatalyst.
- Appraise the scale-up of the epoxidation reaction in the best experimental condition, in

terms of product yield, in fed-batch mode.

- Study the copolymerization of limonene oxide and cyclic anhydrides via ring-opening polymerization mediated by the ionic liquid BMI·Fe₂Cl₇.
- Evaluate the production of nanoparticles via miniemulsification/solvent evaporation method using the synthesized copolymer.
- Assess the effect of the thermal and photo polymerization mediated RAFT aqueous dispersion of HPMA, NIPAM, and BzMA to prepare a series of diblock copolymer nano-objects via aqueous PISA.
- Verify the effect of reaction parameters including RAFT agents, DP of the core-forming block, and the monomer concentration to prepare a series of diblock copolymer nano-objects.

In order to better present the key issues and the obtained results, this thesis is divided into six chapters.

Chapter 2 gives a concise description of terpenes, limonene, and some prospects in the synthesis of epoxides mediated by enzymes. Besides, it presents a review of the literature concerning polymer synthesis using ionic liquids, preparation of polymer nanoparticles, polymer synthesis mediated by RAFT and by PET-RAFT polymerization via aqueous PISA.

Chapter 3 involves the epoxidation of R-(+)-limonene to 1,2-Limonene oxide mediated by low-cost immobilized *Candida antarctica* lipase fraction B. In this study, the effect of various operation parameters like enzyme amount, acyl donor concentration, oxidant concentration, R-(+)-limonene concentration, reaction time, and temperature on 1,2-limonene oxide yield was evaluated.

In Chapter 4, limonene oxide (LO), derived from orange peel, is used as a monomer to obtain polyesters with different cyclic anhydrides. The ionic liquid (LI) 1-n-butyl-3-methylimidazolium heptachlorodiferrate (BMI·Fe₂Cl₇) is used as a catalyst for ring-opening polymerization. Regarding, their potential use in medicine as nanodevices for drug delivery, poly(phthalic anhydride-co-limonene oxide) (PPALO) nanoparticles (NPs) were also produced and cross-linked with tetrathiol via thiol-ene reaction followed by assessing NPs *in vitro* cytotoxicity.

In Chapter 5, details of the RAFT and the PET-RAFT methods used to fabricate several diblock copolymer nano-objects, such as spherical and vesicles via aqueous PISA are described.

The impact of various process parameters on synthesis is discussed in this section. Different initiators, chain transfer agents (CTAs), monomers, and photocatalysts were applied. Additionally, the proof for the controlled/living polymerization is provided based on a kinetic analysis.

Finally, **Chapter 6** summarizes important conclusions of the thesis and contemplates possible future perspectives.

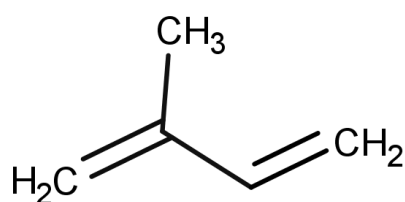
2 LITERATURE REVIEW

This chapter will present a compilation of the available literature on the pertinent subjects of this work. Firstly, the main information about terpenes, limonene, and some prospects in the synthesis of epoxides mediated by enzymes will be introduced. Then, some important biocatalysts and chemical catalysts will be described. The current state of the art of polymer synthesis using ionic liquids will be presented, besides a brief review of the preparation of polymer nanoparticles. Finally, summary state of the art of polymer synthesis via RAFT and PET-RAFT polymerization.

2.1 TERPENES

Terpenes are defined as materials with molecular structures containing isoprene units (2-methyl-1,3-butadiene) (Figure 1). These compounds are found abundantly in the oils of plants and flowers. They are classified based on the number and structural organization of carbons formed by the linear arrangement of isoprene units followed by cyclization and rearrangements of the carbon skeleton (ZWENGER; BASU, 2008; OUELLETTE; RAWN, 2015; LUDWICZUK; SKALICKA-WOŹNIAK; GEORGIEV, 2017).

Figure 1 – Chemical structure of isoprene (2-methyl-1,3-butadiene).

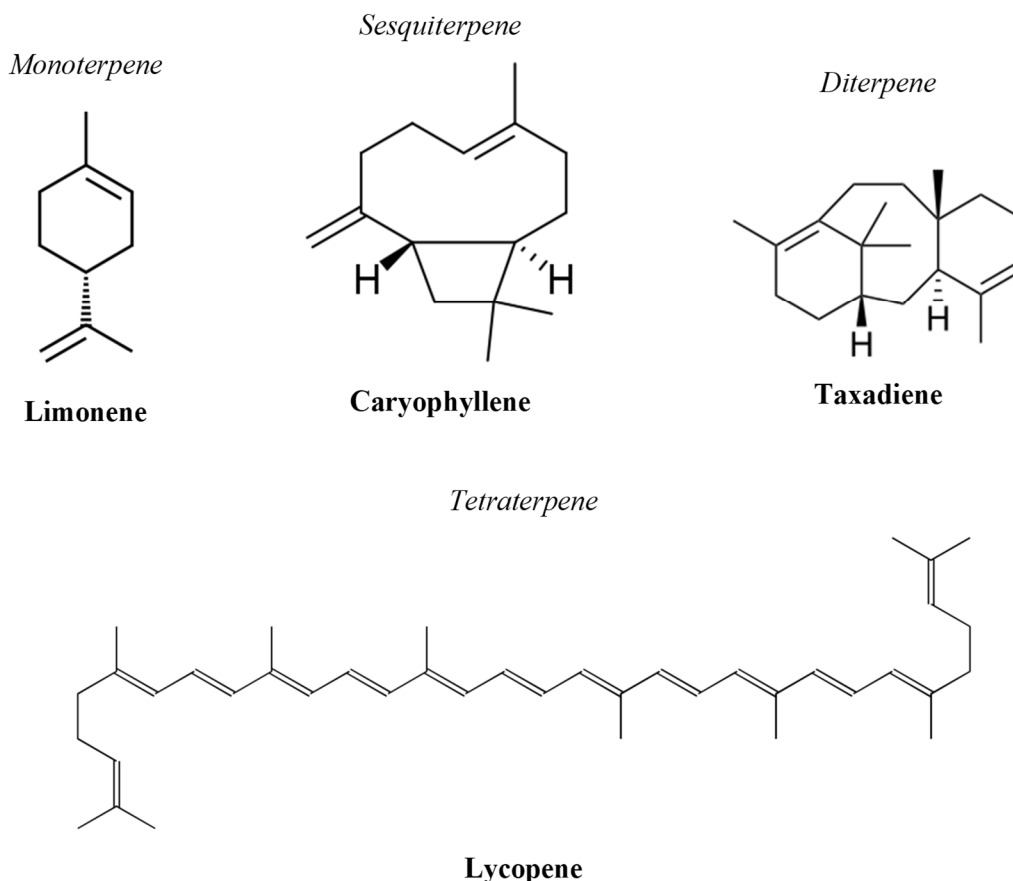


Source: Author.

The monoterpenes, the simplest terpene class, contain two isoprene units, and sesquiterpenes have three isoprene units. Examples of these structures are shown in Figure 2 using bond-line structures. Diterpenes, triterpenes, and tetraterpenes contain 4, 6, and 8 isoprene units, respectively (OUELLETTE; RAWN, 2015). Most of the terpenes are colorless, fragrant liquids that are lighter than water and volatile with steam. A few of them are solids e.g., camphor. All are soluble in organic solvents and usually insoluble in water. Most of them are

optically active and they are easily oxidized nearly by all the oxidizing agents (YADAV; YADAV; GOYAL, 2014).

Figure 2 – Structures and classifications of Terpenes



Source: Author.

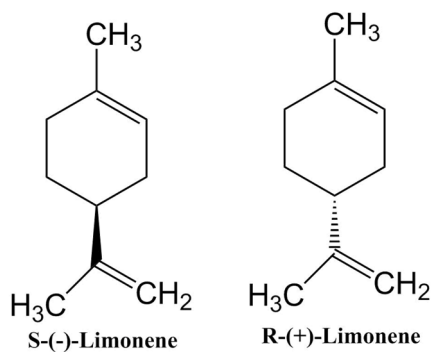
Various catalytic chemical processes of terpenes have been developed for the production of valuable products via isomerization/rearrangement (STOLLE; ONDRUSCHKA; HOPF, 2009), hydrogenation (HUDAYA et al., 2016), oxidation (MUTZEL et al., 2016), hydration (MC; MI, 2015), hydroformylation (DA SILVA et al., 2007), cyclization (ZHANG et al., 2017), and epoxidation (BARRERA ZAPATA; VILLA; MONTES DE CORREA, 2006; RAFIEE-MOGHADDAM et al., 2014; GUIDOTTI; PALUMBO, 2016; RANGANATHAN et al., 2016). The main terpenes, which can be considered as possible renewable platform chemicals, are pinene, limonene, carene, geraniol/nerol, citronellol, citral, and citronella (CORMA; IBORRA; VELTY, 2007). Among the terpenes, R-(+)-limonene stands out, which will be discussed in the next topic.

2.1.1 R-(+)-limonene

Limonene (4-isopropenyl-1-methylcyclohexene) is a monoterpene compound that has many applications in the chemical industry. It is extracted from citrus oil, produced by more than 300 plants species, which results in a highly abundant raw material (SELL, 1999; CIRIMINNA et al., 2014; FELIPE; BICAS, 2017), limonene corresponds to 90% of the oil extracted from the orange peel (BONON, 2012). In addition, in the world scenario, orange production is around 49.7 million tons per year (KIRT, 2021), with Brazil being the leader, with a harvest of more than 11 million tons of the fruit in the production of 2020/21 (BRAGA, 2020), about 80% of Brazilian production is destined for obtaining juice with peel and fixed oil as by-products of commercial value.

Limonene is a colorless or pale yellow liquid with a molecular weight of $136.23 \text{ g mol}^{-1}$ and with a characteristic citrus smell (R-(+)-limonene) or pine smell (S-(-)-limonene) (Figure 3). These two isomers occur due to the presence of a chiral center on the fourth carbon atom in the cycle.

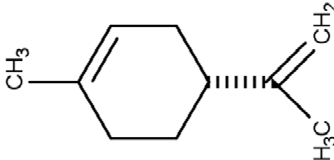
Figure 3 – The isomers of limonene



Source: Author.

Moreover, in nature, limonene occurs often in the form of a racemic mixture. From these two isomers of limonene, R-(+)-limonene exhibits a wider range of applications (MALKO; WRÓBLEWSKA, 2016). The R-(+)-limonene occurs in the peels of citrus fruits, such as sweet orange, tangerine, lemon, and lime, and is characterized by having good solubility in methanol and ethanol as well as in acetone and benzene (PUBCHEM, 2019a). Table 1 presents the identification and main physical properties of R-(+)-limonene.

Table 1 – Identification and main physical properties of R-(+)-limonene.

IUPAC Name	(4R)-1-methyl-4-prop-1-en-2-ylcyclohexene
CAS registry number	5989-27-5 or 65996-98-7
EINECS number	227-813-5
Formula	C ₁₀ H ₁₆
Structure	
Molecular weight	136.24 g mol ⁻¹
Boiling point	175.5-176.0 °C
Melting point	-74.35 °C
Water solubility	13.8 mg L ⁻¹ (25 °C)
Density	0.8411 g cm ⁻³ (20 °C)

Source: PUBCHEM (2019a)

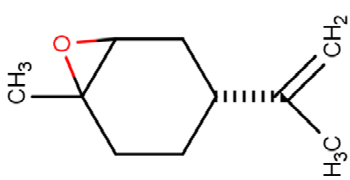
Limonene is widely used as a flavoring agent in food, cosmetic and medical industries (i.e., chewing gum, perfume, ointment, hand cleanser, para-pharmaceutical products) (EDRIS, 2007; REN, 2017), agriculture (e.g. insecticide) (TRIPATHI et al., 2003), organic industry (e.g. biodegradable polymers) (MALKO; WRÓBLEWSKA, 2016), and other areas. Because of its low toxicity and non-water soluble nature, limonene is increasingly being used as an environmentally friendly substitute for toxic and caustic solvents such as fluorinated and chlorinated organic solvents (GU; JÉRÔME, 2013; REN, 2017), and for epoxides synthesis (MANDELLI et al., 2001; MICHEL, 2012; WIEMANN; FALTL; SIEBER, 2012; WRÓBLEWSKA, 2014), which has attracted considerable attention in recent years. The epoxidation reaction of R-(+)-limonene produces isomeric forms of both limonene monoepoxide and diepoxide (CIRIMINNA et al., 2014). The epoxidation of limonene is incredibly attractive as their epoxides are key and versatile reagents for various reactions and the manufacturing of biopolymers. Furthermore, limonene epoxidation processes increase their added value as epoxides are of great interest for the drug, flavor, and fragrance industry (SIENEL; RIETH; ROWBOTTOM, 2000; YAN; XIAO; KOU, 2010). In this way, the next

topics of this literature review will approach the main characteristics and synthesis of 1,2-limonene oxide.

2.1.2 Limonene oxide

Limonene oxide is also known as limonene-1,2-epoxide, limonene monoxide or 1,2-limonene oxide. It is, in fact, the most important member of the terpene family for the perfume industry and is widely used as raw material in manufacturing a range of important commercial products (HERRERO et al., 2000; MALKO; WRÓBLEWSKA, 2016). The compound is an active cycloaliphatic epoxide with low viscosity, and it may also be used with other epoxides and cyclic monomers in applications including metal coatings, varnishes, printing inks, and biodegradable polymers (CORMA; IBORRA; VELTY, 2007; MICHEL, 2012). Table 2 presents the identification and main physical properties of the 1,2-limonene oxide.

Table 2 – Identification and main physical properties of the 1,2-limonene oxide.

IUPAC Name	1-methyl-4-prop-1-en-2-yl-7-oxabicyclo[4.1.0]heptane
CAS registry number	1195-92-2
EINECS number	214-805-1
Formula	C ₁₀ H ₁₆ O
Structure	
Molecular weight	152.23 g mol ⁻¹
Boiling point	113 - 114 °C (50 torr)
Density	0.930 g cm ⁻³ (20 °C)

Source: PUBCHEM (2019b)

The 1,2-limonene oxide occurs naturally in the essential oils of *Cymbopogon densiflorus* (ROYALS; LEFFINGWELL, 1966) and *Elyonurus hensii* (LOUMOUAMOU et al., 2017). At industrial scale, limonene oxide is usually synthesized via the stoichiometric peracid reaction process, thus the development of potentially sustainable alternatives to this

route has attracted great attention (CORMA; IBORRA; VELTY, 2007). Regarding the synthesis of this epoxide using chemical routes, several studies are available in the literature, as possible seen in Table 3.

Table 3 – Literature review of the 1,2-limonene oxide synthesis.

Substrates	Catalyst	Best condition	Yield (%)	Reference
R-(+)-limonene, H₂O₂¹	Al ₂ O ₃	Catalyst 250 mg; MR ² Limonene to H ₂ O ₂ ¹ 4:8; Temperature 89.85 °C; Time 4 h.	70	(MANDELLI et al., 2001)
R-(+)-limonene, H₂O₂¹	MTO ³	Catalyst 0.5 mol%; MR ² Limonene to H ₂ O ₂ ¹ 100:10; Temperature 25 °C; Time 60 min.	77	(MICHEL et al., 2012)
R-(+)-limonene, H₂O₂¹	Zeolite type catalysts: TS-1 and Ti-SBA-15	Catalyst 3 wt%; MR ² Limonene to H ₂ O ₂ ¹ 1:2; Temperature 120 °C and 80 °C; Time 24 h.	59 and 64	(WRÓBLEWSKA, 2014)
R-(+)-limonene, H₂O₂¹	PW-Amberlite	Catalyst 18 g L ⁻¹ ; Limonene: 0.66 M H ₂ O ₂ ¹ : 1.33 M; Temperature ~40 °C; 800 rpm; Time 120 min.	NR ⁴	(WRÓBLEWSKA, 2014)
R-(+)-limonene, O₂ molecules	Photocatalyst Silylated P25	Limonene: 1 mM Solar light simulator with Xe lamp (1500W); Room Temperature; Time 2 h.	~47	(CIRIMINNA et al., 2018)
R-(+)-limonene, H₂O₂¹	Tungsten-based polyoxometalates	MR ² Catalyst to Limonene 0.005:4 MR ² Limonene to H ₂ O ₂ 4:1; Temperature ~50 °C; Time 120 min; Solvent-free.	100	(GUNAM RESUL et al., 2018)
R-(+)-limonene, H₂O₂¹	Ti-SBA-15	Catalyst 3 wt%; MR ² limonene: H ₂ O ₂ 1:1; Temperature 80 °C; Time 3 h.	48.7	(WRÓBLEWSKA; MALKO; WALASEK, 2018)
R-(+)-limonene, NaIO₄⁵	Mn salophen@MWCNT	Catalyst 0.06 mmol; Limonene: 1 mmol NaIO ₄ ⁵ : 2 mmol; Room temperature; Time 3.5 h.	~61	(TANGESTANINEJAD et al., 2010)

R-(+)-limonene, TBHP⁶	Ti-MCM-41	Catalyst 25 mg; MR ² Limonene to TBHP ⁶ 1:1.1; Temperature ~90 °C; 500 rpm; Time 24 h.	~73	(GUIDOTTI et al., 2011)
R-(+)-limonene, TBHP⁶	Mo(VI) complexes	Catalyst 0.5 wt% MR ² Limonene to TBHP ⁶ 100:200; Temperature 80 °C; Time 4 h.	~30	(CINDRIĆ et al., 2017)
R-(+)-limonene, H₂O₂¹	Amberlyst-15	Catalyst 1mol% H ₂ O ₂ 1equiv. 30%H ₂ O ₂ (aq); Solvent-free Temperature 50 °C; Time 1 h.	~94	(CUNNINGHAM et al., 2020)

¹ H₂O₂ – Hydrogen peroxide

² MR – Molar ratio

³ MTO – Methyltrioxorhenium

⁴ NT – Not reported

⁵ NaIO₄ – Sodium periodate

⁶ TBHP – Tert-butyhydroperoxide

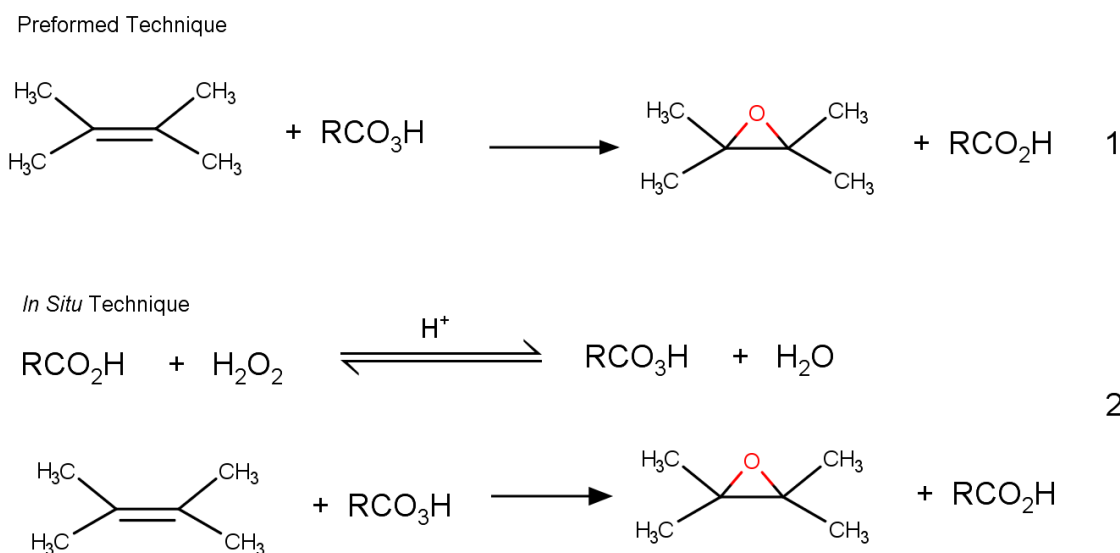
As may be seen, a large body of work has been done on the heterogeneous catalytic epoxidation of limonene using chemical routes. The catalysts used include heterogenized Mn–salen, silylated, as well as polyoxometalates, Ti-substituted zeolites and mesoporous materials, molybdenum complexes, and hydrotalcites. As oxidants, H₂O₂, organic peroxides (TBHP), and oxygen have been used. However, more studies are needed to investigate the viability of the 1,2-limonene oxide synthesis using alternative environmentally friendly epoxidation processes.

2.2 EPOXIDATION

Epoxidation occurs when a cyclic ether is formed at the location of an unsaturated bond along the chains by the addition of oxygen atoms. In which, a C=C double bond is converted into an epoxide, which is the simplest form of cyclic ethers (GUNSTONE, 1996). Epoxides are classified as a member of ethers, having partially positive charged carbons and a Lewis-basic oxygen atom in a three-membered ring system (DAKE, 1996; SIENEL; RIETH; ROWBOTTOM, 2000; NAKANO; NOZAKI, 2007). The chemical equations showing the major reactions involved in epoxidation can be observed in Figure 4, where the symbol ‘R’ represents the alkyl group of the carboxylic acid. It is a second-order reaction and is very

exothermic (ca. 250 kJ/mol), besides it is stereospecific; cis olefins give cis epoxides and trans olefins give trans epoxides (SIENEL; RIETH; ROWBOTTOM, 2000).

Figure 4 – The chemical equations involved in the epoxidation, with preformed peracid (1) and epoxidation methods with *in situ* formed peracid (2).



Source: Latourette et al. (1960)

The epoxidation of vegetable oils is a well-known reaction with patented applications since 1946 (TERRY; WHEELER, 1949; TARAMASSO et al., 1983; WULFF; WATTIMENA, 1983). There are four major categories of epoxidation processes: conventional chemical treatment, acid ion exchange resin (AIER) method, metal-catalyzed epoxidation, and chemo-enzymatic (TAN; CHOW, 2010).

The first practical synthesis of epoxides from a preformed peracetic acid was reported in 1945 by Findley, Swern, and Scanlan (1945). It is the most widely used process of epoxidation, so-called the Prilezhaev process, based on peroxycarboxylic acids (typically peracetic or performic acid), by reacting a carboxylic acid with concentrated hydrogen peroxide. In which, the *meta*-chloro perbenzoic acid (m-CPBA) is a widely applied epoxidation agent (HUSSAIN et al., 2014). This process performs industrially on large scale (SAURABH et al., 2011). The presence of strongly acidic components leads to several disadvantages: (i) side reactions, due to acid-catalyzed epoxide ring-opening; (ii) difficult separation of acid by-products, whose presence may be detrimental for further applications; (iii) problematic disposal of the salts formed during the neutralization step; and (iv) corrosion problems to the reaction plant (GUIDOTTI; PALUMBO, 2016).

To minimize the drawback of using strong mineral acids such as concentrated sulphur acid as catalysts in conventional epoxidation method, it was suggested by Gurbanov and Mamedov (2009) to employ the ion-exchange resin as the catalyst in synthesizing peroxy acids, followed by epoxidation the unsaturated vegetable oil with the *in situ* formed peroxy acids (TAN; CHOW, 2010). In this process, the peroxy acid is obtained by reaction of H₂O₂ with carboxylic acid (HCOOH/CH₃COOH). The peroxy acid interacts with the catalyst by way of entering the pores of the catalyst. Thus when AIER is loaded into the reactor its pores get filled with peroxy acid (CAMPANELLA; BALTANÁS, 2004).

Therefore, with the objective to improve the efficiency and the degree of epoxidation of the process, new methods have been studied, such as metal-catalyzed epoxidation using high-valence catalysts. In this process, the peracid oxidant is obtained *in situ* when a carboxylic acid (usually acetic acid) reacts with hydrogen peroxide in the presence of mineral acids that act as catalysts, which can be titanium, molybdenum or tungsten (TAN; CHOW, 2010; SAURABH et al., 2011; CINDRIĆ et al., 2017; GUNAM RESUL et al., 2018). However, these procedures still have shortcomings, the requirement of preformed catalysts, the use of halogenated solvents, and the relevant formation of by-products (GUIDOTTI; PALUMBO, 2016).

In this way, the search for an alternative environmentally friendly epoxidation process has prominence in the industrial and academic scenario and the use of non-toxic biocatalysts, such as immobilized enzymes, has become an advantageous option. Enzymatic epoxidation methods have the advantage of high selectivity, as they do not lead to any undesired ring-openings of the epoxides. Even more, this technique has stronger points than using inorganic catalysts, including the following: mild reaction conditions, i.e., neutral pH of the reaction mixture; formation of stable hydroperoxides, i.e., no need for acetic or formic acid addition; high regio- and stereoselectivity; significant suppression of side reactions, and high conversion. These methods are particularly suitable for the epoxidation of oleochemicals since both carboxyl group and C=C unsaturation are in the same reactant molecule (VLČEK; PETROVIĆ, 2006; GUIDOTTI; PALUMBO, 2016).

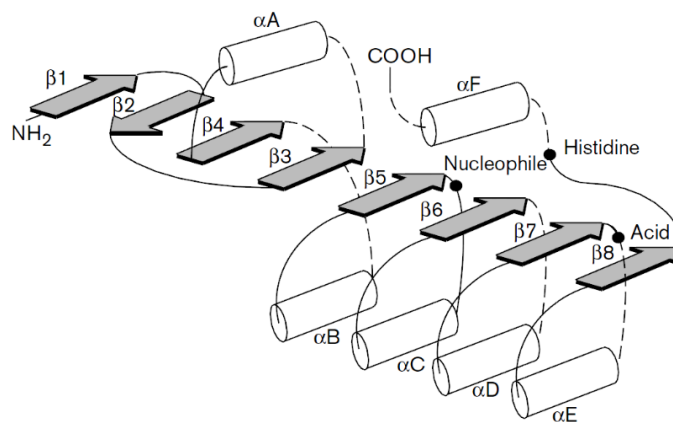
There are several enzymes that catalyze epoxidations (LIN et al., 2016). They belong to the oxydoreductase (EC 1.x.x.x) or hydrolase (EC 3.x.x.x) enzyme classes. Chloroperoxidase is a member of the haloperoxidases family and catalyzes the stereoselective epoxidation of alkenes with good yields (ALLAIN et al., 1993; HU; HAGER, 1999; PIANTINI et al., 2011). Monooxygenases, such as cytochrome P-450, catalyze the insertion of an oxygen atom from O₂ into an organic substrate in many metabolic pathways depending on the substrate structures.

The main drawback with these enzymes is that they are dependent on a cofactor and require NADPH recycling, which in preparative chemistry can be achieved by the use of microbial cells (MCCLAY; FOX; STEFFAN, 2000; KUBO et al., 2006; LIN et al., 2016). Other examples, as lipoxygenases, peroxygenases, perhydrolases also have been used (TIRAN et al., 2012). Lipases have been used for the indirect epoxidation of alkenes with hydrogen peroxide through the formation of peroxy acids (SVEDENDAHL et al., 2008) and it will be further discussed in the next topic.

2.2.1 Epoxidation mediated by lipases

Lipases (triacylglycerol hydrolases, EC 3.1.1.3) are the best candidates to catalyze reactions based on organic media, once they are highly regio- and enantio-selective, versatile, highly stable, and low commercial cost, and able to catalyze innumerable organic syntheses (BJÖRKLING et al., 1992; LEMOULT; RICHARDSON; ROBERTS, 1995; PETKAR et al., 2006). They are α/β hydrolases (Figure 5), which have a molecular weight of around 40 to 50 kDa, with about 300 amino acid residues. In living organisms, they are the enzymes responsible for the hydrolysis of acylglycerides (HAUSMANN; JAEGER, 2010). A large number of lipases have interfacial activation and catalytic activity only when they encounter an aqueous-organic phase interface. The phenomenon is explained by the "lid opening" when a helical oligo-peptide unit shielding the enzyme active site (generally a "catalytic triad" of the amino acids - serine, histidine, and aspartate) moves to expose the active site on interaction with a hydrophobic interface (REETZ, 2002; SECUNDO et al., 2006; HAUSMANN; JAEGER, 2010). This way, this hydrophobic region may be adsorbed and stabilized to any hydrophobic surface, such as oils (named interfacial activation), hydrophobic proteins, and another open form of lipase or even hydrophobic supports (MANOEL et al., 2015; ARANA-PEÑA; LOKHA; FERNÁNDEZ-LAFUENTE, 2018; RIOS et al., 2018).

Figure 5 – Secondary structure diagram of the ‘canonical’ α/β hydrolase fold. The location of the catalytic triad is indicated by black dots. Dashed lines indicate the location of possible insertions. α Helices and β strands are represented by white cylinders and gray arrows, respectively.



Source: Nardini and Dijkstra (1999)

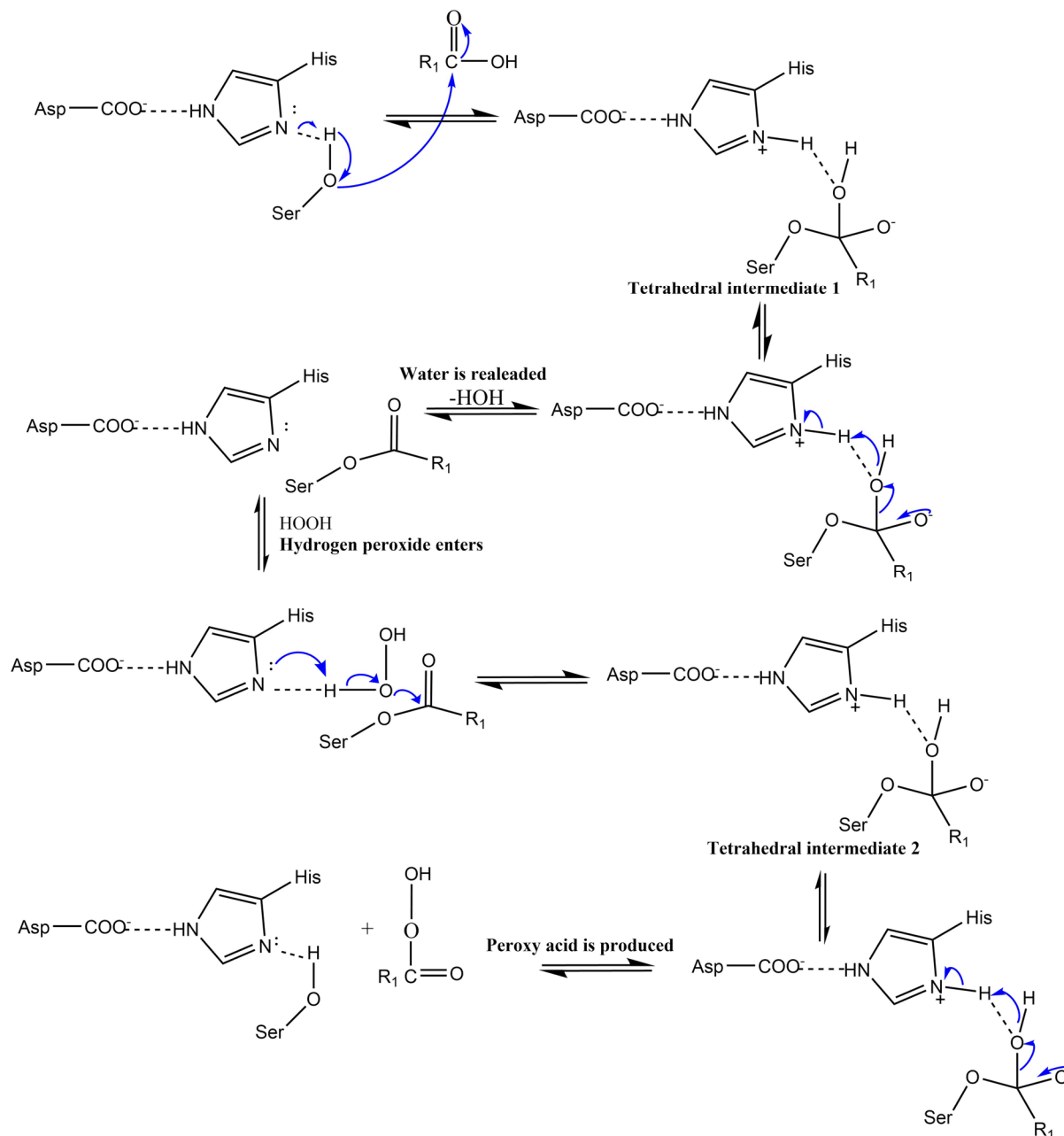
Lipases produced by different strains of genus *Candida* sp. are among the most widely used enzymes for biocatalytic purposes, especially *Candida antarctica* lipase B (CAL-B), for which an enormous number of different applications have been reported (DOMÍNGUEZ DE MARÍA et al., 2005), among them, epoxidation reactions.

The lipase-mediated epoxidation reactions occur via the formation of an acyl-enzyme intermediate between the carbonyl carbon of the carboxylic acid and serine residue at position 105, Ser105. Next, a hydrogen bond is formed between a carbonyl carbon atom of the enzyme and the hydrogen peroxide, in which the attack is facilitated by this bond (Figure 6). Then, the carboxylic peracid generated leaves the active site of the enzyme, it ready to attack the unsaturated bonds along with the fatty acid (SVEDENDAHL et al., 2008).

Nowadays, lipase properties can be improved by using different tools. Microbiology, by means of metagenomics, has made a huge number of new enzymes available, some of them of unknown origin, but with new and interesting features. The genetic tools, such as mutagenesis and directed evolution, have improved the enzyme properties for specific problems (stability or activity in a particular medium, activity versus a substrate) (FACIN et al., 2019). Thus, old techniques, such as chemical modification or immobilization, have lost relevance in the preparation of an industrial biocatalyst (RUEDA et al., 2016). Thus, even though these enzymes may be used in the free form, the possibility of lipase immobilization emerges as an alternative to overcome some misfortunes in the lipase-catalyzed reaction, such as limited solubility and thermal, mechanical, and operational stability of the enzyme, as well as the

impossibility of catalyst reuse, leading to high production costs hindering large-scale applications (BORNSCHEUER, 2003; MOHAMAD et al., 2015).

Figure 6 – Mechanism of lipase-catalyzed perhydrolysis reaction.

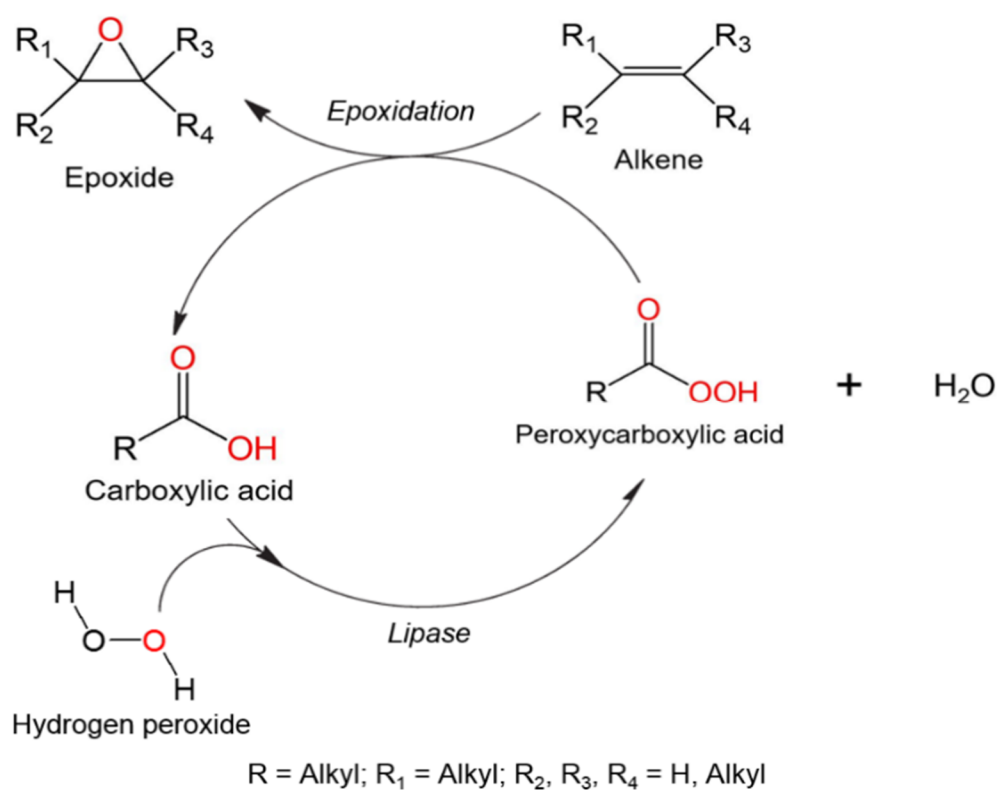


Source: Abdulmalek et al. (2014)

Immobilized enzymes on supports, especially in low-cost supports, can offer some advantages such as increased activity, specificity, and selectivity; improved structural stability; and easy recovery (DATTA; CHRISTENA; RAJARAM, 2013; MERYAM SARDAR, 2015; XIE; ZANG, 2018; FACIN et al., 2019). Many biotechnological applications have been

successfully established using immobilized lipases for the epoxidation of vegetable oils and alkenes (Table 4). Among these, the first work started with Björkling, Godfredsen, and Kirk (1990). They used *Candida antarctica* lipase B (CAL-B) in the presence of an organic solvent, carboxylic acid, and aqueous hydrogen peroxide (H_2O_2) to form peroxy-carboxylic acid, which epoxidized alkenes (Figure 7). Pure products were obtained in yields greater than 90% after 24 h of the experiment.

Figure 7 – Epoxidation of alkenes by lipase-catalyzed perhydrolysis of carboxylic acids.



Source: Melchioris et al. (2019)

Table 4 – Literature review of the epoxidation of vegetable oils and alkenes using immobilized lipases.

Educt	Lipase derived from	Best condition	Conv¹. (%)	Reference
Cyclohexene 3-Ethylpent-2-ene Tetramethyl-ethylene	<i>Candida antarctica</i> <i>Mucor miehei</i> <i>Humicola</i> sp. <i>Candida cylindracea</i> <i>Pseudomonas</i> sp.	Enzyme 175 mg; Alkene: 15 mmol; OC ² : 1.7 μmol; RT ³ ; Time 24 h.	>90	(BJÖRKLING; GODTFREDSSEN; KIRK, 1990)
Cyclic alkenes	<i>Candida antarctica</i> <i>Humicola</i> sp. <i>Pseudomonas</i> sp. <i>Candida cylindracea</i>	Enzyme 4,86 g; Alkene: 586 mmol; TA ⁴ : 59.2 mmol; H ₂ O ₂ ⁵ : 896 mmol; RT ³ ; Time 24 h.	98	(BJÖRKLING et al., 1992)
Rapeseed oil Sunflower oil Soybean oil Linseed oil	<i>Candida antarctica</i>	Enzyme 0.05 mol; MR ⁶ H ₂ O ₂ :C=C bonds 1.5:1 RT ³ ; Time 16 h.	>90	(RÜSCH GEN. KLAAS; WARWEL, 1999)
α-pinene	<i>Candida antarctica</i>	Enzyme 120 mg; Terpene: 10 mmol; OC ² : 5 mmol; H ₂ O ₂ ⁵ : 60 mmol Temperature 50 °C; Time 2.5 h.	>45	(SKOURIDOU; STAMATIS; KOLISIS, 2003b)
(+)-terpinen-4-ol cis-verbenol terpineol R-(+)-limonene α-pinene	<i>Candida antarctica</i> <i>Candida rugosa</i> <i>Mucor miehei</i> , among others.	Enzyme 50 mg; Terpene: 0.5 mmol; H ₂ O ₂ ⁵ : 10 mmol; OC ² : 10 mmol Temperature 30 °C; Time 24 h.	>99 ⁸	(MOREIRA, 2008)
Soybean Oil	<i>Candida antarctica</i>	Enzyme 4 wt%; Oil: 8 wt%; MR ⁶ H ₂ O ₂ :C=C bonds 1:1 Temperature 50 °C; Time 4 h.	>80	(VLČEK; PETROVIĆ, 2006)
(+)-3-carene	<i>Candida antarctica</i>	Enzyme 50 mg; Terpene: 5 mmol; OC ² : 10 mmol; H ₂ O ₂ : 10 mmol; RT ³ ; Time 1.5 h.	>99	(MOREIRA; NASCIMENTO, 2007)

Sunflower oil methyl esters	<i>Candida antarctica</i>	Enzyme 100 mg; Oil: 1 g; H ₂ O ₂ ⁵ : 1 mL; OC ² : 10 mmol Temperature 30 °C; Time 16 h.	>99	(SCHNEIDER et al., 2009)
α-pinene R-(+)-limonene	<i>Candida antarctica</i>	Enzyme 50 mg; Terpene: 1 mmol; H ₂ O ₂ ⁵ : 1.1 mmol; RT ³ ; Time 24 h.	79 ⁷	(TZIALLA et al., 2009)
R-(+)-limonene	<i>Candida antarctica</i>	Enzyme 1 g; Terpene: 25 mM; H ₂ O ₂ ⁵ : 50 mM; OC ² : 50 mM Temperature 40 °C; Time 24 h.	>98	(WIEMANN; FALTL; SIEBER, 2012)
Citronellol	<i>Candida antarctica</i> <i>Rhizomucor miehei</i> <i>Mucor miehei</i>	Terpene: 2 mmol; H ₂ O ₂ ⁵ : 5 mmol; OC ² : 2 mmol; Temperature 25 °C; Time 24 h.	>99	(DA SILVA; NASCIMENTO, 2012)
Jatropha Curcas Oil	<i>Candida antarctica</i>	Enzyme 7 wt%; MR ⁶ H ₂ O ₂ :C=C bonds 3.5:1 Lauric Acid: 23 % Temperature 50 °C; Time 7.5 h.	>93	(RAFIEE-MOGHADDAM et al., 2014)
R-(+)-limonene α-pinene 3-carene	⁹ <i>Candida antarctica/ Palladium</i>	Enzyme 50 mg; Terpene: 0.5 mmol; Temperature: 25–30 °C; Time 16 h.	>76	(RANGANATHAN et al., 2015)
Karanja oil	<i>Candida antarctica</i>	Enzyme 5 wt%; Oil: 10 g; MR ⁶ H ₂ O ₂ :C=C bonds 1.25:1; Temperature 30 °C; 400 rpm; Time 9 h.	>80	(BAJWA et al., 2016)
R-(+)-limonene α-pinene 3-carene	<i>Candida antarctica</i>	Enzyme 60 mg; Terpene: 100 mM; H ₂ O ₂ ⁵ : 500 mM; OC ² : 70 mM Temperature 40 °C; Time 6 h.	>62	(RANGANATHAN et al., 2016)

R-(+)-limonene α-pinene 3-carene	<i>Candida antarctica</i>	Enzyme 100 mg; Terpene: 10 mmol; H ₂ O ₂ ⁵ : 12.5 mmol; OC ² : 2.5 mmol; Solvent-free; Temperature 60 °C; Time 8 h.	>82	(RANGANATHAN; ZEITLHOFFER; SIEBER, 2017)
R-(+)-limonene	<i>Candida antarctica</i>	Immobilized enzyme: 1000 mg; Limonene: 25 mM; H ₂ O ₂ ⁵ : 50 mM; OC ² : 50 mM; Solvent: Toluene; Temperature 50 °C; Time 2 h.	>75	(SALVI; YADAV, 2020)

¹ Conv – Conversion² OC – Octanoic acid³ RT – Room temperature⁴ TA – Tetradecanoic acid⁵ H₂O₂ – Hydrogen peroxide⁶ MR – Molar ratio⁷ Yields of α -pinene, not reported to limonene⁸ Conversion of R-limonene⁹ Combination of hydrogen peroxide production with lipase mediated epoxidation

As may be seen in Table 4, the applicability of chemo-enzymatic epoxidation using lipase has been demonstrated with different substrates, such as several fatty acids, fatty acid esters including vegetable oils, and other olefins. In which, the most utilized and the most efficient biocatalyst was found to be the immobilized lipase B from *Candida antarctica*. This suggests that this lipase is more resistant to the toxic media formed by the hydrogen peroxide and organic solvent. Specifically, the lipase-mediated epoxidation of the R-(+)-limonene has shown promising results in the last years, employing immobilized CalB in organo-modified supports (TZIALLA et al., 2009), immobilized CalB in polyacrylic supports with different bindings (non-ionic adsorption, cationic adsorption, and covalent) (WIEMANN; FALTL; SIEBER, 2012), and Novozym 435 (industrial immobilized CalB) (MOREIRA, 2008; RANGANATHAN et al., 2016). All works emphasized the search for efficient, low-cost, and durable catalysts. Further, the enzyme cost is among the important factors determining the economics of the process. High enzyme stability, the possibility to recycle the enzyme, and the low cost of the immobilized enzyme are therefore highly desirable for the economics of the process.

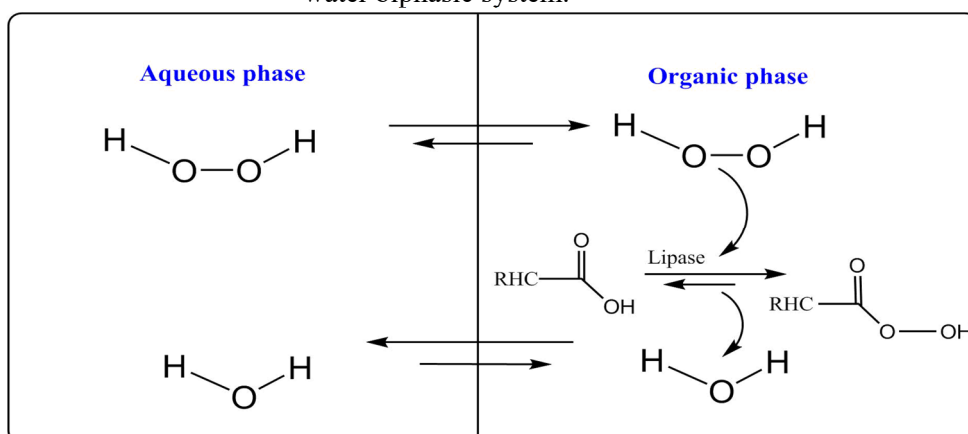
Chemo-enzymatic epoxidation is influenced by various reaction parameters, such as enzyme amount, oxidant concentration, acyl donor concentration, terpene concentration, temperature, and reaction time (RANGANATHAN, 2018).

The enzyme amount needs to be carefully chosen to maximize product formation without significantly deactivating them. Several studies have reported that an increase in the amount of biocatalyst increased the epoxidation rate (SKOURIDOU; STAMATIS; KOLISIS, 2003a; ORELLANA-COCA et al., 2005; MOREIRA, 2008; RANGANATHAN et al., 2016). However, this process reaches the point where all substrates are bound to the enzyme and an increase the catalyst concentration may cause a decrease in yield due to substrate limitations (CAUSSETTE; MARTY; COMBES, 1997; ROBINSON, 2015). This is similar to what was reported by Ankudey, Olivo, and Peeples (2006); Bhattacharya (2011); Sun et al. (2011); Ranganathan, Zeitlhofer, and Sieber (2017) that an excess of enzyme did not lead to an increase in conversion and sometimes it even led to a decrease of the product yield in the epoxidation reactions.

The concentration of the oxidizing agent, such as hydrogen peroxide, has been shown to be the most critical parameter influencing reaction rate and epoxidation (AOUF et al., 2014). Hydrogen peroxide is an important reagent for the formation of peracids from carboxylic acids (ORELLANA-COCA et al., 2005). In addition, a low concentration of hydrogen peroxide

(<30%) is already a highly attractive oxidant as it is an easy to handle and low cost, mild and environmentally benign reagent with high active oxygen content, providing only water as a by-product (ARAMENDÍA et al., 2001; LEI et al., 2006). Björkling, Godtfredsen, and Kirk (1990) and Björkling et al. (1992) reported that exposure of the enzyme to high concentrations of this oxidizing agent resulted in a degree of lipase deactivation. Therefore, a fed-batch process addition of hydrogen peroxide to the reaction medium has been shown to increase the yields of peroxycarboxylic acids (ORELLANA-COCA et al., 2005; ANKUDEY; OLIVO; PEEPLES, 2006). Two distinct phases are formed when aqueous hydrogen peroxide is added to the reaction medium (Figure 8). The immobilized enzyme on hydrophobic support is mainly located in the organic phase, while the H_2O_2 partitions in both phases (aqueous and organic), being at a higher concentration in the aqueous phase (ORELLANA-COCA et al., 2005).

Figure 8 – Schematic presentation of the mass transport of hydrogen peroxide and water in an organic-water biphasic system.

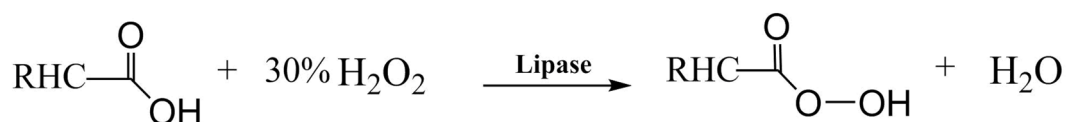


Source: Adapted from Orellana-Coca et al. (2005)

The literature describes that the oxidizing agent, such as hydrogen peroxide, reacts with the acyl-enzyme complex, formed by the fatty acid and the hydroxyl group of the amino acid serine at the active site, to produce the corresponding percarboxylic acid (Figure 9) (BJÖRKLING; GODTFREDSSEN; KIRK, 1990; FABER, 2011; MILCHERT; MALARCZYK; KŁOS, 2015). Then, the peroxy acid formed is responsible for the epoxidation of the unsaturated bonds. In this fashion, epoxidation of vegetable oils can be carried out using carboxylic acids in catalytic amounts (BJÖRKLING; GODTFREDSSEN; KIRK, 1990). Therefore, the primary factor affecting the affinity between acid and enzyme is the chain length of the fatty acids (DA SILVA; NASCIMENTO, 2012). The most tested fatty acids in this reaction are of medium and long-chain (C_6 – C_{16}), such as hexanoic acid, octanoic acid, decanoic

acid, and hexadecanoic acid (BJÖRKLING; GODTFREDSSEN; KIRK, 1990; MOREIRA; NASCIMENTO, 2007; DA SILVA; NASCIMENTO, 2012). However, it is well documented that the addition of octanoic acid in chemo-enzymatic reactions results in a higher yield of products of interest and is readily soluble in preferred solvents for such reactions, such as toluene (ALVES MOREIRA; BERGLER BITENCOURT; DA GRAÇA NASCIMENTO, 2005; FABER, 2011; DA SILVA; NASCIMENTO, 2012). In addition, peracid reactivity and concentration may also be responsible for lipase denaturation, so the acyl concentration needs to be carefully chosen and investigated (YADAV; DEVI, 2002).

Figure 9 – The reaction of carboxylic acids esters with hydrogen peroxide.



Source: Milchert, Malarczyk and Kłós (2015)

Temperature is also one of the main parameters that influence the reaction rate and conversion. As changes in temperature can have an important influence on substrate solubility and enzyme catalytic properties (AOUF et al., 2014) since higher temperatures promote collisions between enzyme and substrate molecules resulting in accelerated rates of the reaction (PHILLIPS, 1996). Then, the reaction temperature needs to be high enough to attain sufficient reaction rates and to prevent substrate solidification, but should not compromise enzyme stability and lead to high energy costs (BHATTACHARYA, 2011). Hence, previous works have already established the temperature range between 40 and 60 °C as the ideal for performing lipase based epoxidation reactions (BJÖRKLING et al., 1992; RANGANATHAN et al., 2015, 2016). In addition, temperatures above 60 °C promote unselective hydrogenation of substrates (RANGANATHAN et al., 2015). Corroborating with Table 4, this shows that the reactions were performed at different temperatures, ranging from 25 °C to 60 °C.

Based on the reports in the literature, there is much information around the synthesis of epoxides, and it was possible to note that the rate of epoxidation increases with increasing process temperature, and with a certain range of initial hydrogen peroxide concentrations (10–50 wt%) and amount of lipase. Other important parameters are also described, such as the amount of solvent (usually toluene), the molar ratio of hydrogen peroxide to unsaturated bonds, type of oil or unsaturated acid. In this way, the chemo-enzymatic epoxidation exhibits the

highest selectivity among the mentioned epoxidation methods and it is highly stereoselective. In addition, in the chemo-enzymatic epoxidation process of vegetable oils, the highest efficiency and reaction rates were achieved at moderate temperatures (25 °C to 60 °C), in biphasic systems, and the catalyst amount range of 5 - 20 %wt.

However, the search for new systems, more efficient and economical, has been gaining space in industry and academia, which makes interesting and viable the investigation of the synthesis of 1,2-limonene oxide for applications in polymerization processes, for example.

2.3 LIMONENE OXIDE POLYMERIZATION

The use of natural products or renewable monomers for the synthesis of new materials has clearly become an important topic in polymer science. Then, the developments of systems that meet the demand for green chemistry with more efficient and diverse catalytic reactions deserve attention. From this perspective, the ring-opening polymerizations of epoxides natural oils have been investigated in different previous studies, and mainly using Lewis acids as a catalyst (ANDJELKOVIC et al., 2005; LI et al., 2005; SILVESTRE; GANDINI, 2008; KUKHTA; VASILENKO; KOSTJUK, 2011).

Polymerization via coordination ring-opening of epoxides has been intensively studied since the late 1950s, and various coordinative catalysts mainly based on aluminum and zinc alkyls have been developed (BOOTH; HIGGINSON; POWELL, 1964; VANDENBERG, 1969; CRIVELLO et al., 1996; DEL RIO et al., 2010; TROTT; GARDEN; WILLIAMS, 2019). In this context, limonene oxide is an interesting monomer, and it can be considered a green alternative to cyclohexene oxide (TAHERIMEHR; PESCARMONA, 2014), which was polymerized via radiation-induced cationic polymerization, reported by Aikins and Williams (1985), one of the pioneers in this process.

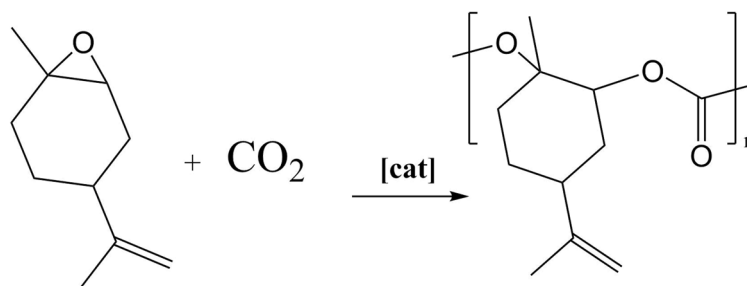
However, other polymers are interesting, for example, the insertion of other monomers, such as carbon dioxide or cyclic anhydrides, into the polymerization process together with limonene oxide, providing attractive materials for various applications. In addition, the use of two distinct monomer sets allows for facile tuning of properties and post-polymerization modification (HAUENSTEIN; AGARWAL; GREINER, 2016; BRANNIGAN; DOVE, 2017). In this context, polyesters are the most widely used biodegradable synthetic polymeric biomaterials (MIAO et al., 2014). In the same way, aliphatic polyester is an important class of these polymers, responsible for various applications such as drug delivery

systems, artificial tissues, and common materials. All of this is possible due to its biocompatibility and biodegradability characteristics (NISHIDA; TOKIWA, 1993; OKADA, 2002; JESKE; DICICCIO; COATES, 2007; BRANNIGAN; DOVE, 2017). Then, polyesters can be synthesized by polycondensation, by self-polycondensation, or by ring-opening polymerization (OKADA, 2002).

Aliphatic polyesters from AB-type monomers are commonly produced by chain-growth ring-opening polymerization (LONGO; SANFORD; COATES, 2016) and a variety of initiators and catalysts have been employed, such as organo-catalysts, metal alkoxides, and various metal complexes (ALBERTSSON; VARMA, 2003).

In that case, the copolymerization with CO₂ using low-cost Zn, Al or Fe homogeneous catalysts to yield polycarbonate structures (Figure 10) (BYRNE et al., 2004; AURIEMMA et al., 2015a, 2015b; PEÑA CARRODEGUAS et al., 2015; HAUENSTEIN et al., 2016; PARRINO et al., 2018) has led to promising results, opening the door for future investigations applicable to a wide class of polymers. The polymerizations allowed reaching 40 – 90% conversion after 2 to 48 hours, molecular weights (M_n) of up to 10.000 g mol⁻¹ were achieved and with a temperature of the polymerization reaction between 25 and 80 °C.

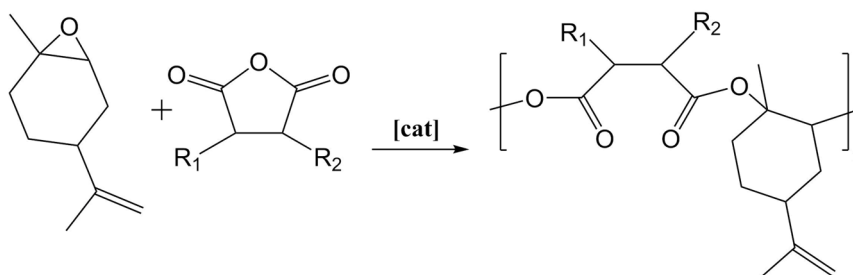
Figure 10 – Copolymerization of limonene oxide and CO₂.



Source: Poland and Darensbourg (2017)

In this same context, other researches have catalytically coupled limonene oxide with different cyclic anhydrides (Figure 11), such as maleic anhydride or phthalic anhydride, to produce polyesters with molecular weights (M_n) from 4000 g mol⁻¹ to 36000 g mol⁻¹, using as active catalysts the (β -diiminate)Zn-alkoxide complexes for the ring-opening (JESKE; DICICCIO; COATES, 2007).

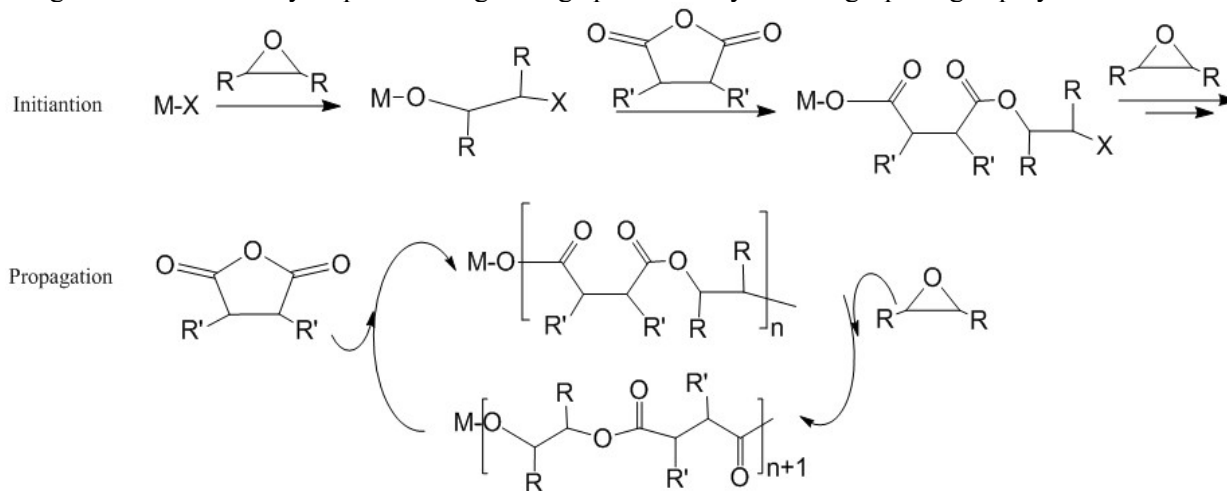
Figure 11 – Copolymerization of limonene cyclic and anhydride oxides.



Source: POLAND; DARENSBOURG (2017)

In addition, Figure 12 illustrates the generic elementary reactions which are proposed to occur during epoxide–anhydride ring-opening copolymerizations, helping to understand each step of the process. These polymerizations require the application of an initiator/catalyst. This species is often a single site metal complex of the form L-M-X, formed for an “L” that is an ancillary ligand, an “M” is the metal site at which catalysis occurs, and an “X” that is the initiating group and site at which propagation proceeds. Polymerization is terminated often by temperature reduction, monomer removal, by the addition of water or acids (PAUL et al., 2015).

Figure 12 – Elementary steps occurring during epoxide–anhydride ring-opening copolymerizations.



Source: PAUL et al. (2015)

Performing a literature search about copolymerization involving such monomers, Table 5, summarizes the works related to the synthesis of these polyesters in the last decades. As may be seen, there are few studies available in the literature on the copolymerization of limonene oxide and cyclic anhydrides.

Table 5 – Literature review of the copolymerization of limonene oxide and cyclic anhydrides.

Monomers	Catalyst	Best condition	Best results	Reference
Limonene oxide and maleic anhydride	zinc 2-cyano- β -diketiminatate complex	Catalyst: 1 mol%; Time: 24 h; Solvent: Toluene; Temperature: 60 °C;	M_n : 12000 g mol ⁻¹ ; PDI: 1.1; T_g : 62 °C; LO conv. ³ : 55 %;	(JESKE; DICICCIO; COATES, 2007)
Limonene oxide and diglycolic Anhydride	zinc 2-cyano- β -diketiminatate complex	Catalyst: 0.33 mol%; Time: 16 h; Solvent: Toluene; Temperature: 70 °C;	M_n : 36000 g mol ⁻¹ ; PDI: 1.2; T_g : 51 °C; LO conv. ³ : 81 %;	(JESKE; DICICCIO; COATES, 2007)
Limonene oxide and camphoric anhydride	Metal complexes based on the tetradentate salen	MR ¹ Catalyst: Monomer 1:100; Time: 9 h; Cocatalysts: ² PPN ⁺ Cl ⁻ Solvent: Toluene; Temperature: 100 °C;	M_n : 8100 g mol ⁻¹ ; PDI: 1.3; LO conv. ³ : 100 %;	(ROBERT; DE MONTIGNY; THOMAS, 2011)
Limonene oxide and phthalic anhydride	Metal t-Bu- salophen complexes	MR ¹ Catalyst: Monomer 1:250; Time: 3 h; Bulk; Cocatalysts: ² PPN ⁺ Cl ⁻ Temperature: 130 °C;	M_n : 9700 g mol ⁻¹ ; PDI: 1.4; LO conv. ³ : 94 %;	(NEJAD et al., 2013)
Limonene oxide and phthalic anhydride	Bimetallic aluminum complex	MR ¹ Catalyst: Monomer 1:250; Time: 2 h; Solvent: Toluene; Temperature: 130 °C;	M_n : 4360 g mol ⁻¹ ; PDI: 1.15; T_g : 88.3 °C; LO conv. ³ : 91 %;	(ISNARD et al., 2017)
Limonene oxide and phthalic anhydride	Phenoxy-based aluminum complexes	MR ¹ Catalyst: Monomer 1:125; Time: 8 h; Cocatalysts: ³ DMAP Solvent: Toluene; Temperature: 110 °C;	M_n : 2750 g mol ⁻¹ ; PDI: 1.07; T_g : 35.6 °C; PA conv. ⁵ : 89 %;	(ISNARD et al., 2019)
Limonene oxide and phthalic anhydride	Chromium complex	Catalyst: 0.005 mmol Epoxide: 8 mmol Time: 24 h; Solvent: Toluene; Temperature: 130 °C;	M_n : 2780 g mol ⁻¹ ; PDI: 1.17; T_g : 91 °C; LO conv. ³ : 98 %;	(RYU et al., 2020)

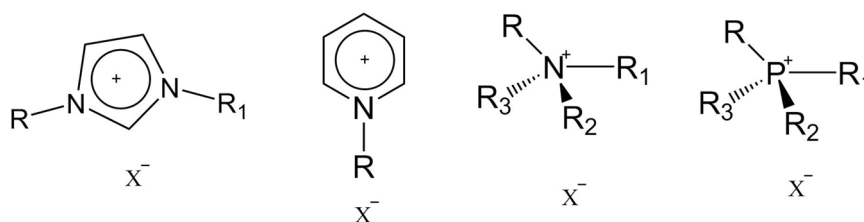
¹MR – Molar ratio²Bis(triphenylphosphoranylidene)ammonium chloride³LO conv. – Conversion of limonene oxide⁴DMAP – 4 - (N,N dimethylamino)pyridin⁵PA conv. – Conversion of phthalic anhydride

These reports showed the synthesis of polyesters using monomers from renewable resources, employing several catalysts, such as metal-porphyrinate and metal-salen complexes. The works are important to improve the sustainability of epoxide/anhydride copolymerization. However, it is relevant to note that phthalic anhydride is not currently a commercial product of renewable origin, but research reports that bioderivation is possible from renewable resources (MAHMOUD; WATSON; LOBO, 2014; LIN; IERAPETRITOU; NIKOLAKIS, 2015), confirming its potential application. In fact, these polymerization reactions are attractive but need to be coupled with the insertion of new catalysts and monomers combinations that will further expand the range of renewable polymers that can be synthesized. In addition, due to difficulties in completely removing initiators/catalysts from polyesters, it is essential to look for initiators/catalysts containing metals that are not harmful to human organisms (ALBERTSSON; VARMA, 2003), aiming at applying these polymers in the biomedical area. In this context, the next topic will show the use of an ionic liquid as a catalyst in ring-opening polymerization reactions.

2.3.1 Ionic liquids

Ionic liquids are compounds formed by an ion, where cations are usually derived from organic molecules and anions derived from inorganic molecules (Figure 13) (LIAW et al., 2012). They have thermal stability, wide application temperature range, and low vapor pressure properties, which makes them very useful for green replacements of volatile organic solvents (WELTON, 1999; CLARKE et al., 2018), electrolytic materials for batteries (YE; RICK; HWANG, 2013), nanocomposites (AWAD et al., 2004) and catalysts/initiators in reactions polymerizations (KAHVECI et al., 2008; ALVES et al., 2018). However, most work on ionic liquids in polymerization systems is related to their use as a solvent or as additives in the reaction system (VIJAYARAGHAVAN; MACFARLANE, 2012).

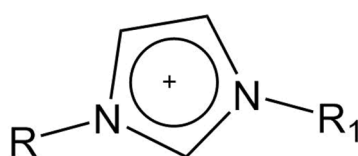
Figure 13 – Composition of typical ionic pairs present in ionic liquids.



Source: RODRIGUES (2013)

In particular, imidazolium-based ionic liquids have unique physicochemical properties, especially those derived from 1,3-dialkylimidazolium cation (Figure 14), due to their liquid state over a wide temperature range, high conductivities, high thermal and chemical stability, and low viscosities, required for a multitude of applications (CHIAPPE et al., 2013).

Figure 14 – Examples of cations derived from 1,3-dialkylimidazolium.



1a R = R₁ = Me

2a R = Me, R₁ = Et

3a R = Me, R₁ = Pr

4a R = Me, R₁ = Bu

Source: Rodrigues (2013)

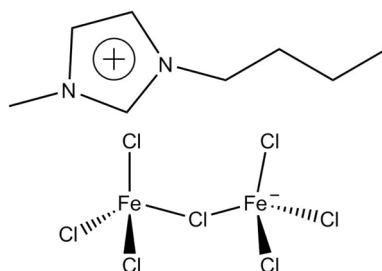
However, functionalized ionic liquids have attracted great interest from scientists and industry, in particular as organo-catalysts, due to their high catalytic potential (ŠEBESTA; KMENTOVÁ; TOMA, 2008; OLIVEIRA et al., 2011). Both the cation and anion of ionic liquids are potential targets for structural and compositional modification, providing unique characteristics (DAVIS, 2002). Thus, the ionic liquids have donor and acceptor patterns, its Lewis acidity can be modulated by the relative amount of the compounds (DA SILVEIRA NETO et al., 2004). A review of the literature on the use of LIs as initiators/catalysts of polymerization reactions have shown that there are just a few works in this field (DING; RADOSZ; SHEN, 2005; LIU et al., 2013; KHOLKHOEV; BURDUKOVSKII; MOGNONOV, 2014; BEREZIANKO; VASILENKO; KOSTJUK, 2018, 2019). The works reported significant improvements in the synthesis of polymers via cationic polymerization using ionic liquids as initiators/catalysts in terms of monomer conversion and polydispersity.

In this context, the study of the synthesis of ionic liquids for applications in polymerization processes has attracted the attention of numerous researchers. Therefore, the utilization of the ionic liquid BMI·Fe₂Cl₇ (Figure 15) as initiator/catalyst in ring-opening polymerization is interesting, because it has Lewis acids incorporated in its structure and iron atoms, which is an environmentally viable metal, being a compound of low cost of production (RODRIGUES, 2013).

Table 6 summarizes the works related to the synthesis of polymers using the ionic liquid BMI·Fe₂Cl₇. Studies with this ionic liquid have been investigated since 2014 by our research group, with the University of Brasilia (UnB) as partners. The works report efficient cationic polymerizations of styrene using different techniques (mass, emulsion, miniemulsion)

(RODRIGUES et al., 2015; ALVES et al., 2018; MIGUEZ, 2018; PATROCINIO et al., 2019); ϵ -caprolactone ring cationic polymerization (LEITE, 2018) and also ϵ -caprolactone polymerization in inverse miniemulsion (SILVA et al., 2019).

Figure 15 – Chemical structure of the catalyst BMI·Fe₂Cl₇



Source: Rodrigues et al. (2015)

Table 6 – Literature review of the polymerizations using the ionic liquid BMI·Fe₂Cl₇

Monomers	Polymer process	Condition	Results	Reference
Styrene	Cationic polymerization in bulk	¹ MR IL ² :Monomer 1:1000; Time: 15 min; Solvent: Toluene Temperature: 70 °C;	M _w : 8672 g mol ⁻¹ ; Conv. ³ : >80%;	(RODRIGUES et al., 2015)
Styrene	Cationic polymerization in miniemulsion	¹ MR IL ² :Monomer 1:1000; Time: 6 h; Temperature: 90 °C;	M _v : 2230 kg mol ⁻¹ ; Conv. ³ : 88%;	(ALVES et al., 2018)
Styrene	Cationic polymerization in emulsion	¹ MR IL ² :Monomer 1:500; Time: 24h; Temperature: 90 °C;	M _w : 1099 kg mol ⁻¹ ; Conv. ³ : 75%;	(PATROCINIO et al., 2019)
Caprolactone	Ring opening polymerization	¹ MR IL ² :Monomer 1:1000; Time: 4h; Temperature: 70 °C;	M _w : ≈ 12 kg mol ⁻¹ ; Conv. ³ : >60%;	(LEITE, 2018)
Caprolactone	Ring opening polymerization in inverse miniemulsion	¹ MR IL ² :Monomer 1:550; Time: 24h; Temperature: 60 °C;	M _w : 1681g mol ⁻¹ ; Conv. ³ : 100%;	(SILVA et al., 2019)
Styrene	Cationic polymerization in miniemulsion	¹ MR IL ² :Monomer 1:1000; Time: 8h; Temperature: 85 °C;	M _w : 1800 kg mol ⁻¹ ; Conv. ³ : 80%;	(AGNER et al., 2020)

¹MR – Molar ratio

²IL – Ionic Liquid

³Conv. – Conversion

As seen, there are few studies available in the literature on polymerization using ionic liquid BMI·Fe₂Cl₇. Moreover, no other works were found on the copolymerization of epoxides,

as limonene oxide, and cyclic anhydrides applying ionic liquids as a catalyst. However, research involving these systems is important since they have been successfully used in polymerization reactions, reducing reaction time, promoting high catalytic activity, being an alternative to conventional catalysts. In addition, to give noble destinations for the synthesized polymers, combined with great versatility, nanoparticles emerge and are best described in the next topic. Furthermore, the surface functionalization of these polyester nanoparticles is relatively straightforward due to the presence of pendant double bonds in the polymer chain.

2.4 PREPARATION OF POLYESTER NANOPARTICLES

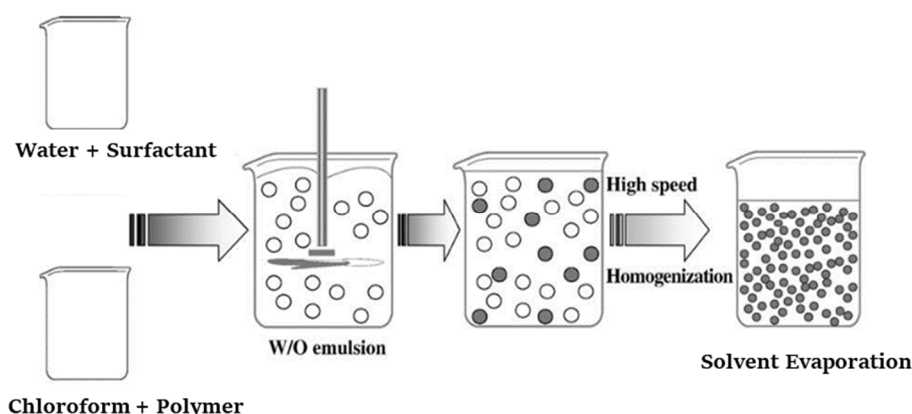
Nano-biotechnology has grown in recent decades and has attracted a lot of attention for numerous applications, mainly due to the growing potential of imaging techniques, drug delivery approaches, sensor technology, and diagnostic purposes. Various confined systems have been used for the formation of nanoparticles with controlled characteristics, such as size, size distribution, and morphology (RALIYA et al., 2016). Among different systems, the use of miniemulsions is often preferred because it allows efficient control of these characteristics (ANTON; BENOIT; SAULNIER, 2008).

Miniemulsions are emulsions with a uniform and extremely small droplet size, typically in the range of 20–200 nm (SOLANS et al., 2005). To prepare a miniemulsion it is necessary to apply mechanical energy to the system by means of high-shear devices; these methods are of the high energy, such as high-pressure homogenizers, or ultrasound generators (LANDFESTER; EISENBLÄTTER; ROTHE, 2004; DELMAS et al., 2011). Emulsion types can be classified into different groups, such as oil-in-water (O/W), water-in-oil (W/O), and multiple emulsions (WANG et al., 2015). In addition, the formation of the nanoparticle may be occasioned either by *in situ* polymerization of a monomer in the miniemulsion droplets or by precipitation of a preformed polymer, for example via the solvent-evaporation method (PINTO REIS et al., 2006). The latter being the focus of this work.

The method of solvent evaporation involves three steps (Figure 16). In the first step, the polymer is dissolved in a volatile organic solvent. Then, the resultant solution is added to the aqueous phase containing surfactant under high-shear stirring to form a miniemulsion. After the formation of stable miniemulsion, the organic solvent is evaporated either by increasing the temperature under reduced pressure or by continuous stirring (PINTO REIS et al., 2006; CHEABURU-YILMAZ; KARASULU; YILMAZ, 2019). Volatile, partly water soluble

solvents such as dichloromethane or chloroform have been widely used (GHADERI; GHANBARZADEH; HAMISHEHKAR, 2015). Our research group has been conducting studies in this area since 2013, works by Leimann et al. (2013), Peres et al. (2017), Mattos dos Santos et al. (2018) and Guindani et al. (2019) showed that nanoparticles were successfully produced using the solvent evaporation technique, confirming the efficient method and well established in the present group.

Figure 16 – Schematic representation of the miniemulsification /solvent evaporation technique



Source: Adapted from Pinto Reis et al. (2006)

Therefore, the main interest in polyester nanoparticles (NPs) preparation, using, for example, the poly (phthalic anhydride-*co*-limonene oxide), allows the functionalization of this polymer via exposed double bonds on the surface of NPs with thiol groups present in protein residues, forming biofunctional materials (DONDONI, 2008; LOWE, 2010; HAUENSTEIN; AGARWAL; GREINER, 2016), resulting in a potentially important material primarily for medical applications. Thiol-ene reactions are a simple and adaptable methodology for preparing functionalized and/or cross-linked polymers using combinations of multifunctional alkenes and thiols (HOYLE; LEE; ROPER, 2004). This reaction can be used to perform post-polymerization modifications, allowing the introduction of several different chemical groups into the polymer chains, forming materials with fascinating characteristics, such as decreasing polymer crystallinity, improving its degradation properties, and even affinity for specific tissue types and modify their mechanical and physicochemical properties (DONDONI, 2008; DARENSBOURG et al., 2014; ZUO; CAO; FENG, 2015; HAUENSTEIN; AGARWAL; GREINER, 2016; MACHADO; SAYER; ARAUJO, 2017; CHIARADIA, 2019). There are no

studies in the literature on poly(phthalic anhydride-limonene oxide) nanoparticles, allowing expanding the use spectrum of polyesters from renewable resources for noble applications.

Nanoparticles can be formulated and optimized depending on the application. To achieve the properties of interest, different preparation techniques are available. These techniques either use previously synthesized polymer or nanoparticles are directly formed during polymerization, such as in emulsion, miniemulsion, microemulsion, interfacial, controlled/living radical polymerization (NAGAVARMA et al., 2012; MUSYANOVYCH; LANDFESTER, 2014).

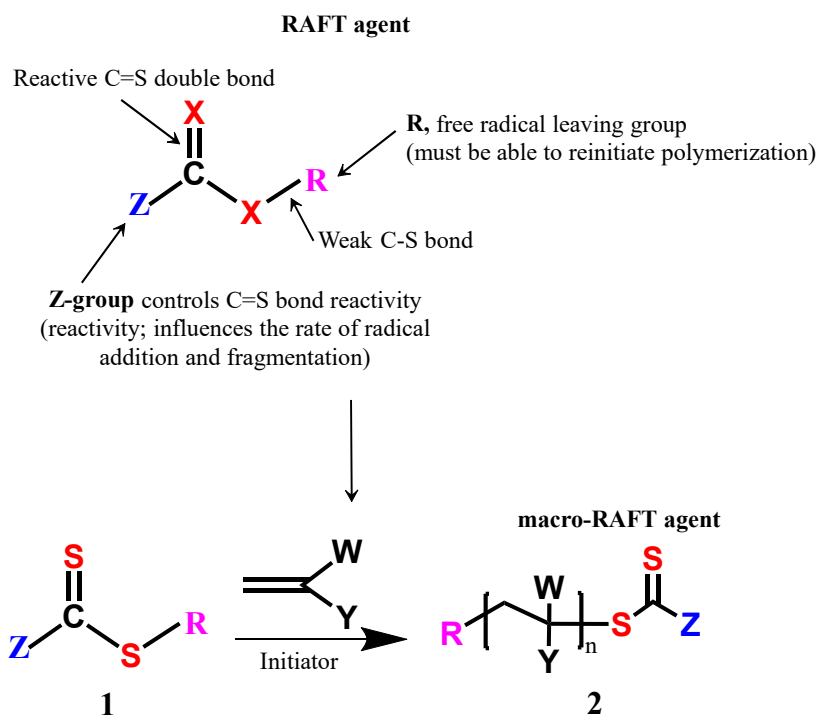
2.5 BLOCK COPOLYMER SYNTHESIS BY RAFT POLYMERIZATION

Reversible Addition-Fragmentation chain Transfer (RAFT) is a controlled radical polymerization method that employs the same monomers, initiator, solvents, and reaction conditions as conventional free radical polymerizations. The difference is the addition of a specific chain transfer agent (CTA), commonly referred to as RAFT agent. Reports of radical addition-fragmentation processes first appeared in the synthetic organic chemistry literature in the early 1970s (DAVIES; PARROTT, 1978; RAMAIAH, 1987), and the first examples of RAFT polymerization, reported in 1995, made use of so-called macromonomer chain transfer agents (macro-CTA) (KRSTINA et al., 1995). The basis of the RAFT mechanism is dependent on the chain transfer steps, which involves a reversible transfer of a functional chain end-group (typically a thiocarbonylthio group, $Z-C(=S)S-R$) between the dormant chains (macro-RAFT agent or macro-CTA) and the propagating radicals. The overall process (Figure 17) is comprised of the insertion of monomers between the R- and $Z-C(=S)S$ -groups of a RAFT agent, which forms the α and ω end-groups of the majority of the resulting polymeric chains (PERRIER, 2017). At the completion of the RAFT polymerization, most of the chains are still living, which means that at the ω -end there is the thiocarbonylthio group. This end-capped homopolymer can be seen as a macro-CTA agent and can be used to re-initiate the polymerization with a second different monomer, thereby achieving complex architectures such as block copolymers (BELLOTTI; SIMONUTTI, 2021).

RAFT polymerization can be performed in homogeneous (e.g. bulk or solution) or in heterogeneous media conducted successfully in emulsion, or dispersion polymerization based on a self-assembly approach (PERRIER, 2017; NOTHLING et al., 2020). This method enables to use of a broad range of different monomers to produce polymers with defined structures,

such as spheres, worms, or vesicles depending on the precise reaction conditions (MOAD; RIZZARDO; THANG, 2005; FIELDING et al., 2013; HORNING et al., 2013; WARREN; ARMES, 2014; SUGIHARA, 2019).

Figure 17 - Representation of the RAFT agents and macro-RAFT formation.

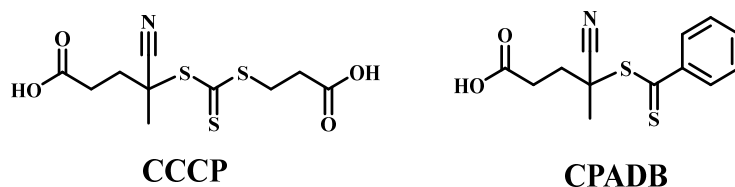


Source: Adapted from Keddie et al. (2012)

2.5.1 RAFT agents

Optimal control in RAFT polymerization requires the selection of an appropriate RAFT agent for the monomer(s) to be polymerized and the reaction conditions. Efficient control of chain transfer and the likelihood of retardation or inhibition is determined by addition and fragmentation rates and the groups Z and R play critical roles in determining the outcome of polymerization (KEDDIE et al., 2012). The most effective reagents for RAFT polymerization are certain thiocarbonylthio compounds, where X is sulfur (Figure 17). Thiocarbonylthio RAFT agents include certain dithioesters, trithiocarbonates, xanthates, dithiocarbamates, and other compounds. Being 4-(((2-carboxyethyl) thio)carbonothioyl)thio)-4-cyanopentanoic acid (CCCP) and 4-Cyanopentanoic acid dithiobenzoate (CPADB) commercially available RAFT agents (Figure 18), that are known to lead to well-controlled polymerizations for methacrylic monomers (MOAD; RIZZARDO; THANG, 2008; XU et al., 2015; DOCHERTY; DERRY; ARMES, 2019; HATTON et al., 2019).

Figure 18 - Structure of commercially available RAFT agents: CCCP and CPADB.



Source: Author

Related to the structure of the RAFT agent, the Z group is responsible to activate and deactivate the thiocarbonyl double bond of the RAFT agent and the R or leaving group, which determines the partition coefficient of the RAFT agent. The radical $R\bullet$ should also be a good homolytic leaving group, relative to the propagating radicals generated, to have good control over polymerization. A key feature of the process is that the thiocarbonylthio groups, present in the initial RAFT agent, are retained in the polymer products (Figure 17). These polymer products are themselves RAFT agents, constituting a dormant form of the corresponding propagating radicals (MOAD; RIZZARDO; THANG, 2011; KEDDIE et al., 2012).

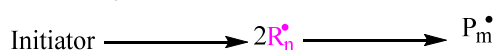
2.5.2 RAFT Polymerization

The accepted mechanism for RAFT polymerization is shown in Figure 19. Initiation is accomplished by a conventional method, as in radical polymerization. Commonly, conventional radical initiators are utilized, such as azobisisobutyronitrile (AIBN) or benzoyl peroxide (BPO), which produce radicals upon thermal decomposition. The step so-called “**initiation**”, the initiator radical adds monomer to form the propagating radical $P_m\bullet$. The next step, in the “**pre-equilibrium**” the radical $P_m\bullet$ makes a reversible attack to the CTA to form an intermediate radical. Which can then fragment the R group from the RAFT agent resulting in $R\bullet$ and a dormant polymer chain. Consequently, the step “**re-initiation**” the new radical $R\bullet$ reinitiates polymerization by reacting with other monomers to form another propagating radical $P_n\bullet$. Thus, the so-called “**main-equilibrium**” is attained when an active radical chain adds to a monomer molecule or other activated chains. In this step, it is possible to get control over molecular weight due the efficient re-initiation between active ($P_m\bullet$ and $P_n\bullet$) and dormant polymer chains ($P_nS(Z)C=S$ and $P_mS(Z)C=S$). In summary, the polymer chains grow in parallel, and the polymer has predictable molecular weight and narrow molecular weight distribution. Finally, the step “**termination**” occurs as in radical polymerization, where radicals react between them and form a polymer or an inactive species (ROWE-KONOPACKI;

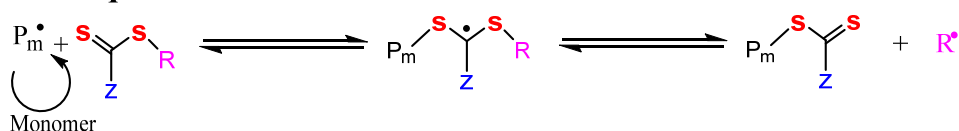
BOYES, 2007; KERN; BOYES, 2014; CAMACHO-CRUZ; VELAZCO-MEDEL; BUCIO, 2020). In addition, the termination reaction could be minimized, due to the existence of thiocarbonylthio end-group in resulting polymeric chains, which also enables participating in RAFT polymerization as RAFT agent, so-called as macro-RAFT agents and other monomers can be polymerized to fabricate multiblock polymers (TIAN et al., 2018).

Figure 19 - Basic reaction steps of the Reversible Addition–Fragmentation Chain Transfer (RAFT) processes: initiation, pre-equilibrium, re-initiation, main-equilibrium, and termination.

Initiation



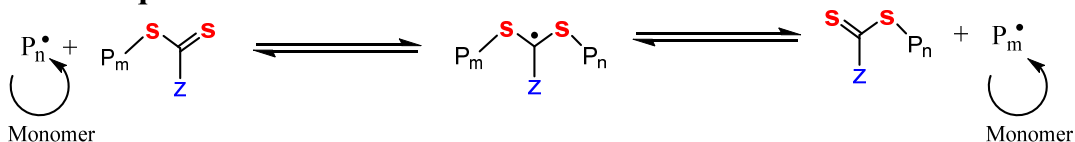
Pre-equilibrium



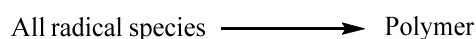
Re-initiation



Main-equilibrium



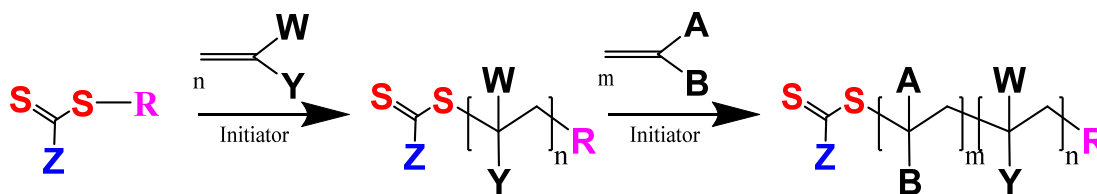
Termination



Source: Adapted from Camacho-Cruz; Velazco-Medel and Bucio (2020)

Block copolymers can be prepared using RAFT polymerization by incorporation of two or more monomers through sequential polymerization processes, with purification before the addition of each monomer. For the synthesis of a simple AB diblock copolymer (Figure 20), the homopolymer formed from an initial RAFT polymerization acts as a macro-RAFT agent for a second polymerization step. This results in the formation of the block copolymer (KEDDIE, 2014).

Figure 20 - Block copolymers by sequential RAFT polymerizations overall RAFT process



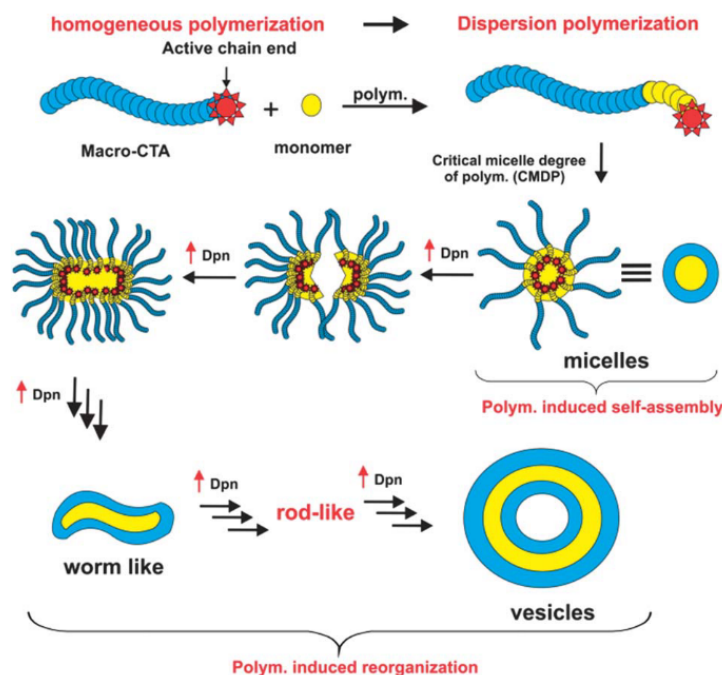
Source: Adapted from Keddie (2014)

RAFT polymerizations can be performed in range of different solvents, including alcohols (JONES et al., 2012; ZHAO et al., 2014), n-alkanes (DERRY; FIELDING; ARMES, 2016), and water (SUGIHARA et al., 2011; BLANAZS; RYAN; ARMES, 2012; CHARLEUX et al., 2012; WARREN; ARMES, 2014; TAN et al., 2015; ZAQUEN et al., 2019a; GUIMARÃES et al., 2021). This body of work focuses on using water as the solvent so only aqueous conditions will be discussed in detail.

2.5.3 RAFT-PISA Polymerization

The development of RAFT polymerization in heterogeneous media has provided new tools to create new macromolecular objects. Polymerization-induced self-assembly (PISA) is probably the best example of this evolution. This method consists in preparing a solvent-swollen polymer corona and a collapsed polymer core and can be self-assembled from different block copolymers in selective solvents. When we connect PISA with RAFT polymerization, the process involves a macromolecular chain transfer agent (macro-CTA) or a macroinitiator is chain-extended with a core forming monomer to form a block copolymer. The molecular weight of the core forming block increases to a certain value, leading to the in situ self-assembly in a selective solvent in which the phase separation occurs. Thus, this polymerization reaction triggers diblock copolymer self-assembly once a sufficiently high degree of polymerization (DP) of the core-forming block is attained (Figure 21) (CORNEL et al., 2021; LUO et al., 2021).

Figure 21 - Evolution of the self-assembly process as polymerization progresses.



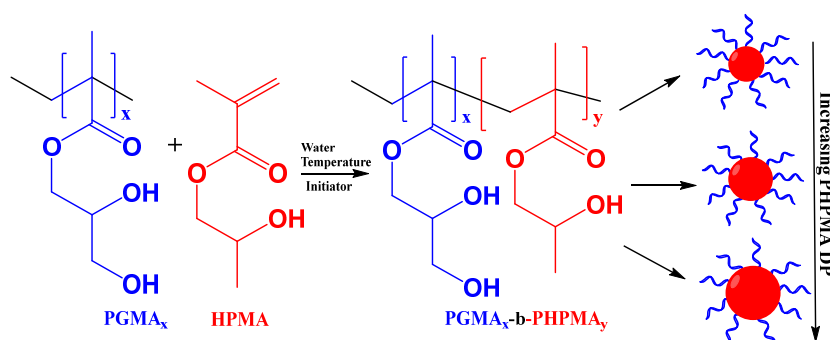
Source: Karagoz et al. (2014)

It is important to emphasize that several polymerization mechanisms in addition to RAFT polymerization, such as ring-opening metathesis polymerization (ROMP) (WRIGHT et al., 2017; VARLAS et al., 2019) and atom transfer radical polymerization (ATRP) (WANG et al., 2017; CAO et al., 2019; SHI et al., 2019) have been introduced into PISA. Although RAFT-mediated PISA has become the most studied PISA method owing to the absence of surfactants, metal catalysts, mild reaction conditions, and tolerance towards various functional groups. The pioneering works involving this system were performed by Ferguson et al. in 2002 and 2005. Since then, a high number of studies have been published using this system, covering the main concepts (BLANAZS; RYAN; ARMES, 2012; ZEHR; RATCLIFFE; ARMES, 2013; KEDDIE, 2014; CANNING; SMITH; ARMES, 2016; PERRIER, 2017), the corresponding formulations for the design of nano-objects (FIELDING et al., 2013; WARREN; ARMES, 2014; TAN et al., 2017; SUGIHARA, 2019; GUIMARÃES et al., 2021) and their applications (KARAGOZ et al., 2014; HATTON et al., 2019). Thermal initiation and photoinitiation are the two most commonly employed initiation methods in RAFT-mediated PISA (CANNING; SMITH; ARMES, 2016; LUO et al., 2021) and will be described in the next section.

RAFT-mediated PISA process has three main routes (1) the synthesis of one block followed by initiation of the second block, (2) the selective post-modification of a preformed diblock copolymer composed of compatible blocks, or (3) a polymer-polymer coupling reaction

(D'AGOSTO; RIEGER; LANSALOT, 2020). A good example of this system is the diblock copolymer poly(glycerol monomethacrylate)-poly(2-hydroxypropyl methacrylate) ($\text{PGMA}_x\text{-b-HPMA}_y$) (Figure 22), which has been extensively studied as a model system (LI; ARMES, 2010; BLANAZS; RYAN; ARMES, 2012; CHAMBON et al., 2012). As the PISA process requires a water-miscible monomer that polymerizes to form a polymer that is soluble in this solvent, there exist limitations to find systems that meet these requirements. Consequently, the $\text{PGMA}_x\text{-b-HPMA}_x$ is a great candidate to understand how each reaction condition influences in the formation of nano-objects (CORNEL et al., 2021).

Figure 22 - Synthesis of sterically stabilized ($\text{PGMA}_x\text{-b-HPMA}_y$) diblock copolymer nanoparticles via PISA utilizing RAFT aqueous dispersion polymerization



Source: Adapted from Li and Armes (2010)

The field of RAFT-PISA has been well-reviewed, and to date, more than 20 reviews have already been published given literature compilation and to provide the reader, both newcomers to the field or experts, with overviews of the topic. Recently, D'agosto, Rieger, and Lansalot (2020) published a review on this subject and discussed the fundamentals of the PISA mechanism, some of the features and limitations, as well as some potential applications. Other reviews were published for guiding the reader to a more in-depth discussion concerning RAFT-PISA (CANNING; SMITH; ARMES, 2016; PENFOLD et al., 2019; MANE, 2020). These reviews provide comprehensive lists of reported RAFT-PISA formulations, perspectives on PISA, highlighting its current potential and recent scientific trends.

2.5.3.1 Thermal RAFT-PISA polymerization

The original and still most widely explored approach to RAFT initiation is through thermally labile radical initiators, such as 2,2'-azobisisobutyronitrile (AIBN), for oil soluble compounds (MOAD, 2019a), and for water soluble compounds other azo-initiators, such as

azobis(4-cyanovaleric acid) (ACVA), half-life time of 10 h at 69 °C (PERRIER, 2017) and 2,2'-Azobis[2-(2-imidazolin-2-yl)propane] dihydrochloride (AIPD), the half-life of 10 h at 44 °C (NAGAO; HOSHINO; MIURA, 2019). The thermal initiator and reaction temperature must be carefully selected to provide an adequate radical flux at the desired polymerization temperature (NOTHLING et al., 2020). The choice of the thermal initiator is important since is a factor to obtain control over RAFT polymerization. High ratios of the RAFT agent to initiator should be employed, to maintain a low radical flux. Further, the choice of the initiator is dependent on its half-life at the desired reaction temperature and its initiation ability relative to the monomer employed. The longer the half-life of the initiator at the desired temperature, the longer is the duration of radical production, and thereby, the RAFT polymerization is kept active for a longer time (MISHRA; KUMAR, 2012).

The key to success for the RAFT process is the source of radicals and influences on (1) polymerization rate, as it is related to radical concentration, (2) control since the number of radicals generated determines the number of dead chains in the system, and (3) reaction conditions, such as temperature, solvent, reaction time, etc. In addition, the RAFT process requires the continuous addition of (re)initiating radicals to compensate for unavoidable termination events and thereby sustain polymer chain growth (SEMSARILAR; ABETZ, 2021).

RAFT is not limited to thermal initiation; recent studies have shown that RAFT can be conducted by photoinduced electron-transfer (PET).

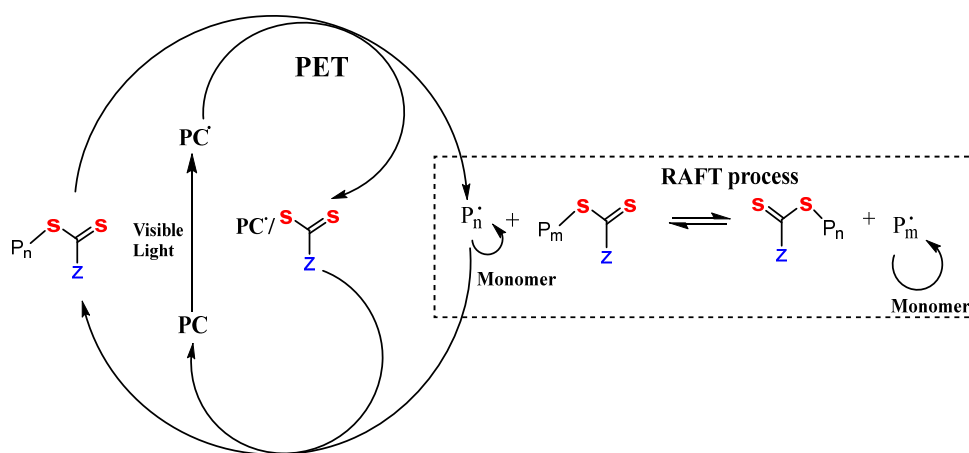
2.5.3.2 Photo RAFT-PISA polymerization

RAFT polymerization can also be undertaken using light as an energy source. This can be achieved for photosensitive RAFT agents, photoinitiators, and photocatalysts. Photocatalysts have been used in photoinduced electron/energy transfer reversible addition-fragmentation chain transfer (PET-RAFT) (SEMSARILAR; ABETZ, 2021).

RAFT mediated by photoinduced electron-transfer (PET) is typically performed at room temperature and employs a photoredox catalyst (PC[•]), activated by visible light. PET-RAFT has been shown to be widely applicable to a variety of catalysts, including metallo-complexes (*fac*-[Ir(ppy)₃], Ru(bpy)₃Cl₂, chlorophyll A, and zinc porphyrins) and organic compounds (e.g., the dye Eosin Y, the photocatalyst 10-phenylphenothiazine, and some tertiary amines) (PERRIER, 2017).

This polymerization method is similar to conventional RAFT, though it is initiated by photochemical means, and in PET-RAFT the thiocarbonylthio-containing chain transfer agent (CTA) acts not only as the transfer agent, but also as the initiating species. Here, the excited state photocatalyst interacts with the CTA to generate the initiating radical (ALLEGREZZA; KONKOLEWICZ, 2021). The accepted mechanism can be seen in Figure 23. Based on the proposed mechanism, radicals can be generated through an energy transfer pathway from the excited state photocatalyst ($PC \rightarrow PC^*$). Under light irradiation, the RAFT agent is reduced to provide radicals, along with the formation of oxidized photoredox catalyst. These radicals initiate the monomer to become a propagating radical and enter the equilibrium of the activation/deactivation chain transfer process. Different from the photodissociation RAFT agent, this PET-RAFT system can minimize the formation of dead chains and restrict the irreversible light degradation reaction by not using the exogenous radical initiators (TIAN et al., 2018).

Figure 23 - Proposed mechanism for PET-RAFT process. Note: PC: photocatalyst; PET: photoinduced electron transfer.



Source: Adapted from Tian et al. (2018)

Boyer's group reported the first RAFT polymerization that was activated by photoinduced electron transfer process by use of tris[2-phenylpyridinato-C₂, N]iridium(III) (Ir(ppy)₃) irradiated under visible light (XU et al., 2014). Many other works have been studied using abundant metals as photocatalysts, such as zinc tetraphenylporphyrin (ZnTPP) (SHANMUGAM; XU; BOYER, 2015; XU et al., 2016). Heterogeneous catalyst systems, where the photocatalytic species is immobilized onto a solid substrate, have also been explored (CHU et al., 2018; ZHU et al., 2020). These systems are interesting since they allow catalyst

reuse and easy purification, important aspects for the scale-up of the process using PET-RAFT (SHANMUGAM et al., 2018).

Phommalsack-Lovan et al. (2018) published an interesting review about the emergence of the PET-RAFT technique, summarized the rapid advances in this area and important publications. Recently, Allegranza and Konkolewicz (2021) approached more deeply this topic in their review with a focus on the mechanism as well as literature compilation since 2014.

As can be seen, the use of this technique is recent and needs to explore since it is a green process that allows easy access to different light sources, minimization of waste, compatibility with other synthetic approaches, broad availability and recyclability of photocatalysts, selectivity, and oxygen tolerance (PHOMMALYSACK-LOVAN et al., 2018).

2.6 FINAL CONSIDERATIONS REGARDING THE STATE OF THE ART

Based on the literature review exposed in this chapter, there is an insufficiency of studies investigating low-cost green alternatives for limonene oxide synthesis via lipase-mediated epoxidation. In this way, biocatalysis using new low-cost immobilized preparations contributes to the economic viability of the process and improves the range of options in the use of these biocatalysts. In addition, due to the growing demand for clean technologies, allied to the production of biocompatible and bioresorbable materials, there is great interest in this area, numerous studies are reported in the literature with this purpose. However, the main innovation of this work is to interconnect all these topics, using renewable resources to produce new materials, employing new polymerization methods and catalysts free of toxic waste, enabling employment in the biomedical area, and expanding the range of materials available to the population.

RAFT-PISA polymerization was shown to be a relatively recent and versatile approach with great potential for the preparation of nano-objects as spheres, worms, and vesicles. The combination with photoinduced electron-transfer (PET) allows performing the polymerization under milder and more environmentally friendly conditions. On the other hand, the power of the PET-RAFT process remains somewhat underexplored once it requires the development of efficient and selective photocatalysts for fine control of the reaction, as well new approaches linked to green chemistry.

3 EPOXIDATION OF R-(+)-LIMONENE TO 1,2-LIMONENE OXIDE MEDIATED BY LOW-COST IMMOBILIZED *Candida antarctica* LIPASE FRACTION B

The aim of this work was to synthesize 1,2-limonene oxide by lipase-mediated epoxidation reaction (Figure 24). This research evaluated the efficiency of a new immobilized preparation with low-cost material from *Candida antarctica* fraction B (NS 88011). This study also investigated the effect of various reaction parameters on 1,2-limonene oxide yield, like enzyme amount, acyl donor concentration, oxidant concentration, R-(+)-limonene concentration, reaction time, and temperature.

The results of this chapter are published in Industrial & Engineering Chemistry Research as “Epoxidation of (R)-(+)-Limonene to 1,2-Limonene Oxide Mediated by Low-Cost Immobilized *Candida antarctica* Lipase Fraction B.” “Reprinted with permission from MELCHIORI, M. S. et al. Copyright 2019 American Chemical Society.”

Graphical abstract

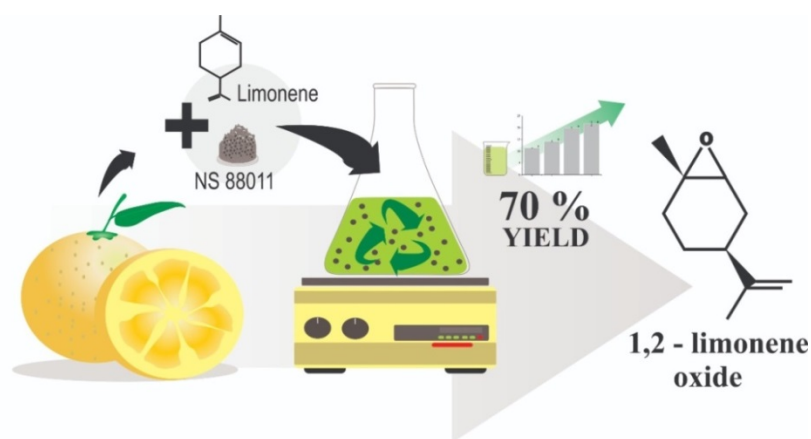
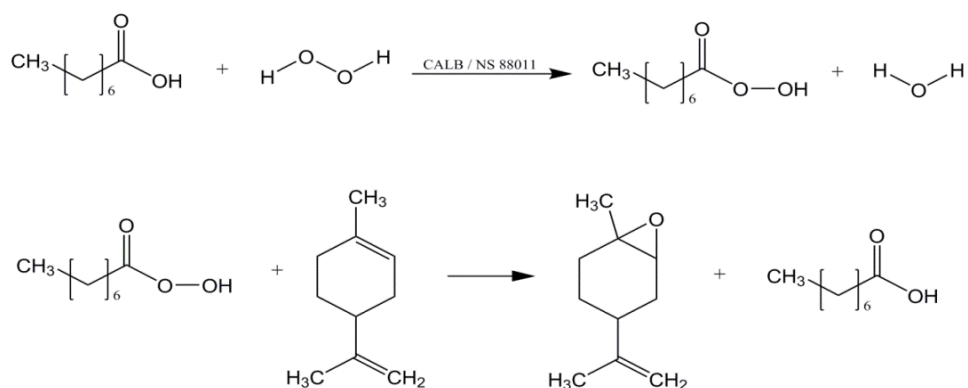


Figure 24 – Schematic structure of epoxidation reaction using immobilized CALB as catalyst (NS 88011).



3.1 MATERIAL AND METHODS

3.1.1 Enzymes and chemicals

Novozymes® kindly donated both immobilized *Candida antarctica* lipase fraction B (CalB), Novozym 435 and NS 88011, with enzymatic activity of 54.6 ± 0.7 U/g and 54.2 ± 0.5 U/g, respectively (SÁ et al., 2018). The Novozym 435 is obtained by the adsorption method and consists of CalB on a hydrophobic macroporous polymer (Lewatit VP OC 1600, Bayer) based on methyl and butyl methacrylic esters cross-linked with divinylbenzene (PÄIVIÖ; PERKIÖ; KANERVA, 2012). The NS 88011 is a new enzymatic preparation consisting of CalB immobilized on a hydrophobic polymeric resin. It was formulated by Novozymes® to provide a more economically feasible support for the production of compounds on an industrial scale (POLLONI et al., 2018). Sá et al. (2018) reported that NS 88011 material has smaller surface area ($15.16 \text{ m}^2/\text{g}$), total pore volume (0.02613 cc/g), and average pore diameter (68.96 \AA) than Novozym 435.

R-(+)-Limonene (97%) and (+)-Limonene 1,2-epoxide (isomeric mix) (97%) were obtained from Sigma Aldrich. Hydrogen peroxide (35% aqueous solution) (Neon) and Octanoic acid (98%) (Sigma Aldrich) were used as substrates. Toluene ($\geq 99.9\%$) (Neon) was used as the solvent. Ethyl acetate (Dinâmica) was used in gas chromatography injections, and acetone (Dinâmica) was used to wash the enzyme for reuse tests. Sodium bicarbonate (saturated solution, Dinâmica) and anhydrous sodium sulfate (Vetec) were employed for 1,2-limonene oxide purification. All other chemicals used were of analytical grade.

3.1.2 Reaction conditions

The epoxidation reaction was carried out in the fed-batch configuration using 20 mL of toluene as solvent. Reactions were performed by adding 40, 70, and 250 mM of octanoic acid; 40, 70, and 100 mM of R-(+)-limonene; 100, 250, and 500 mM of H_2O_2 (35% aqueous solution); and 1, 5, 10, and 20% of the biocatalyst NS 88011 in relation to the total amount of substrates (octanoic acid and H_2O_2 (35% aqueous solution)). The aqueous solution of H_2O_2 was added to the medium throughout the first 60 min of reaction, homogeneously distributed by adding equal amounts every 5 min. After the end of H_2O_2 addition, the mixture was incubated for additional 60 min, reaching 120 min total reaction time. The reaction was carried out under

permanent magnetic stirring (500 rpm) in a sealed round bottom flask at 40, 50, and 60 °C, all performed in duplicate. The Novozym 435 was also used at the best reaction condition (maximum yield obtained) to compare with NS 88011 results. Aliquots of 500 µL from the organic phase were withdrawn at different time intervals and adequately diluted for quantification via Gas Chromatography (GC).

3.1.3 Reuse cycles assay

The enzyme reuse involved to apply the exact same immobilized units of enzymes over three reaction cycles for the same reaction setup. The recuperation of the immobilized enzyme after each reaction was made by vacuum filtration using glass funnel and filter paper. The enzymes were washed with acetone (w/v ratio of 1:20) three times to remove the product and substrate residues (TOMKE; RATHOD, 2015). Then, they were dried for 20 h at 60 °C and reused in a new fresh reaction batch. This procedure was repeated for each reuse cycle.

3.2 LIMONENE OXIDE QUANTIFICATION

All reactional medium samples were diluted in ethyl acetate and analyzed in a Gas Chromatograph (Shimadzu GC 2010) coupled to an auto-injector (Shimadzu AOC 5000), equipped with a DB-5 column (27 m length x 0.25 mm internal diameter x 0.25 µm film thickness), and flame ionization detection (FID) detector. The samples were injected into the column initially at 60 °C, after a holding time of 1 min, the temperature increased at 10 °C/min until 170 °C, and increased at 70 °C/min until 270 °C, with a final holding time of 3 min (RANGANATHAN et al., 2016). The 1,2-limonene oxide corresponding peak of each chromatogram was analyzed by a previously prepared (+)-1,2-limonene oxide (isomeric mix) (97%), and the determination of the limonene oxide concentration, C , (mg/mL) was carried out using the linear regression shown in Equation 1 ($R^2 = 0.9962$). The yield for limonene oxide, Y , was calculated using Equation 2.

$$C = 146013x \quad (1)$$

$$Y = 100 \frac{C_t}{C_0} \quad (2)$$

in which C_t is the 1,2-limonene oxide concentration after the epoxidation, and C_0 is the initial limonene concentration (added to epoxidation reaction).

3.3 INITIAL REACTION RATE

The initial reaction rate was calculated by Equation 3,

$$r = \frac{\Delta Z}{\Delta t} \quad (3)$$

in which r is the initial rate of reaction ($\mu\text{mol min}^{-1} \text{g}^{-1}_{\text{enzyme}}$), ΔZ is the first increment in the formation of 1,2-limonene oxide ($\mu\text{mol g}^{-1}_{\text{enzyme}}$), and Δt is the reaction time interval (min) evaluated (ZENEVICZ et al., 2016).

3.4 SCALE-UP AND 1,2-LIMONENE OXIDE PURIFICATION

The scale-up, from 20 to 600 mL, was performed with the fed-batch configuration using the reaction setup that resulted in the highest yield. A 1000 mL glass reactor equipped with magnetic stirring was charged with R-(+)-limonene (40 mM), octanoic acid (70 mM), and NS 88011 (5% in mass). The reactor was heated up to 50 °C by using a sand bath. The aqueous solution of H₂O₂ was added dropwise to the stirring solution for 60 min (until 250 mM). The resulting two-phase mixture was stirred vigorously at 500 rpm and 50 °C. The reaction was completed at 60 min.

The 1,2-limonene oxide purification was conducted by removing chemicals and enzymes after 60 min of the epoxidation reaction. First, the immobilized enzymes were filtrated using a granulometric sieve. The product was dissolved in a saturated solution of sodium bicarbonate (1:4 in volume related to the organic phase) 5 to 7 time-fold to ensure complete neutralization of the residual acid. Then, the organic phase was recuperated by liquid-liquid extraction, and filtrated under vacuum with anhydrous sodium sulfate to remove the remaining water (RANGANATHAN et al., 2016). Finally, the organic phase was submitted to evaporation in a rotary evaporator (R3 BUCHI) with a coupled vacuum pump (V-700 BUCHI) for removing residual toluene. After evaporation, the 1,2-limonene oxide obtained was isolated using cylindrical silica columns (11 x 1.5 cm), packed with n-hexane and using a 9:1 mixture of n-hexane:ethyl acetate as eluent (MOREIRA, 2008). Then the purified 1,2-limonene oxide was analyzed by gas chromatography as previously described.

¹H NMR analyses of the purified 1,2-limonene oxide were recorded in deuterated chloroform (CDCl₃) using a Bruker Ascend spectrophotometer at 200 MHz. Chemical shifts (δ) are reported in part per million (ppm) relative to intern standard tetramethylsilane (TMS, $\delta = 0$ ppm) used to calibrate chemical shift.

3.5 RESULTS AND DISCUSSION

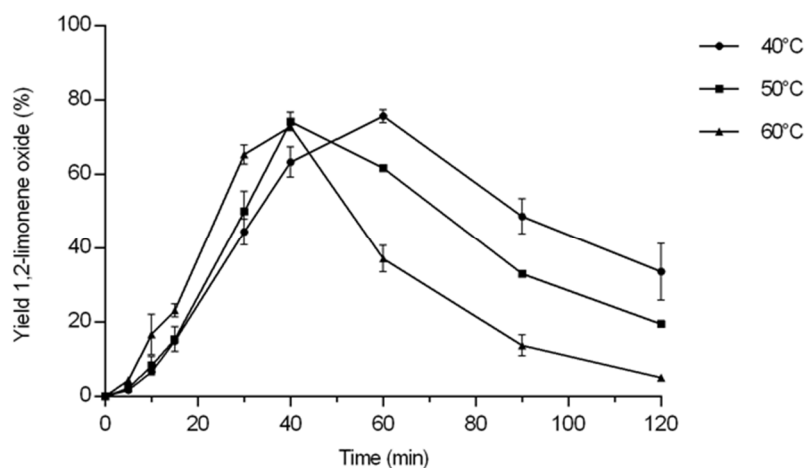
3.5.1 Optimization of the enzyme-catalyzed epoxidation conditions

3.5.1.1 Temperature

To evaluate the effect of the temperature (40, 50, and 60 °C), all other parameters were kept constant. Previous works had already established this temperature range as the ideal for performing lipase based epoxidation reactions (BJÖRKLING et al., 1992; RANGANATHAN et al., 2015, 2016). Temperature values above 60 °C promote unselective hydrogenation of substrates (RANGANATHAN et al., 2015), and, thereby, affect the yield of hydrogen peroxide. Moreover, the range studied is recommended by the biocatalyst fabricant for higher productivity (KRISTENSEN; XU; MU, 2005). The initial reaction conditions were defined according to Ranganathan et al. (2016): R-(+)-limonene 100 mM, hydrogen peroxide (35% aqueous solution) 500 mM, octanoic acid 70 mM, and 20% of NS 88011 in relation to the substrates, all in toluene.

The temperature range studied presented low influence in the system using NS 880011 (Figure 25), once all three temperatures were adequate to reach high yield. The yield values ranged from 63.33 to 74.24% after 40 min of reaction, in which the highest was observed at 50 °C. Therefore, this temperature was applied in all following experiments. These results are in agreement with studies of Rafiee-Moghaddam et al. (2014) that reported high yields using Novozym 435 in the epoxidation reactions at the same temperature. It is important to note that longer periods of time resulting in decreased yields of 1,2-limonene oxide, due to by-product formation, such as diepoxide.

Figure 25 – Influence of temperature in the 1,2-limonene oxide biosynthesis using NS 88011 as catalyst, using 100 mM of R-(+)-limonene, 70 mM of octanoic acid, 500 mM of hydrogen peroxide (35% aqueous solution), and 20% in mass of NS 88011 in solvent toluene. The line connecting the experimental points is a guide for the eye.



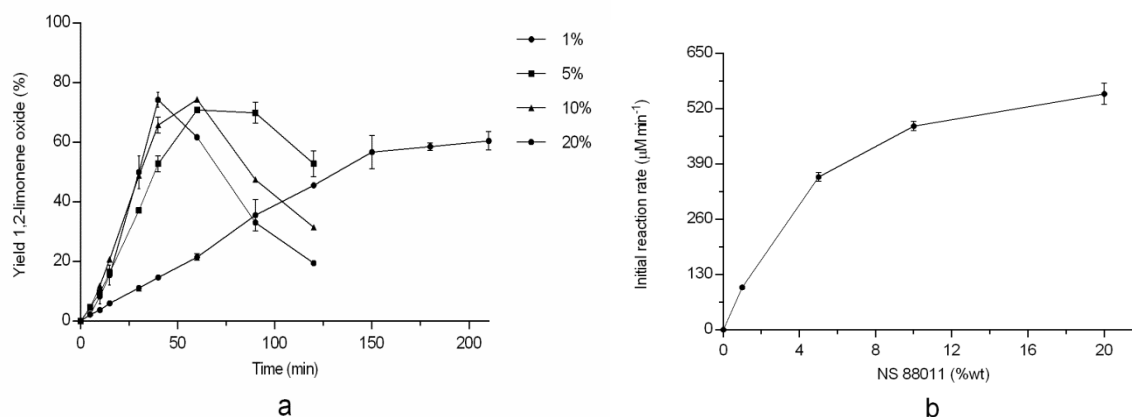
3.5.1.2 Enzyme concentration

The effect of enzyme concentration on the conversion rate of the R-(+)-limonene into 1,2-limonene oxide was studied for the range of 1 to 20% in mass related to limonene and octanoic acid amount. Reaction formulation and condition were R-(+)-limonene 100 mM, hydrogen peroxide (35% aqueous solution) 500 mM, octanoic acid 70 mM, and temperature at 50 °C.

In Figure 26a, it can be seen that when lipase concentration increases, the production of 1,2-limonene oxide also increases. This effect already was observed in other works (SKOURIDOU; STAMATIS; KOLISIS, 2003a; MOREIRA, 2008; RANGANATHAN et al., 2016), and can be highlighted by plotting the rate of 1,2-limonene oxide formation as a function of the NS 88011 mass fraction, as shown in Figure 26b. One can see that the reaction rate increased as lipase mass fraction increased, approaching a plateau at 20% of the enzyme, demonstrating the saturation of the system. The highest epoxidation rates were obtained using 10 and 20% of NS 88011, resulting in a rate of 479 and 555 $\mu\text{M min}^{-1}$, respectively. When 5% of NS 88011 was used, the rate was 359.5 $\mu\text{M min}^{-1}$. Despite resulting in lower rates than the values for 10 and 20% of NS 88011, this enzyme concentration was selected for the following experiments based on the cost-benefit ratio, once both 5 and 20% of NS 88011 resulted in 1,2-limonene oxide yield over 70 mol% and the required reaction time was relatively low for

both (60 min and 40 min, respectively). In the absence of the biocatalyst and the hydrogen peroxide, there was no product formation.

Figure 26 – Effect of enzyme loading (% in mass) on: a) yield of 1,2-limonene oxide (mol%), and b) initial reaction rates ($\mu\text{M min}^{-1}$). Conditions: NS 88011 as catalyst, 100 mM of R-(+)-limonene, 70 mM of octanoic acid, 500 mM of hydrogen peroxide (35% aqueous solution), solvent toluene, and 50 °C. The line connecting the experimental points is a guide for the eye.

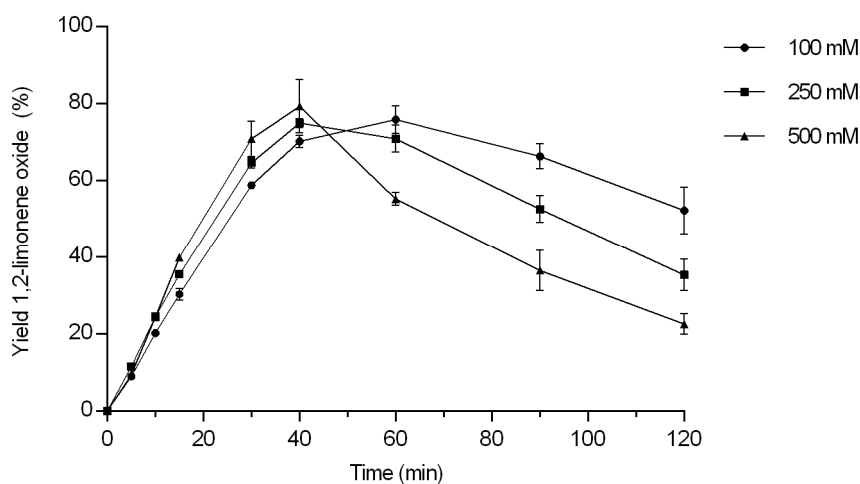


3.5.1.3 Oxidant concentration

The optimal concentration of oxidant is essential since its excess can induce the formation of by-products while a lesser concentration may result in deficient activity of the catalyst system, and, consequently, a reduced yield for the desired product (MICHEL, 2012). For this purpose, different amounts of hydrogen peroxide at 50 °C were examined. The reaction conditions used R-(+)-limonene 40 mM, octanoic acid 70 mM, and 5% in mass of NS 88011.

As depicted in Figure 27, the higher the oxidant concentration, the higher the catalytic activity. It was evident that increasing the presence of H_2O_2 accelerates the reaction. However, it also significantly promotes the deactivation of the biocatalyst, promoting inhibition and decreasing the selectivity towards 1,2-limonene oxide. Bhattacharya (2011) reported similar results. Thus, it can be observed that 1,2-limonene oxide production was greater during the first 30 min. In the assay with 500 mM of hydrogen peroxide, after 40 min, the yield of 1,2-limonene oxide decreased quickly due to by-product formation. Consequently, hydrogen peroxide concentration of 250 mM led to the highest yield and selectivity, within a reasonable reaction time. Thus, this was the hydrogen peroxide concentration applied in the following experiments.

Figure 27 - Yield of 1,2-limonene oxide (%) obtained at varying H_2O_2 concentrations. Conditions: 5% in mass of NS 88011 as catalyst, 40 mM of R-(+)-limonene, 70 mM of octanoic acid, 100 to 500 mM of hydrogen peroxide (35% aqueous solution), solvent toluene, and 50 °C. The line connecting the experimental points is a guide for the eye.



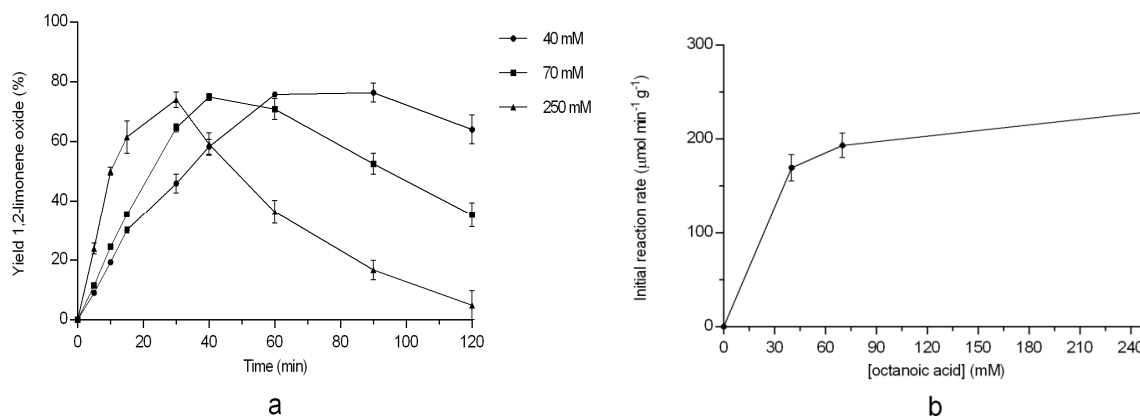
3.5.1.4 Octanoic acid concentration

Three octanoic acid concentrations (40, 70 and 250 mM) were studied keeping other parameters constant. Figure 28b presents the results of the impact of octanoic acid concentration on the initial reaction rate of the epoxidation. It was reported in previous works that the use this acid is the preferred acyl donor for epoxidation reactions mediated by lipase not only due to its ability to undergo reaction with the enzyme but also since it is easily soluble in the preferred solvent for such reactions, e.g., toluene (SKOURIDOU; STAMATIS; KOLISIS, 2003a; ALVES MOREIRA; BERGLER BITENCOURT; DA GRAÇA NASCIMENTO, 2005; TZIALLA et al., 2009; WIEMANN; FALTL; SIEBER, 2012; RANGANATHAN et al., 2016). Therefore, the octanoic acid is an acyl donor, and it is involved in the catalytic step directly interacting with the enzyme, its effect on the reaction itself is significant, and this factor has also been thoroughly reviewed along the years (BHATTACHARYA, 2011).

Increasing levels of octanoic acid accelerates the reaction, as shown in Figure 28b, achieving an initial reaction rate of $228.96 \mu\text{mol min}^{-1} \text{g}^{-1}$ for 250 mM of acid. However, in Figure 28a, one can see that the highest acid concentration quickly decreased the 1,2-limonene oxide yield, which may represent a substrate inhibition phenomenon. It might be due to the formation of an ineffective substrate complex between the excess of octanoic acid and the enzyme, as observed for the epoxidation of citronellol (DA SILVA; NASCIMENTO, 2012) and α -pinene (SKOURIDOU; STAMATIS; KOLISIS, 2003a). Therefore, since 70 mM of acid

showed the highest yield in a reasonable time (40 min), it was selected for the following reactions.

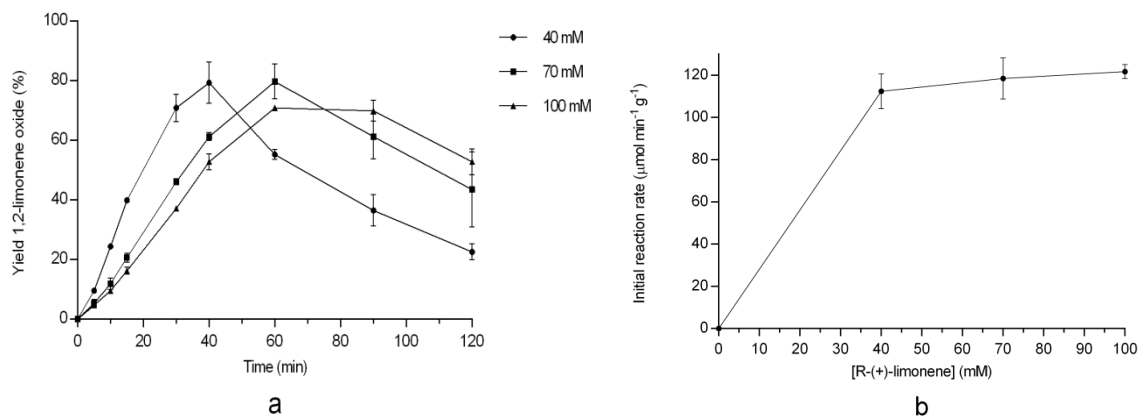
Figure 28 – Effect of octanoic acid concentration (mM) on: a) yield 1,2-limonene oxide (%); b) initial reaction rates ($\mu\text{mol min}^{-1} \text{g}^{-1}$). Conditions: 5% in mass of NS 88011 as catalyst, 40 mM of R-(+)-limonene, 40 – 250 mM of octanoic acid, 250 mM of hydrogen peroxide (35% aqueous solution), solvent toluene, and 50 °C. The line connecting the experimental points is a guide for the eye.



3.5.1.5 R-(+)-limonene concentration

R-(+)-limonene constitutes the reactive phase and is the educt with which the intermediate peroxy-octanoic acid reacts to form the final product, 1,2-limonene oxide. The effect of varying the R-(+)-limonene concentration (at fixed H_2O_2 , octanoic acid and NS 88011 concentrations) on the initial reaction rate is shown in Figure 29. As seen, an increase in R-(+)-limonene concentration has not influence on the initial reaction rate (Figure 29b). This behavior is due to the excess of limonene in relation to the acid and peroxide. Thus, this result indicates that, under the studied conditions, the enzymatic reaction responsible for the formation of the peroxy-octanoic acid is the rate-limiting step of this chemo-enzymatic epoxidation.

Figure 29 – Effect of R-(+)-limonene concentration (mM) on: a) yield 1,2-limonene oxide (%); and b) initial reaction rates ($\mu\text{mol min}^{-1} \text{g}^{-1}$). Conditions: 5% in mass of NS 88011 as catalyst, 40 to 100 mM of R-(+)-limonene, 70 mM of octanoic acid, 500 mM of hydrogen peroxide (35% aqueous solution), solvent toluene, and 50 °C. The line connecting the experimental points is a guide for the eye.



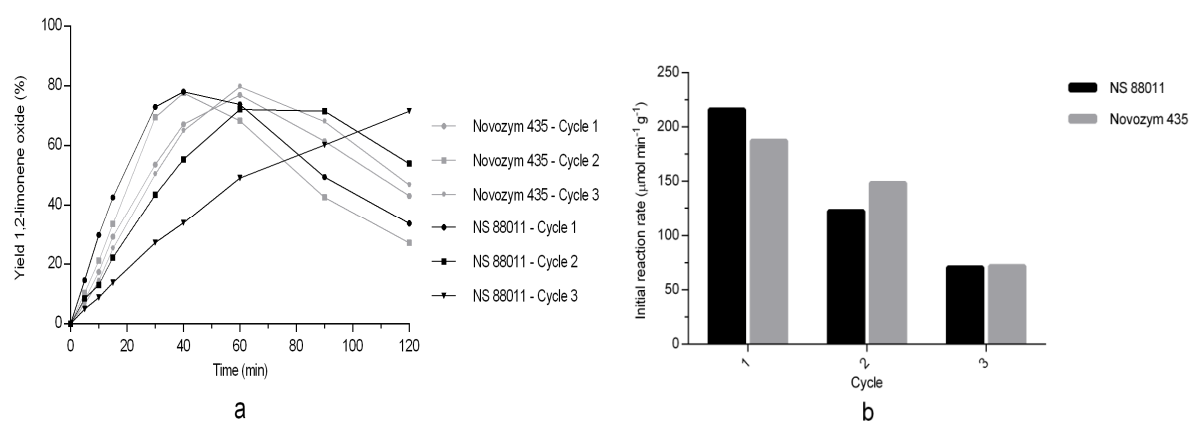
3.5.2 Successive cycles using NS 88011 lipase

The reuse of the NS 88011 was investigated for the epoxidation of R-(+)-limonene at 50 °C. The reaction was performed for 120 min, after which the enzyme was separated, washed, and added to fresh substrate. The enzyme reuse is one of the main goals of the immobilization processes, mainly due to the high cost associated with enzymes in the industrial processes, which sometimes can hinder their application as a catalyst (MOHAMAD et al., 2015). Usually, it is considered that an enzyme can be reused until 50% of the initial activity (WHITAKER; DEKKER, 1995).

In this work, it was possible to reach 3 reuse cycles for the NS 88011 with solvent, as shown in Figure 30. However, the epoxidation rate decreased throughout the subsequent cycles, reducing from 216.07 to 70.80 $\mu\text{mol min}^{-1} \text{g}^{-1}$ (Figure 30b). This behavior was expected and can be explained by the exposition of some amino acids of the enzyme, that were protected. Then, during reaction cycles, as the reuse increases, these amino acids suffer oxidation by H_2O_2 , resulting in a loss in enzymatic activity (TÖRNVALL et al., 2007). Nevertheless when comparing the performance of the process with Novozym 435 (Figure 30), the results were similar, which justifies the use of a low-cost biocatalyst for the system. Tziaila et al. (2009) reported 4 reuse cycles for the *Candida antarctica* B (Cal B lipase) immobilized before reducing enzyme activity to 50% of the initial value. However, Méndez-Sánchez et al. (2014) reported 3 reuse cycles for the commercial *Rhizomucor miehei* lipase immobilized but, unfortunately, the reuse of the enzyme led to a premature and dramatic decrease in activity, these results suggest the denaturalization of the enzyme with a prolonged exposure to H_2O_2 ,

justifying the result observed in Figure 30. Decreases in lipase activity in subsequent alkene epoxidation processes have also been reported by other authors (BJÖRKLING; GODTFREDSSEN; KIRK, 1990).

Figure 30 – Performance of NS 88011 and Novozym 435 over three cycles in a fed-batch reactor on: a) yield 1,2-limonene oxide (%); and b) initial reaction rates ($\mu\text{mol min}^{-1} \text{g}^{-1}$). Conditions: 5% in mass of enzyme, 40 mM of R-(+)-limonene, 70 mM of octanoic acid, 250 mM of hydrogen peroxide (35% aqueous solution), solvent toluene, and 50 °C. The line connecting the experimental points is a guide for the eye.

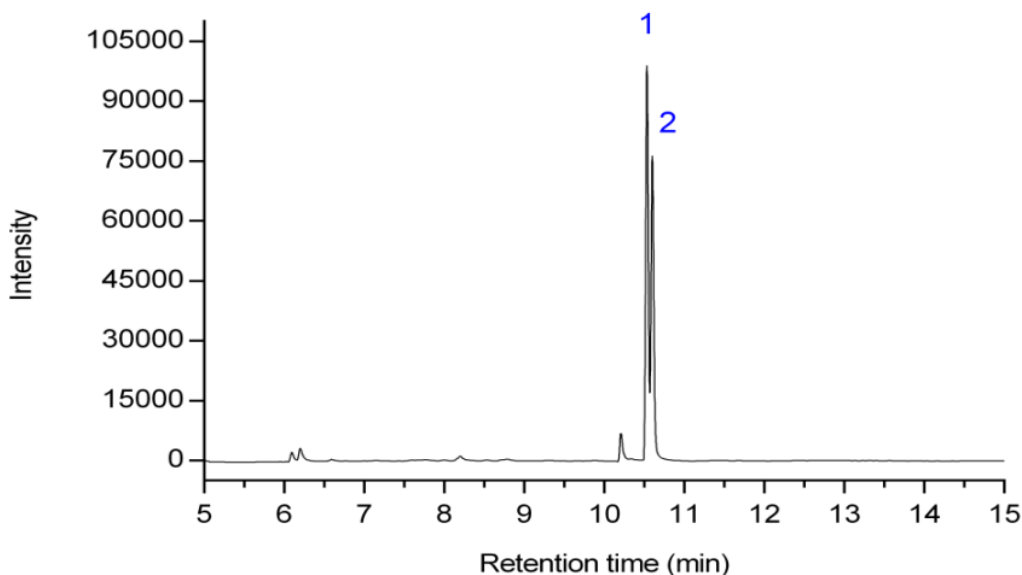


3.5.3 Scale-up and purification of 1,2-limonene oxide

After the establishment of experimental process conditions, a validation run was performed in addition to a scale-up and complemented by the design of a purification procedure. The 1,2-limonene oxide yield was 78% in the scale-up conditions, indicating that the results found in Figure 30 are reproducible on a larger scale. Although the reaction yield was 78%, the subsequent steps involving neutralization of the octanoic acid with saturated sodium bicarbonate as well as the utilization of the silica gel column chromatography led to the loss of some product, therefore, the isolated yield after product purification was 30%.

The 1,2-limonene oxide obtained from a fed-batch epoxidation reaction was purified by liquid-liquid extraction to remove the non-reacted acid and isolated using silica gel column chromatography. After concentrating the sample, the GC analysis (Figure 31) showed a purity of 95% in an area normalization analysis, with 1,2-limonene oxide retention time of 10.536 min.

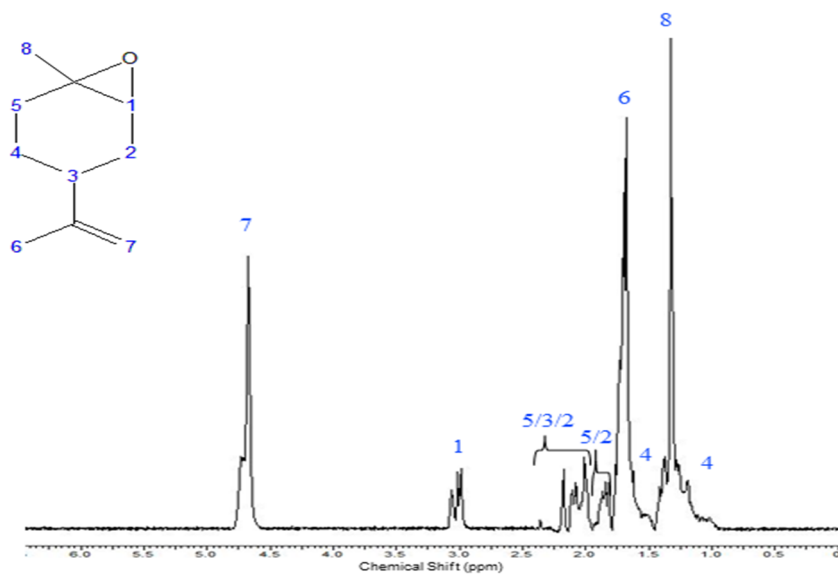
Figure 31 – Chromatogram of the 1,2-limonene oxide in ethyl acetate after purification using column chromatography on silica gel. Peak 1: cis-limonene internal epoxide; Peak 2: trans-limonene internal epoxide.



The purified final product was analyzed by ^1H NMR (200 MHz, CDCl_3 , δ) as shown in Figure 32. It showed chemical shifts at 4.70 (d, 2H), 3.07 (t, 1H), 2.14 (m, 1H), 1.86 (m, 2H), 1.74 (m, 2H), 1.71 (s, 3H), 1.55 (m, 2H), and 1.32 (s, 3H), which correspond to the specific chemical shifts of the 1,2-limonene oxide molecule. All spectroscopic data were consistent with those reported in literature (FERRANDI et al., 2015).

It is important to emphasize that in these epoxidation reactions limonene reached conversions above 98%, however, the focus of this work was the quantification of 1,2-limonene oxide in terms of yield and subsequent purification. In the experiments, the presence of by-products, such as 1,2-8,9-limonene diepoxide, was observed, which explains why 1,2-limonene oxide did not reach 100% yield.

Figure 32 – ^1H NMR spectrum of the 1,2-limonene oxide in CDCl_3 after purification using column chromatography on silica gel (n-hexane:ethyl acetate 9:1).



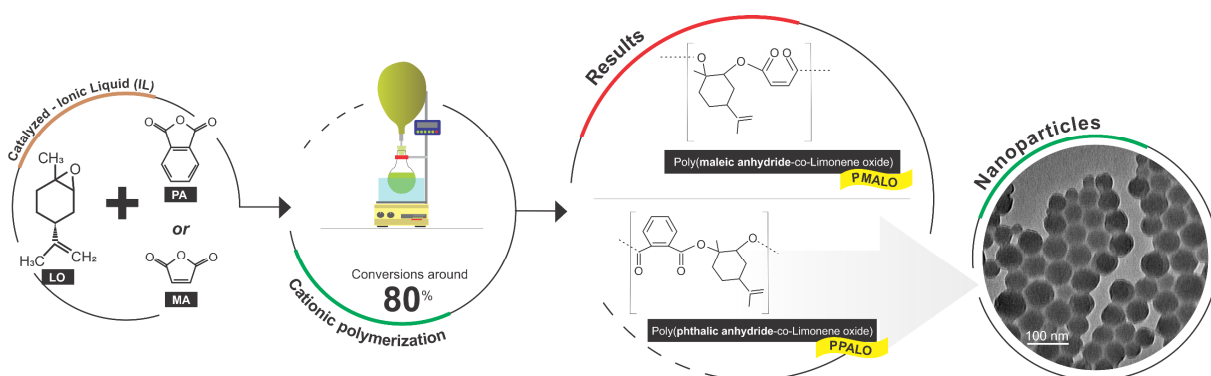
3.6 Conclusions

This work showed for the first time the epoxidation reaction of R-(+)-limonene mediated by the *Candida antarctica* lipase fraction B immobilized with a low-cost material, so-called NS 88011. Yields above 70% were reached in organic solvents, at a low substrate concentration and under moderate temperature, with an assurance in costs reduction. Results revealed that there are no major differences on the epoxidation reaction when using different support material of the biocatalyst as Novozym 435 and NS 88011. Some loss of enzyme activity occurred during the reuse cycles, suggesting that the enzyme was oxidized by hydrogen peroxide, aggrassing the microaqueous interface and leading to enzyme deactivation. The scale-up of the best fed-batch condition indicated a good reproduction of the 1,2-limonene oxide yield. The present results showed a route for 1,2-limonene oxide biotechnological production with a low-cost system.

4 COPOLYMERIZATION OF LIMONENE OXIDE AND CYCLIC ANHYDRIDES CATALYZED BY IONIC LIQUID BMI·Fe₂Cl₇ AND CYTOTOXICITY STUDIES

The development of more sustainable materials derived from renewable resources has increasingly gained attention from society, including scientists, engineers as well as polymer producers. In this work, limonene oxide (LO), derived from orange peel, is used as a monomer to obtain polyesters with different cyclic anhydrides, as phthalic anhydride (PA) or maleic anhydride (MA). The ionic liquid (LI) 1-n-butyl-3-methylimidazolium heptachlorodiferrate (BMI·Fe₂Cl₇) is used as a catalyst for ring-opening polymerization. As a proof-of-concept, poly(phthalic anhydride-co-limonene oxide) (PPALO) nanoparticles (NPs) were produced and cross-linked with tetrathiol followed by assessing NPs in vitro cytotoxicity (blood compatibility and cell viability).

This research evaluated the efficiency of a new catalyst, the ionic liquid BMI·Fe₂Cl₇, on this polymerization system to develop a bio-derived polymer containing unsaturation that could be further used for cross-linking or modification by thiol-ene reactions with potential for biomedical and pharmaceutical applications.



Graphical abstract

4.1 MATERIAL AND METHODS

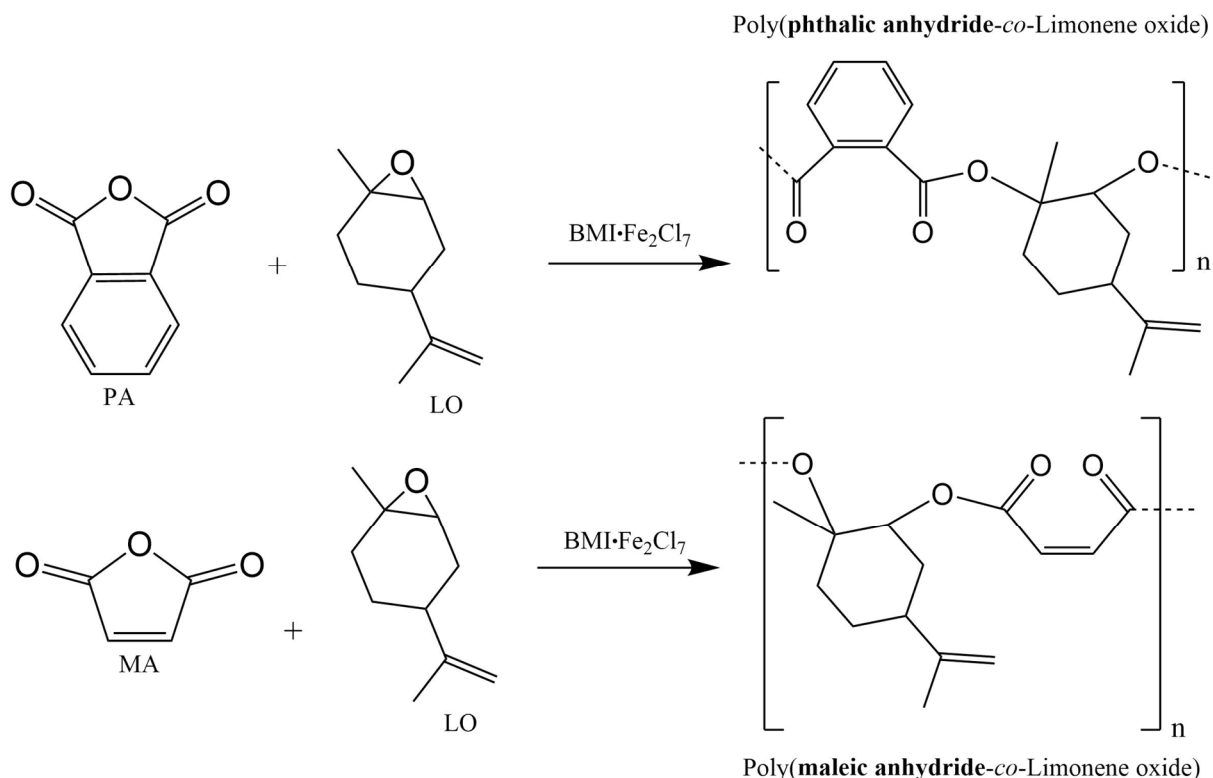
4.1.1 Chemicals

Polymerizations were performed using (+)-Limonene 1,2-epoxide (isomeric mixture) (97%) (LO, monomer, Sigma-Aldrich), Phthalic Anhydride (99%) (PA, monomer, Sigma-Aldrich), Maleic Anhydride (99%) (MA, monomer, Fluka), 1-n-butyl-3-methylimidazolium heptachlorodiferrate ($\text{BMI}\cdot\text{Fe}_2\text{Cl}_7$, ionic liquid IL), synthesized as reported by Rodrigues et al., (2015) and distilled Toluene ($\geq 99.9\%$) (Solvent, Neon). Nanoparticles were prepared using Sodium Dodecyl Sulfate (SDS, surfactant, Alpha Aesar), Tetrakis(3-mercaptopropionate) of Pentaerythritol ($>95\%$) (PETMP, Sigma-Aldrich), and 2,2-Dimethoxy-2-phenylacetophenone (DMPA, photoinitiator, donated by IGM resins). Anhydrous deuterated chloroform (CDCl_3) from Sigma-Aldrich was used as a solvent for the $^1\text{H-NMR}$ analyses. All other chemicals used were of analytical grade.

4.1.2 General procedure for ring-opening polymerization using $\text{BMI}\cdot\text{Fe}_2\text{Cl}_7$

Polymerization reactions were carried out following a procedure adapted from the one described by Nejad et al. (2013) at a constant temperature ($110\text{ }^\circ\text{C}$) under magnetic stirring (450 rpm) and nitrogen atmosphere in a Schlenk round-bottom flask. The $\text{BMI}\cdot\text{Fe}_2\text{Cl}_7$ and MA or PA were directly weighed into the Schlenk flask, using IL:LO:MA or PA molar ratios of 1:100:100, then the reaction flask was purged by successive vacuum and nitrogen cycles. The distilled toluene constituting 50 wt% of the reaction medium was added to the Schlenk flask with a syringe under magnetic stirring for 10 min for complete solubilization of the anhydride and ionic liquid. In sequence, the second monomer, LO, was added with a syringe. The polymerizations were conducted for 300 min. After the stipulated reaction time, polymerizations were stopped by the addition of an excess of a nucleophilic chain transfer agent, methanol with a small amount of ammonium hydroxide (0.1 vol%). The polymer obtained was dried at $60\text{ }^\circ\text{C}$ in a forced convection oven until constant weight, and the monomer conversion was determined gravimetrically. All reactions were performed in triplicates. The general scheme for the synthesis of poly(phthalic anhydride-*co*-limonene oxide) (PPALO) is shown in Figure 33.

Figure 33 - Synthesis of polyesters from limonene oxide (LO) and phthalic anhydride (PA) or maleic anhydride (MA) using the ionic liquid $\text{BMI}\cdot\text{Fe}_2\text{Cl}_7$ as catalyst.



4.1.3 Poly(phthalic anhydride-co-limonene oxide) (PPALO) nanoparticles preparation

The NPs were prepared according to the miniemulsification/solvent evaporation method as described elsewhere (GUINDANI et al., 2019). The organic phase was obtained by mixing the pre-synthesized PPALO (400 mg), and chloroform as solvent (4 g). The aqueous phase, constituted by water (14 g) and surfactant SDS (0.2% w/w), was added to the organic phase and the mixture was stirred for 10 min. Subsequently, the coarse emulsion was sonicated for 2 min (10 s pulse on, 10 s pulse off) with an amplitude of 60%. An ice bath was used to prevent the temperature increase during sonication. After sonication, the miniemulsion was left in a thermostatic bath with a temperature of 40 °C until complete solvent evaporation. The purification of the nanoparticles dispersion was carried out by centrifugation ($12.600 \times g$, for 60 min). The supernatant containing the excess surfactant was removed and the NPs re-dispersed in distilled water. This process was performed twice. Purified nanoparticle dispersions were stored in a refrigerator (4 °C). The nanoparticles preparation protocol was performed in duplicate.

4.1.4 Crosslinking of Poly(phthalic anhydride-co-limonene oxide) (PPALO) nanoparticles

The PPALO NPs were cross-linked via thiol-ene reactions between the pending double bonds in the polymer chain and pentaerythritol tetrakis(3-mercaptopropionate) (PETMP). The purified dispersion containing PPALO NPs was placed in a flask containing PETMP and photoinitiator 2,2-dimethoxy-2-phenylacetophenone (DMPA), under a nitrogen atmosphere. The reaction was conducted under UV light (365 nm, 1,53 mW cm⁻²) for 4 h with continuous magnetic stirring. The distance between the reaction medium and the UV lamp was 4 cm. PETMP was used in sufficient amounts to consume 50% of the double bonds. DMPA content was fixed in 1% (mol), relative to the total amount of thiol groups from PETMP present in the reaction medium. After the reaction, the aqueous dispersion containing cross-linked nanoparticles was stored in a refrigerator (4 °C).

4.1.5 Characterization

4.1.5.1 Polymer characterization

Monomer conversion. Determined by gravimetric analysis based on limonene oxide. **Molecular weight and polymer chain topology.** Determined by Matrix-assisted laser desorption ionization time-of-flight mass spectrometry (MALDI-TOF). These analyses were carried out on a Bruker Autoflex III smartbeam spectrometer. 2,5-dihydroxybenzoic acid (DHB) was used as a matrix, being dissolved in a methanol/water solution (70% v/v methanol) in a concentration of 20 mg mL⁻¹. Samples were solubilized in tetrahydrofuran (THF) and then mixed into the matrix solution in a 1:6 volume ratio. Analyses were performed in both reflector positive mode and linear positive mode.

Chemical composition. Determined by Nuclear Magnetic Resonance (NMR), ¹H NMR and ¹³C NMR spectroscopies were performed on a Bruker AC-200F NMR, operating at 200 MHz for ¹H NMR and 50 MHz for ¹³C NMR. Chemical shifts are reported in ppm relative to tetramethylsilane (TMS) 0.01% (v/v) ($\delta=0.00$). All samples were solubilized in CDCl₃ ($\delta = 7.27$ for ¹H NMR, and $\delta = 77.0$ for ¹³C NMR). As well, determined by Attenuated Total Reflectance Fourier Transform Infrared spectroscopy (ATR-FTIR) using equipment from Agilent

Technologies, model Cary 600 Series, in the wavenumber range of 4,000 to 600 cm^{-1} and resolution of 4 cm^{-1} .

Glass transition (T_g) temperature. Determined by Differential Scanning Calorimetry (DSC), in which the samples of approximately 5 mg of the dried copolymer were analyzed using a Perkin-Elmer Jade DSC, under inert atmosphere (20 mL min^{-1}), from -30 to 220 $^{\circ}\text{C}$ at a heating rate of 10 $^{\circ}\text{C min}^{-1}$. All calorimetric data were reported for the second heating cycle.

Thermal stability. Determined by thermogravimetric analysis (TGA) performed on the STA 449 F3 Jupiter (Netzsch). The samples were heated from 30 to 1,000 $^{\circ}\text{C}$ to 10 $^{\circ}\text{C min}^{-1}$ under a nitrogen gas flow of 60 mL min^{-1} using approximately 10 mg of polymer.

Before DSC, TGA, RMN, and MALDI-TOF analyses the polymer was purified. The polyester was dissolved in dichloromethane and the ionic liquid and unreacted anhydrides were removed by liquid-liquid extraction using a saturated sodium bicarbonate solution. The organic phase containing the polymer was dried with sodium sulfate anhydride and then the dichloromethane was evaporated.

4.1.5.2 Nanoparticles characterization

Particle morphology. Transmission electron microscopy (TEM) was carried out with a JEM 1011 microscope operated at an acceleration voltage of 100 kV. The nanoparticle dispersions were diluted in distilled water to 0.1% solids content; in sequence, one drop of each diluted sample was placed on a carbon-coated copper grid and dried overnight under room conditions.

Particle size. The size distributions of the PPALO NPs were accessed by TEM images using ImageJ software. Each sample was characterized by the volume-weighted mean diameter $D_{4,3}$ defined as $\sum n_i d_i^4 / \sum n_i d_i^3$, and the number-weighted mean diameter $D_{1,0}$ defined as $\sum n_i d_i^1 / \sum n_i$, where n_i is the number of nanoparticles and d_i is the diameter.

Zeta potential. The zeta (ζ) potential of the nanoparticles was determined by laser doppler anemometry associated with microelectrophoresis using the Zetasizer Nano ZS 3600 equipment from Malvern Instruments. Analysis was conducted after a previous dilution in distilled water (1:10) at 25 $^{\circ}\text{C}$.

4.1.5.3 *In vitro* cytotoxicity assay of the cross-linked nanoparticles

Cell viability assays. The cell viability assays were performed following the methodology described by Feuser et al. (FEUSER et al., 2016). Mouse embryo fibroblast (NIH3T3) cell line was used to evaluate the cytotoxicity of the obtained cross-linked PPALO NPs. Cells were cultured in Dulbecco's Modified Eagle Medium (DMEM) supplemented with 10 wt% of fetal bovine serum (FBS) and 100 U mL⁻¹ penicillin-streptomycin. NIH3T3 cells were maintained at 37 °C in a humidified incubator containing 5 wt% CO₂. After incubation, cells were seeded at 1x10⁴ cells/well in a 96 well plate. After 24 h, cells were treated with cross-linked PPALO NPs (dispersed in PBS-phosphate buffered saline), at four different concentrations: 25, 50, 100, and 200 µg mL⁻¹. After 24 h of incubation, the cells were washed three times with PBS and 100 µL of MTT was added and incubated for 3 h (5% CO₂, 37 °C). Afterward, 150 µL of isopropyl alcohol was added to dissolve the formazan crystals and the absorbance was measured at 540 nm using an Infinite 200 TECAN microplate reader. Experiments were performed in triplicate with three wells for each condition and the results were expressed as the percentage of viable cells in comparison to the control group.

Hemolysis assay. The hemolysis assay was performed following the methodology described by Feuser et al. (FEUSER et al., 2016). The human red blood (erythrocytes) cells were collected from three healthy donors in tubes containing 3.2 wt% of sodium citrate. 4 mL of whole blood was added to 8 mL of a sterile saline solution and the erythrocytes were isolated from serum by centrifugation and (1,500 × g / 10 min) washed three times with saline solution. Following the last wash, the human erythrocytes were diluted in 2 mL of saline solution and then 70 µL of the diluted was added to 930 µL of water or saline. The erythrocytes were treated with samples of the cross-linked PPALO NPs at concentrations of 100, 200, and 400 µg mL⁻¹ and stirred (350 rpm) at 37 °C for 120 min. In sequence, the erythrocytes containing the samples were centrifuged at 10.000 × g for 5 min. Subsequently, 100 µL of supernatant from the sample tube was transferred to a 96 well plate and the absorbance value was measured at 540 nm. As positive and negative controls, 70 µL of the erythrocytes' suspension was incubated with 930 µL of distilled water and saline, respectively. The assays were performed in triplicate. Before cell viability and hemolysis assays, PPALO was purified as previously described.

4.2 RESULTS AND DISCUSSION

The copolymerization of limonene oxide and cyclic anhydrides, such as phthalic anhydride or maleic anhydride, via ring-opening polymerization, using the ionic liquid BMI·Fe₂Cl₇ as the catalyst was evaluated. As can be observed from Table 7, conversions around 80% were obtained, and the molecular weights were approximately 1 x 10³ g mol⁻¹; this might be due to side reactions like transesterification, irreversible chain termination, or partial catalyst deactivation, phenomena also reported by Nejad et al. (2013); or even possible traces of water or hydrolyzed anhydrides present in the monomers, resulting in anhydride diacids, that could act as chain transfer agents and chain stoppers, thereby promoting the molecular weight reduction of the polymers (HATAZAWA et al., 2017).

Table 7 – Results of ring-opening copolymerization of LO with phthalic or maleic anhydrides using the ionic liquid BMI·Fe₂Cl₇ as catalyst.

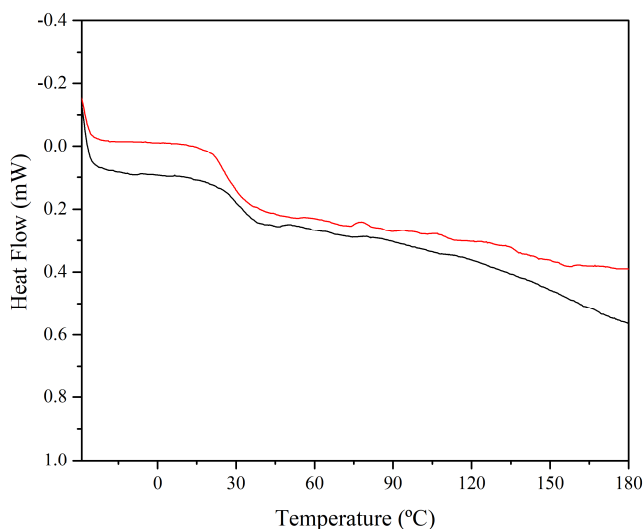
Anhydride	¹ LO conv. (%)	² M _n (g mol ⁻¹)	² M _w (g mol ⁻¹)	² PDI	T _{onset} (°C) ³	⁴ T _g (°C)
Phthalic	78.7 ± 1.7	1521	2044	1.34	234.2	31.0
Maleic	82.5 ± 2.4	1030	2081	2.02	245.0	28.7

Reaction conditions: Molar ratio [IL]:[LO]:[anhydride] 1:100:100; Temperature: 110 °C; Toluene 50 wt%; Reaction time: 300 min. ¹gravimetry of crude reaction mixture. Data are mean ± SD (n = 3). ²MALDI-TOF. ³TGA. ⁴DSC.

However, these results provide new perspectives for polymerization processes using this ionic liquid as a catalyst. Furthermore, it has been demonstrated that it is possible to synthesize a polyester from limonene oxide and cyclic anhydrides using BMI·Fe₂Cl₇ as a catalyst. Even more, low molecular weight polymers can be excellent precursors in the production of nanomaterials, for example, since they require less solvent to produce nanoparticles by miniemulsification/solvent evaporation, being an environmentally friendly alternative.

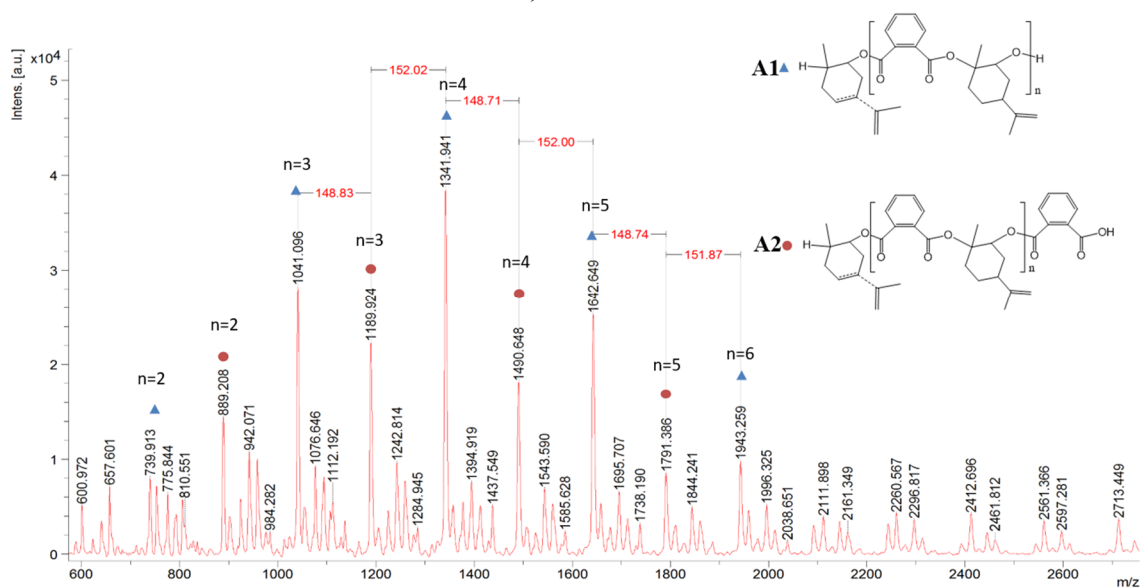
In terms of thermal properties, the prepared copolymers presented *T_g* values below 40 °C (Figure 34) as can be observed from Table 7. Isnard et al. (2019) reported *T_g* values in the same range, 27 to 43 °C, for a polyester obtained with these monomers.

Figure 34 - Second heating DSC curves of PPALO (black) and DSC curves of PMALO (red).



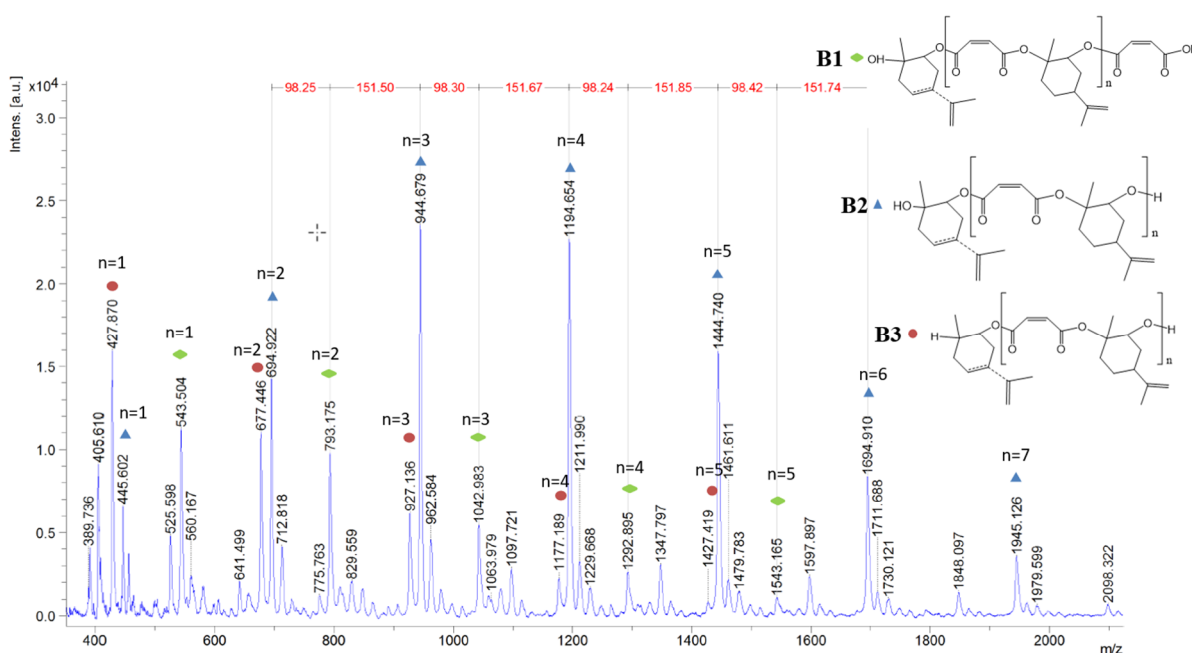
The MALDI-TOF spectrum of PPALO (Figure 35) exhibited a m/z interval of 300 g mol^{-1} between the consecutive peaks, corresponding to a [LO (152 g mol^{-1}) + PA (148 g mol^{-1})] repeating unit, confirming a perfectly alternating structure. In addition, MALDI-TOF spectra were also analyzed to provide more information related to the terminal groups of the PPALO, as shown in Figure 35. The major distribution A1 corresponds to the expected polymer structure with the OH terminal group. Whereas the distribution A2 exhibits the phthalic acid terminal group. The existence of a side reaction might also explain the low molecular weight of the polymers, a similar result was also reported by Nejad et al. (2013).

Figure 35 – MALDI-TOF spectrum of PPALO copolymer synthesized using liquid BMI·Fe₂Cl₇ as catalyst. Reaction conditions: Ratio molar [IL]:[LO]:[anhydride] 1:100:100; Temperature: 110°C; Toluene 50 %wt; Reaction time: 300 min.



In the same way, the MALDI-TOF spectra of poly(maleic anhydride-*co*-limonene oxide) (PMALO) (Figure 36) exhibited an m/z interval of 250 g mol^{-1} between the consecutive peaks, corresponding to a [LO (152 g mol^{-1}) + MA (98 g mol^{-1})] repeating unit, also confirming a perfectly alternating structure.

Figure 36 – MALDI-TOF spectrum of PMALO copolymer synthesized using liquid $\text{BMI-Fe}_2\text{Cl}_7$ as catalyst. Reaction conditions: Ratio molar [IL]:[LO]:[anhydride] 1:100:100; Temperature: $110 \text{ }^\circ\text{C}$; Toluene 50 %wt; Reaction time: 300 min.



Again, to elucidate the terminal groups, more information was collected from the MALDI-TOF spectra and PMALO showed different terminal groups, as shown in Figure 36. The major distribution B2 corresponds to a structure that exhibits polymer chains with two OH terminal groups. The distribution B1 corresponds to the polymeric chains with OH and maleic acid as terminal groups. Finally, the distribution B3 corresponds to the structure that exhibits polymer chains with the end group OH. Similarly, as for the PPALO, for PMALO the occurrence of side reactions might also explain the relatively low molecular weight.

The composition of the obtained polymers was estimated by ^1H NMR (Figure 37) and ^{13}C NMR (Figure 38) analyses, in which the integrals of the epoxide/anhydride sequence signals were compared with those of the sequential epoxide chain, the data are in agreement with the data obtained by Nejad et al. (2013) and by Jeske, Diccio, and Coates (2007) for the similar polymers. All obtained copolymers showed the absence of ether bonds, thus describing perfectly alternating copolymers, as expected from the bulky nature of LO.

Figure 37 – Analysis of ^1H NMR spectra of (1) LO-PA and (2) LO-MA in CDCl_3 , using TMS as the peak reference. Reaction conditions: Ratio molar $[\text{IL}]:[\text{LO}]:[\text{anhydride}]$ 1:100:100; Temperature: $110\text{ }^\circ\text{C}$; Toluene 50 %wt; Reaction time: 300 min.

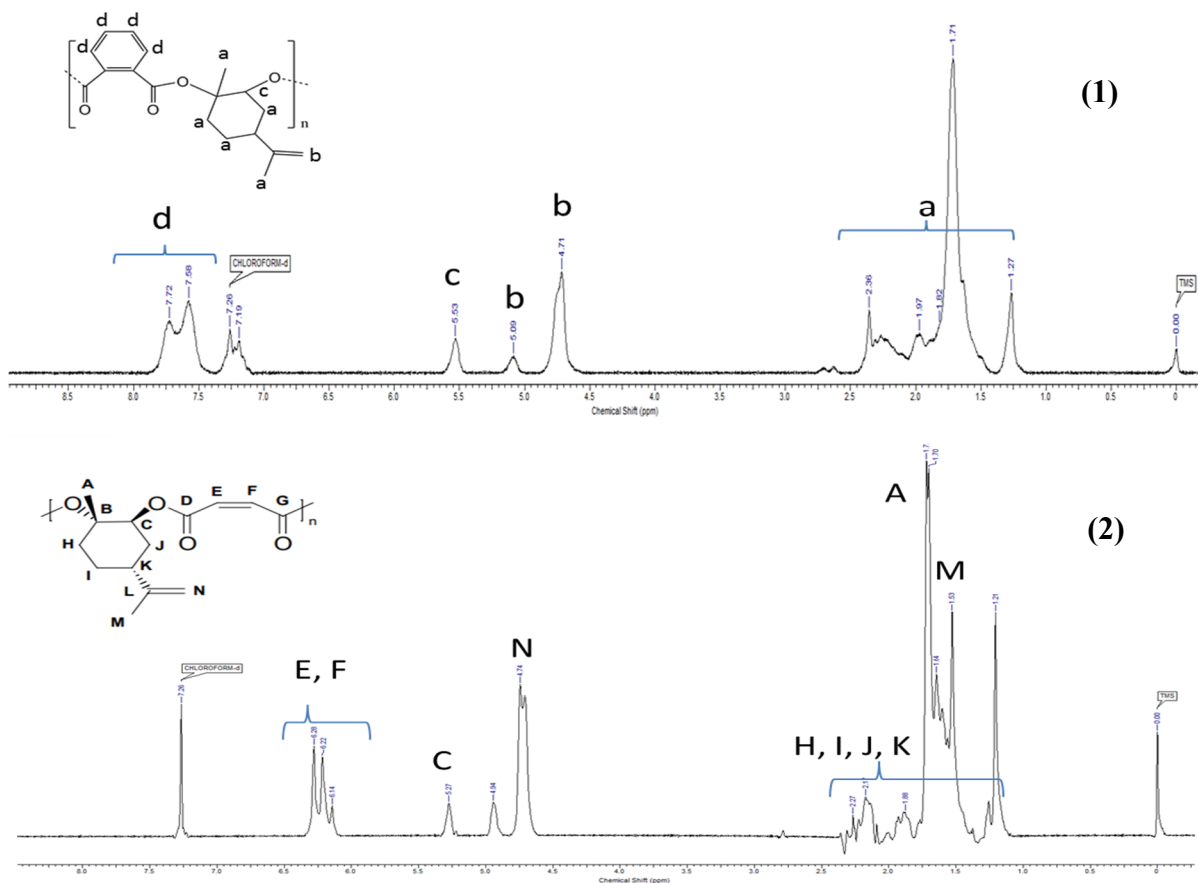
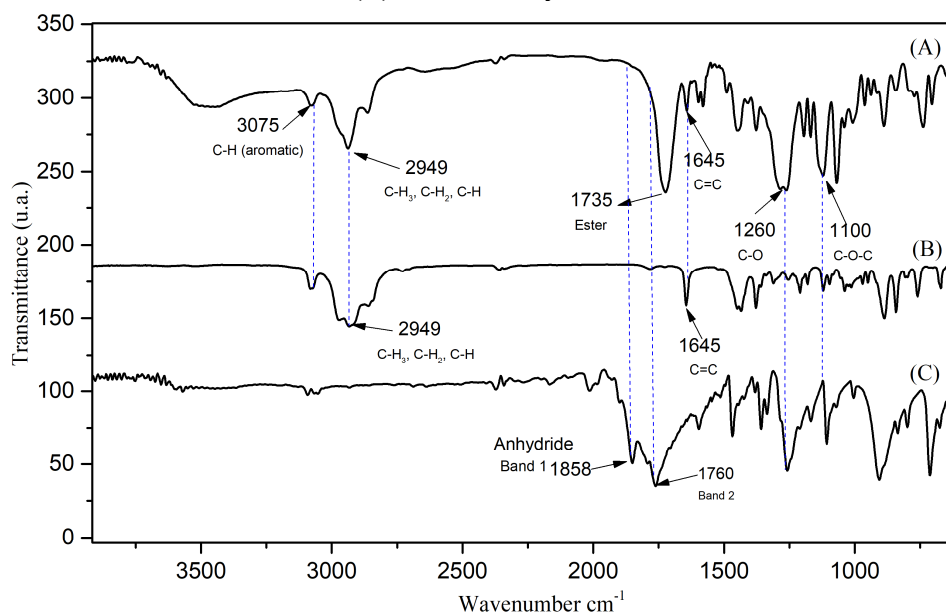


Figure 38 – Analysis of ^{13}C NMR spectra of the LO-PA, using TMS as the peak reference. Reaction conditions: Molar ratios $[\text{IL}]:[\text{LO}]:[\text{anhydride}]$ 1:100:100; Temperature: $110\text{ }^\circ\text{C}$; Toluene 50 %wt; Reaction time: 300 min.



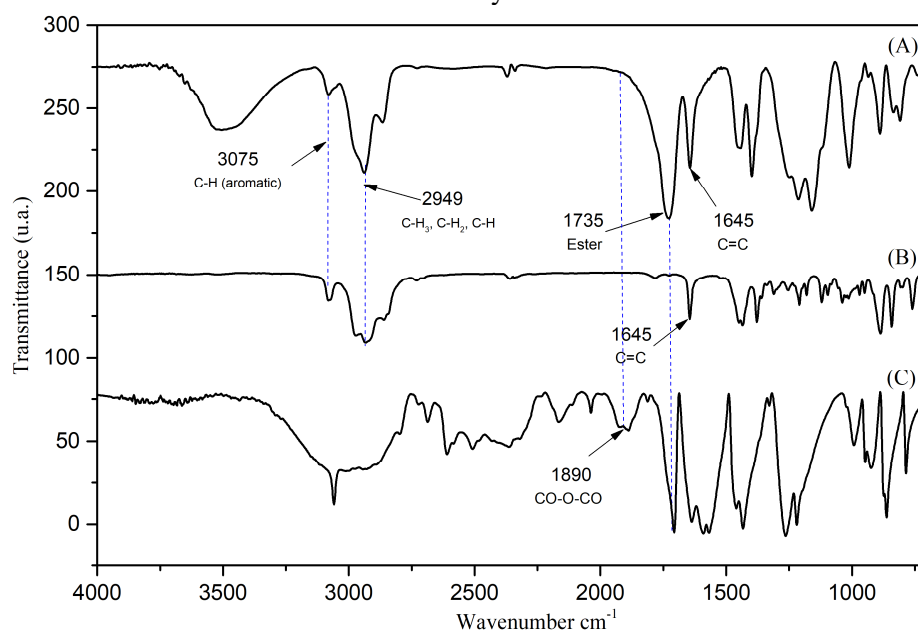
The normalized FTIR spectrum of the polymer obtained by copolymerization of LO with PA, PPALO, is shown in Figure 39. For comparison, normalized FTIR spectra of pure LO and pure PA can be seen in Figure 39. Peaks that can be found in both LO and PA are also present in the spectrum for the copolymer. The spectrum of the prepared polymer confirms the ester linkage. The band assigned to the symmetric stretching vibration of the ester carbonyl group is found at 1735 cm^{-1} (MUNDIL et al., 2015), and the disappearance of the band at 1858 cm^{-1} and 1760 cm^{-1} associated with anhydride ring grouping confirms the efficient opening of the ring (HASE et al., 1976). In addition, the peak at 1645 cm^{-1} originated from the external double bond of limonene oxide is still present in the copolymer, confirming that the double bonds were preserved after polymerization (NORSTRÖM, 2011).

Figure 39 – FT-IR spectra of (A) Poly(phthalic anhydride-*co*-limonene oxide), (B) Limonene oxide, (C) Phthalic anhydride.



In the same way, the normalized FTIR spectrum of the polymer obtained by copolymerization of LO with MA, PMALO, is shown in Figure 40. The spectrum was compared with those of pure LO and MA. The formation of the polyester is confirmed by the presence of a specific symmetric stretching vibration band of the ester carbonyl group at 1735 cm^{-1} . In addition, the disappearance of the band at 1890 cm^{-1} associated with the anhydride ring group confirms the efficient opening of the ring. Even more, the absorption peak at 1645 cm^{-1} is attributed to the $\text{C}=\text{C}$ vibration, indicating the presence of MA and LO (SONG et al., 2008; NORSTRÖM, 2011).

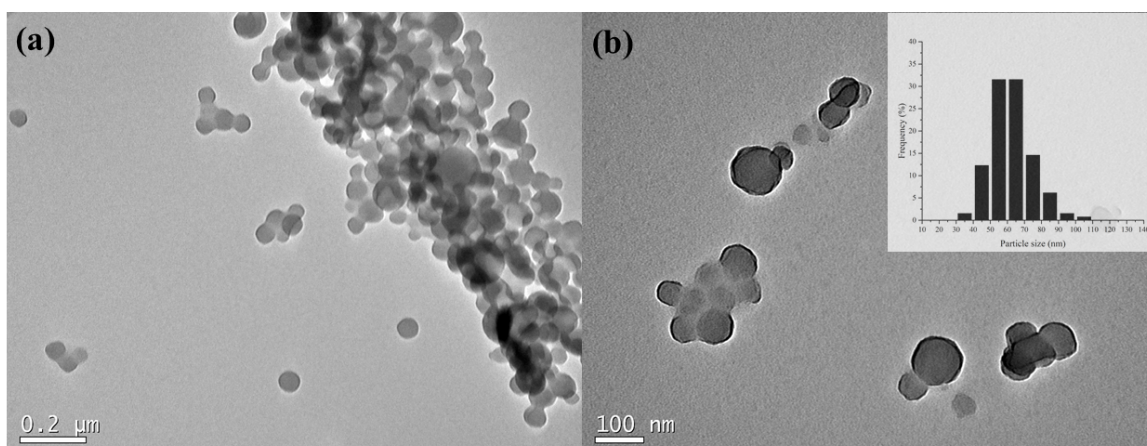
Figure 40 – FT-IR spectra of (A) Poly(maleic anhydride-*co*-limonene oxide), (B) Limonene oxide, (C) Maleic anhydride.



The next step was to evaluate the production of poly(phthalic anhydride-*co*-limonene oxide) nanoparticles (NPs) by the miniemulsification/solvent evaporation method. The nanoparticles were produced with the polymer from item 4.1.3. These results aimed to confirm whether it is possible to produce nanoparticles of appropriate size, distribution, and morphology.

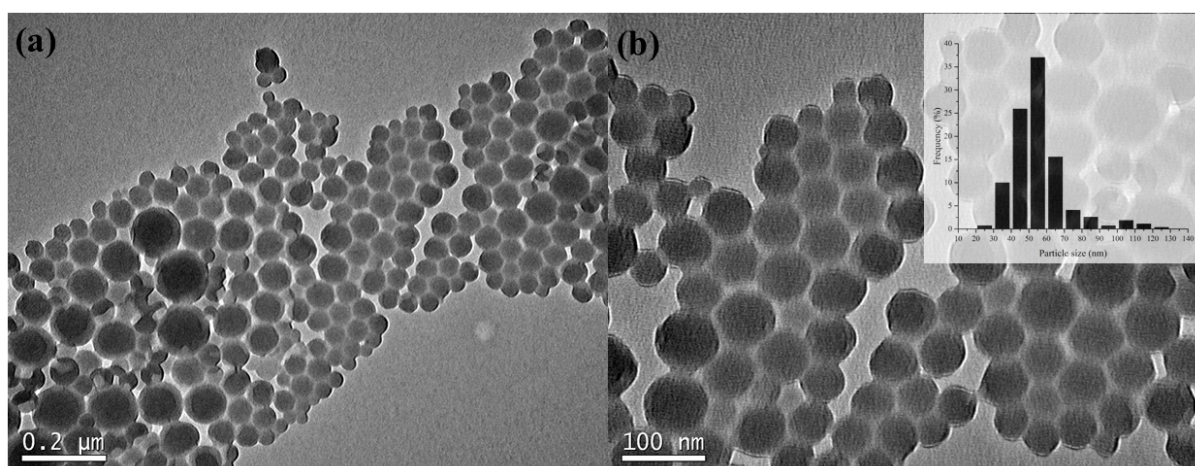
The particle size distribution and morphology of PPALO NPs were analyzed by TEM, as shown in Figure 41. TEM images confirm that the nanoparticles were spherical with the number-weighted mean diameter ($d_{1,0}$) of 63 nm and the volume-weighted mean diameter ($d_{4,3}$) of 70 nm. In addition, the zeta potential at pH 6.4 was determined to be -34.8 ± 1.5 mV, revealing that the dispersion was colloidally stable. The negative charge is associated with the presence of SDS (an anionic surfactant) adsorbed on the surface of the nanoparticles, which may be present even after purification, as this step only removed the SDS in excess (LOOSLI; STOLL, 2017).

Figure 41 - (a) TEM images of PPALO NPs (b) Details of the shape of the particles with higher magnification and size distribution histogram.



Finally, the double bonds from limonene oxide in PPALO chains can be further reacted via thiol-ene mechanism in PPALO NPs to modify the polymer characteristic and the nanoparticle physico-chemical structure. The PPALO NPs were reacted with a tetrathiol compound (PETMP) to obtain cross-linked nanoparticles. After cross-linking, the NPs became insoluble in chloroform, and the morphology and size distribution was accessed by TEM. A typical TEM image of cross-linked PPALO NPs can be seen in Figure 42. The NPs had an approximately spherical shape, with no aggregated structures and the number-weighted mean diameter ($d_{1,0}$) of 56 nm, and the volume-weighted mean diameter ($d_{4,3}$) of 73 nm. It is important to emphasize that after reticulation the resolution of the particles in the TEM images was improved since they became more rigid and stable during the analysis and exposure to the strong electron beam.

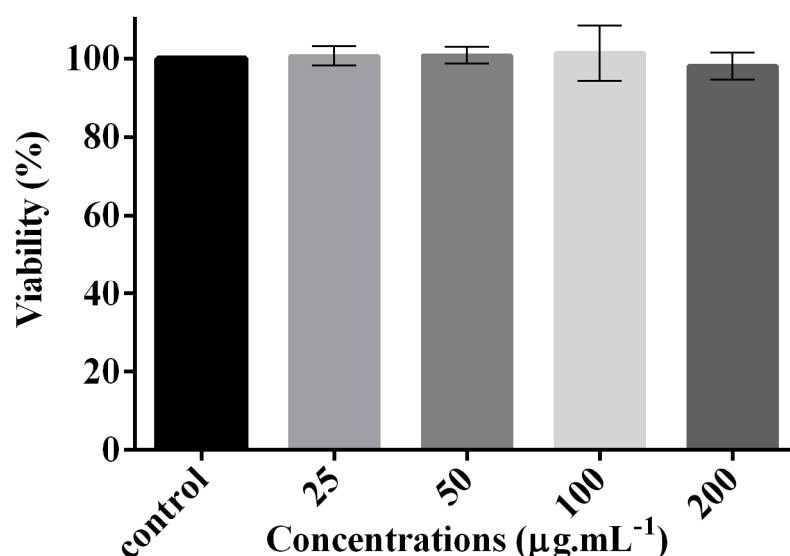
Figure 42 - (a) TEM images of cross-linked PPALO NPs (b) Details of the shape of the particles with higher magnification and size distribution histogram.



We showed the successful crosslinking of PPALO NPs via the thiol-ene reaction keeping their morphology, size, and colloidal stability. This is a remarkable result as it increases the spectrum of application of these polymers obtained from renewable resources. It is important to emphasize that there are no studies in the literature involving the formation of nanoparticles with this polymer. In addition, it provides new ideas for noble applications, further expanding the use of polyesters synthesized by new routes.

To verify the *in vitro* cytotoxic effect of the produced NPs, cell viability assays were performed. As shown in Figure 43, the exposure of NIH3T3 cells to the cross-linked PPALO NPs did not significantly reduce cell viability ($p>0.05$) at any of the tested concentrations (25, 50, 100, and 200 $\mu\text{g mL}^{-1}$). These results are very promising because they indicate the potential of this innovative research into new materials for biomedical applications. It is also important to mention that in accordance with ISO 10993-5:2009 (INTERNATIONAL ORGANIZATION FOR STANDARDIZATION, 2009) for the cell viability higher than or equal to 70% in comparison to the control group, which presents 100% viability, PPALO NPs can be assumed as a non-cytotoxic material.

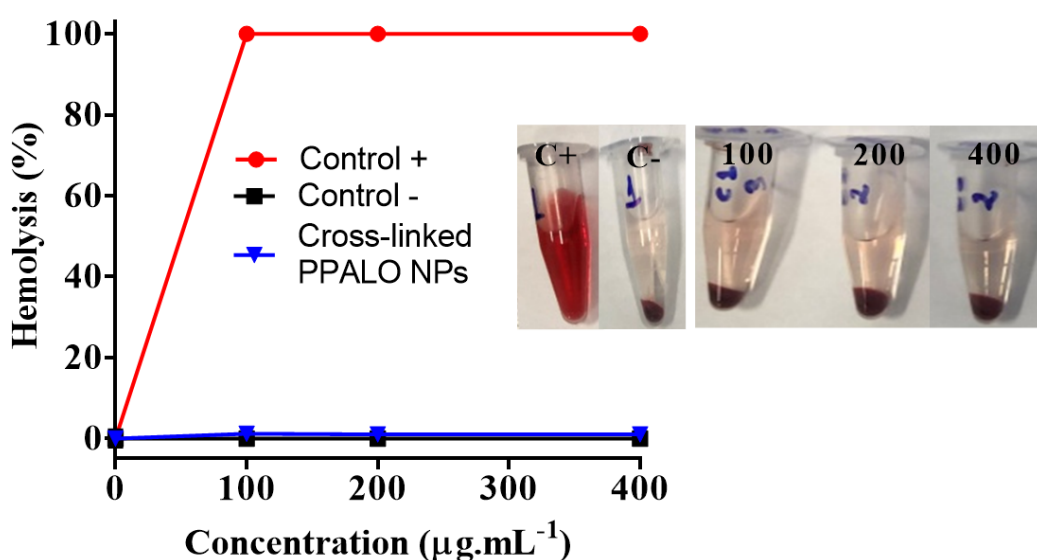
Figure 43 – Cytotoxicity assay. Cytotoxicity effects of different concentrations of PPALO NPs on mouse embryo fibroblast (NIH3T3) cell exposed 24 h. The cell viability was monitored through MTT assay. ($p>0.05$) using one-way ANOVA followed by post-test Bonferroni's.



Finally, to evaluate the hemocompatibility of cross-linked PPALO NPs, hemolysis assays were carried out, as shown in (Figure 44). Hemolysis assay is an indispensable initial step in assessing polymer blood compatibility to identify severe acute toxic red cell reactions

in vivo (DOBROVOLSKAIA; MCNEIL, 2013). Many studies have reported that *ex vivo* hemolysis assays have good correlations with *in vivo* toxicity by the hemolytic effect (LU et al., 2009; JEONG et al., 2017). As shown in (Figure 44), high concentrations of NPs incubated for 2 h did not cause hemolysis to human red blood cells, suggesting that these systems do not have hemolytic capacity, even when administered at high concentrations. The non-hemolytic character confirms the hemocompatibility of cross-linked PPALO NPs. These results are particularly important because they suggest the non-cytotoxicity and future biomedical application of the NPs obtained with material produced via polymerization catalyzed by $\text{BMI}\cdot\text{Fe}_2\text{Cl}_7$.

Figure 44 - Hemolysis assay. Relative rate of hemolysis of human red blood cells upon incubation with PPALO at $50\ \mu\text{g mL}^{-1}$, $100\ \mu\text{g mL}^{-1}$, and $200\ \mu\text{g mL}^{-1}$. The presence of hemoglobin in the supernatant (red) was observed at 540 nm. Data are mean \pm SD (n = 3).



4.3 CONCLUSION

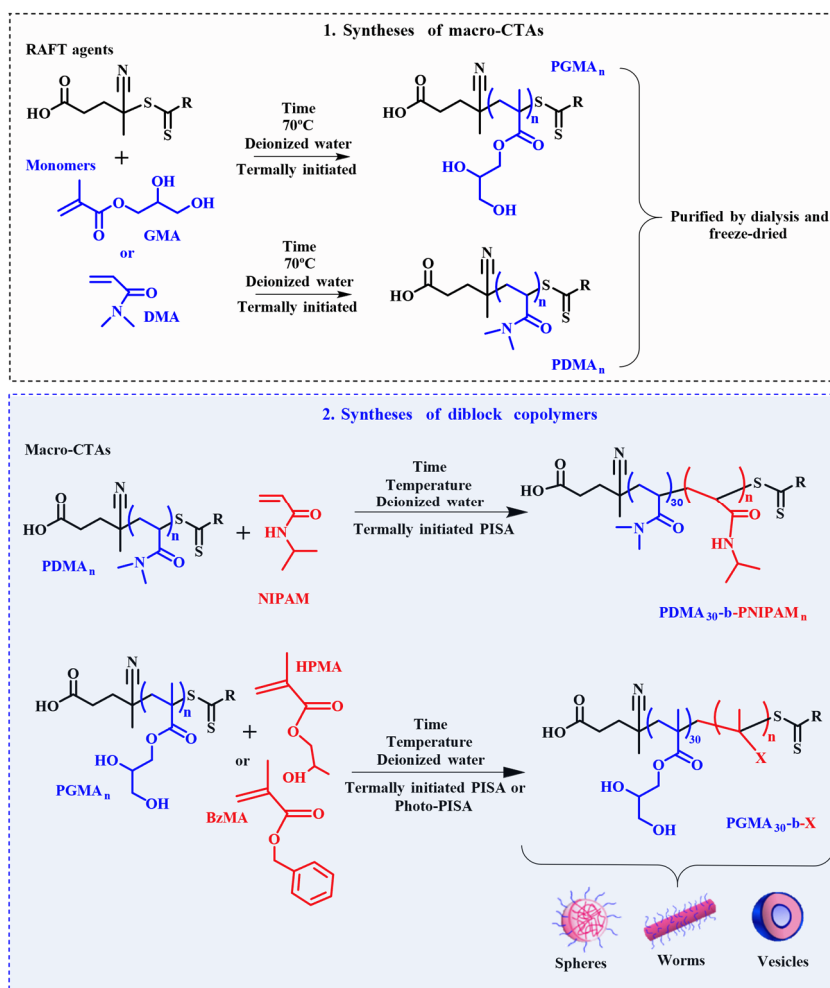
The copolymerization of commercial limonene oxide with cyclic anhydrides, (phthalic and maleic anhydride) mediated by ionic liquid (IL) $\text{BMI}\cdot\text{Fe}_2\text{Cl}_7$ reached conversions around 80% at a catalyst:limonene oxide molar ratio of 1:100. The resulting polymer presented a perfectly alternating structure; number-average molar mass over $1000\ \text{g mol}^{-1}$, and pendant double-bonds that allow posterior modification of the polymer chemical structure. Nanoparticles were successfully produced by the combination of miniemulsion and solvent

evaporation techniques, confirming the efficiency of the method. In addition, the presence of unsaturations in the polymer chain provides a site for modifying this polyester allowing modifications in the polymer structure as, for example, crosslinking the polymer nanoparticles via thiol-ene reaction. Finally, cross-linked PPALO NPs presented high blood compatibility and slightly reduced cell viability at different concentrations, suggesting the biocompatibility of the material with potential for biomedical application.

5 DEVELOPMENT OF NANOSTRUCTURED POLYMERIC SYSTEMS BASED ON REVERSIBLE ADDITION-FRAGMENTATION CHAIN-TRANSFER (RAFT) POLYMERIZATION

The study presented in this chapter was developed at the Max-Planck-Institut für Polymerforschung, in Mainz, Germany, under the supervision of Professor Katharina Landfester and Dr. Calum Ferguson. This period abroad was part of a “sandwich-PhD” program, funded by CNPq. In this work, we exploited thermal and photo polymerization mediated RAFT aqueous dispersion of HPMA, NIPAM, and BzMA to prepare a series of diblock copolymer nano-objects via aqueous PISA (Scheme 1). Two different RAFT agents were evaluated, and poly(glycerol monomethacrylate) (PGMA) and poly(N,N-dimethylacrylamide) (PDMA) were chosen as the macro-RAFT agents. The effects of reaction parameters on thermal and photo-PISA were studied in detail.

Scheme 1 - Steps to produce nano-objects via RAFT-PISA polymerization.



5.1 MATERIAL AND METHODS

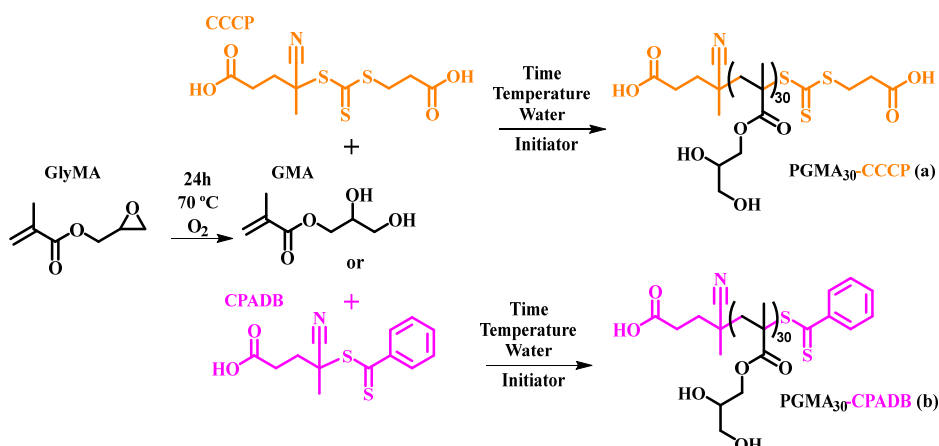
5.1.1 Chemicals

Hydroxypropyl methacrylamide (HPMA, 97%), Glycidyl methacrylate (GlyMA, 97%), N,N-Dimethylacrylamide (DMA, 99%), N-isopropyl acrylamide (NIPAM, 97%) and Benzyl methacrylate (BzMA, 98%) from Sigma-Aldrich were used as monomers. Triethylamine (TEA, $\geq 99.5\%$) from Sigma-Aldrich was used as a reducing agent. 4,4'-Azobis(4-cyanovaleric acid) (ACVA, $\geq 98\%$) from Sigma-Aldrich and 4-cyano-4-(phenylcarbono thioylthio)pentanoic acid 2,2'-Azobis[2-(2-imidazolin-2-yl)propane]dihydrochloride (AIPD) from Tokyo Chemical Industry, Ltd (Tokyo, Japan) were used as initiator in Thermal PISA. 4-Cyanopentanoic acid dithiobenzoate (CPADB, $\geq 95\%$) and 4-(((2-carboxyethyl) thio)carbonothioyl)thio-4-cyanopentanoic acid (CCCP, $\geq 95\%$) from Sigma-Aldrich were used as RAFT agents. Deuterated Dimethyl sulfoxide (DMSO, 95.5%) and Deuterium oxide (D₂O, 99.9%) from Sigma-Aldrich were used as solvents for the ¹H NMR analysis. All chemicals used were of analytical grade. All the chemicals and solvents were used without purification. Millipore quality (18.2 MΩcm) water was used throughout.

5.1.2 Synthesis and purification of PGMA_n and PDMA_n macro-CTAs

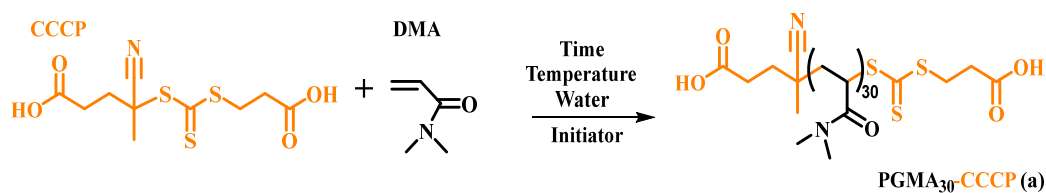
A typical protocol adapted from the one described by Ratcliffe; Ryan, and Armes (2013) for the synthesis of PGMA_n macro-CTA (Scheme 2) is given as follows: initially, the GMA monomer (0.014 mol, 2.00 g) is oxidized at 70 °C overnight to open the epoxy ring and form the glycerol methacrylate in a 40 mL flask equipped with a septum and magnetic stirrer. In sequence, the CPADB or CCCP RAFT agent (0.28 mmol, 0.086 g), and water (21.00 g, to make a 10% w/w solution) were added aiming at a target degree of polymerization (DP) of 50. To this, ACVA initiator (0.056 mmol, 0.016 g, CTA/Initiator molar ratio = 1.0) was added and the resulting pink solution using CPADB and yellow solution using CCCP was sparged with N₂ for 10 min before the sealed flask was immersed in a bath set at 70 °C. The polymerizations were quenched by immersion of the flask in an ice bath and opening it to air. The solution was then purified by dialysis (regenerated cellulose MWCO 1kDa) for 48 h with 2–3 water changes per day and freeze-dried.

Scheme 2 - Syntheses of PGMA macro-CTAs with CCCP (a) and CPADB (b) RAFT agents.



For the synthesis of PDMA_n macro-CTA a typical protocol adapted from the one described by Ma et al., (2017) (Scheme 3) is given: DMA monomer (20 mmol, 2.00 g), CCCP RAFT agent (0.40 mmol, 0.124 g), ACVA initiator (0.081 mmol, 0.022 g, CTA/Initiator molar ratio = 1.0) and water (21.00 g, to make a 10% w/w solution) were added in a 40 mL flask equipped with a septum and magnetic stirrer and the resulting yellow solution was sparged with N₂ for 10 min before the sealed flask was immersed into a bath set at 70 °C. The polymerization was quenched by immersion of the flask in an ice bath and opening it to air. The solution was then purified by dialysis (regenerated cellulose MWCO 1kDa) for 48 h with 2–3 deionized water changes per day and freeze-dried.

Scheme 3 - Synthesis of PDMA macro-CTA with CCCP RAFT agent.



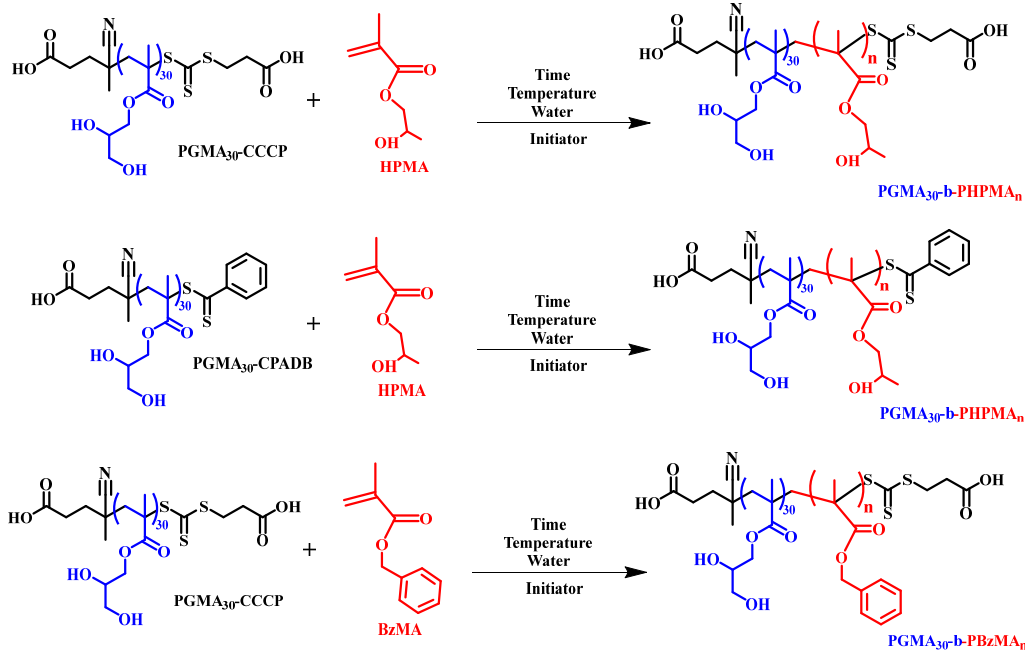
5.1.3 Thermally initiated aqueous RAFT dispersion polymerization to form diblock copolymers

5.1.3.1 Synthesis of PGMA₃₀-b-PHPMA_n and PGMA₃₀-b-PBzMA_n diblock copolymer nanoparticles

A typical protocol adapted from the one described by Blanazs; Ryan; Armes, (2012), and Cunningham et al., (2014) for the syntheses of PGMA₃₀-b-PHPMA_n and PGMA₃₀-b-

PBzMA_n diblock copolymers (Scheme 4) is as follows: PGMA_n macro-CTA (0.200 g) was added to a 40 mL vial equipped with a septum, followed by HPMA or BzMA monomer with a target degree of polymerization (DP) of 50 to 400 and water (varying amounts to result in solids contents varying between 2.5 to 15% w/w). ACVA or AIPD was then added (CTA/ACVA molar ratio = 1.0) and the solution was sparged with N₂ for 10 min. The flask was sealed and immersed in a bath set at 70 °C for ACVA or 45 °C for AIPD. The reaction medium was magnetically stirred for completing monomer conversion and the polymerization was subsequently quenched by exposure to air. Monomer conversions were determined via ¹H NMR and molecular weight distributions were analyzed via GPC. Aliquots of polymer were taken and diluted with water to an appropriate concentration for DLS analysis.

Scheme 4 - Syntheses of PGMA₃₀-b-HPMA_n and PGMA₃₀-b-BzMA_n diblock copolymer nano-objects via thermally initiated PISA in water.

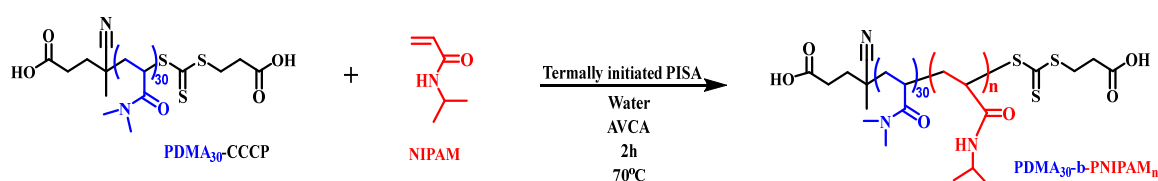


5.1.3.2 Synthesis of PDMA_n-b-PNIPAM_n diblock copolymer nanoparticles

A typical procedure adapted from the one described by Ma et al., (2017) to synthesize PDMA₃₀-b-PNIPAM_n diblock copolymers (Scheme 5) ([M] : [macroRAFT] : [initiator] = 50 to 200 : 1 : 0.2) by aqueous RAFT PISA polymerization with 10 wt% solids content was set up. PDMA₃₀ macro-CTA (0.200 g) was added to a 40 mL round-bottomed flask, followed by NIPAM monomer (DP 50 to 200), and water (solids content 10% w/w). ACVA was then added (CTA/ACVA molar ratio = 1.0) and the solution was sparged with N₂ for 10 min. The flask was

sealed and immersed in a bath set at 70 °C. The reaction medium was magnetically stirred for completing monomer conversion and the polymerization was subsequently quenched by exposure to air. Monomer conversions were determined via ^1H NMR and molecular weight distributions were analyzed via GPC. Aliquots of polymer were taken and diluted with water to an appropriate concentration for DLS analysis. The resulting solution was dialyzed against deionized water multiple times (regenerated cellulose MWCO 3.5 kDa) for 48 h to yield the desired polymer.

Scheme 5 - Synthesis of the PDMA₃₀-b-PNIPAM_n nano-assemblies by RAFT polymerization.



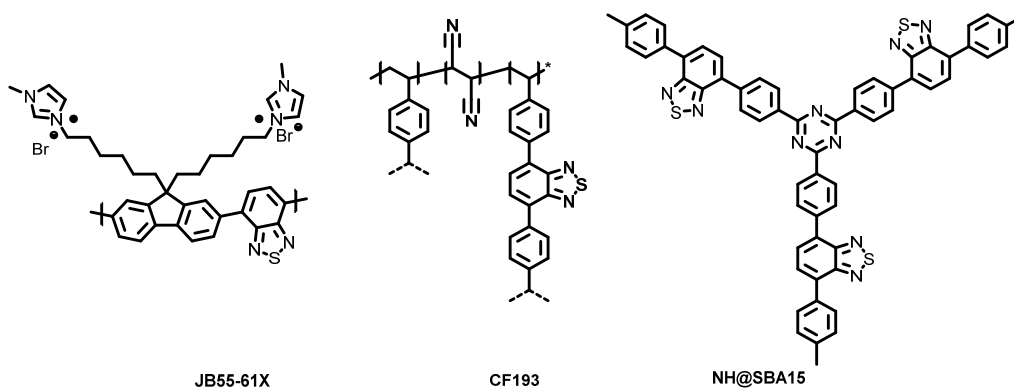
5.1.4 Photocatalysis aqueous RAFT dispersion polymerization of diblock copolymer

5.1.4.1 Synthesis of PGMA₃₀-b-PHPMA_n and PGMA₃₀-b-PBzMA_n diblock copolymer nanoparticles

A typical procedure adapted from the one described by He et al., (2018) to synthesize PGMA_n-b-PHPMA_n and PGMA_n-b-PBzMA_n block copolymers ([M] : [macroRAFT] : [photocatalyst] : [TEA] = 100 to 600 : 1 : 0.01 : 0 to 1) by aqueous RAFT PISA photopolymerization and 10 wt% solids content was set up as follows: PGMA, HPMA or BzMA, photocatalyst (1 wt% related to the macro-CTA), TEA were dissolved in deionized water in a glass vial. The glass vial was sealed with a rubber septum and purged with nitrogen for 10 min. The vial was then irradiated with blue LED light (0.16 W cm⁻², λ 460 nm) at room temperature for completing monomer conversion, before it was quenched by exposure to air and stored in the dark. Conversion of HPMA and BzMA were determined via ^1H NMR. GPC analyses were performed to determine the molecular weight of the samples. Aliquots of polymer were taken and diluted with water to an appropriate concentration for DLS analysis.

All the employed photocatalysts, Figure 45, were synthesized by the Landfester Group at Max-Planck Institute for Polymer: JB55-61X (BYUN; LANDFESTER; ZHANG, 2019), CF193 (FERGUSON et al., 2020), and NH@SBA15 (HUANG et al., 2016, 2017).

Figure 45 - Photocatalysts used for PET-RAFT polymer synthesis.



To start we investigated the synthesis of the second block studying the reaction kinetics and polydispersity. The hydrophilic block was produced by classical thermal RAFT polymerization with the best RAFT agent that promoted good polymerization control. The chain extension of the hydrophilic block was then performed with the best monomer candidate for the hydrophilic block which provided high molecular weight and low D .

5.1.5 Characterization

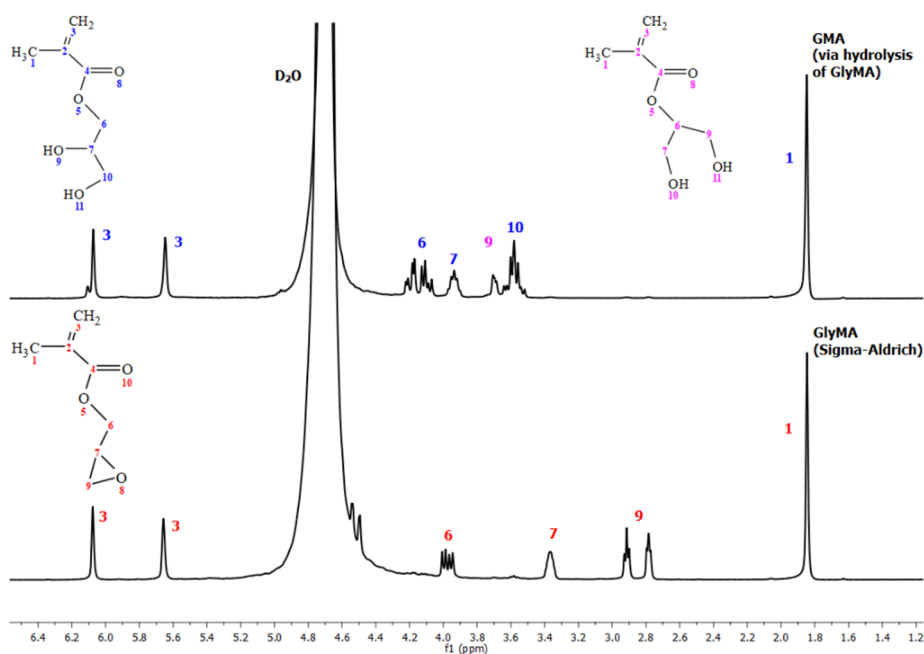
Molecular weight distributions were determined by Gel Permeation Chromatography (GPC) using tetrahydrofuran (THF) or dimethylformamide (DMF) as the mobile phase. The GPC system was a PSS Security of Agilent Technologies 1260 Infinity and was calibrated with a series of poly(methyl methacrylate) (PMMA) M_p 800 to 182,000 g mol^{-1} . **Chemical compositions and conversions were analyzed by** Nuclear Magnetic Resonance (NMR) spectroscopy on a Bruker Advance III with SampleXpress operating at 300 MHz for ^1H using D_2O or DMSO as solvent. Data was reported as chemical shift (δ) measured in ppm. **Intensity average particle diameters and dispersion were measured by** Dynamic Light Scattering (DLS) using a Malvern Zetasizer NanoZS instrument at 25 °C and a fixed scattering angle of 173°. Studies were performed on count rate kept in between 100 and 500 kcps, thereby highly diluting the nanoparticles dispersions, leading to almost translucent samples. All data were averaged over two consecutive runs. **Particle morphology was determined by** Transmission Electron Microscopy (TEM, Jeol 1400) by placing a drop of diluted nanoparticles dispersion onto a 300-mesh carbon-coated copper grid and drying under ambient conditions.

5.2 RESULTS AND DISCUSSION

5.2.1 Synthesis of PGMA_n and PDMA_n macro-CTAs

According to Ratcliffe; Ryan and Armes (2013), GlyMA can be converted into GMA via hydrolysis in deionized water (10% w/w) in the absence of any catalyst. One of the reasons for that, GMA is a relatively expensive specialty monomer and GlyMA is a commodity monomer, being this a highly cost-effective, purely aqueous route to prepare diblock copolymer nano-objects. Herein, we synthesized the GMA monomer according to the reference, and the GMA monomer was directly polymerized *in situ* via RAFT aqueous solution polymerization to produce a PGMA macro-CTA, which can be subsequently chain-extended with other monomers. Figure 46 shows the ¹H NMR spectra of GMA and GlyMA, demonstrating the full transformation of GlyMA to GMA. In addition, no hydrolysis of the ester or polymerization was observed during this process.

Figure 46 - ¹H NMR spectra of glycerol monomethacrylate (GMA, prepared via hydrolysis of glycidyl methacrylate at 10% w/w) and commercial glycidyl methacrylate (GlyMA, Sigma-Aldrich) in D₂O.

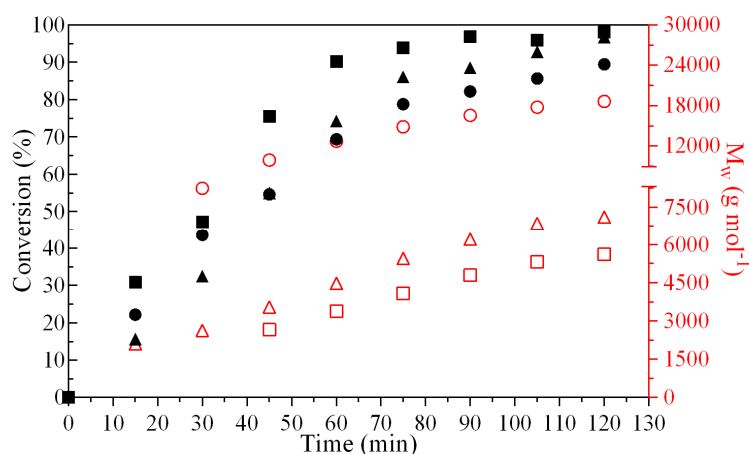


The PGMA macro-CTA was synthesized using CCCP or CPDAB, as commercially available RAFT agents, via RAFT polymerization in deionized water at 70 °C with ACVA as the initiator. These RAFT agents were chosen since providing good control over the

polymerization of more activated monomers (methacrylates and methacrylamides) (MOAD, 2019b). The final composition of PGMA was determined by checking the GMA conversion by ^1H NMR spectroscopy and denoted as PGMA₃₀-CCCP, PGMA₆₀-CCCP or PGMA₃₀-CPADB, depending on the type of RAFT agent and the amount of GMA used. A CTA/initiator molar ratio of 1.0 was selected to ensure a sufficiently fast but controlled homopolymerization.

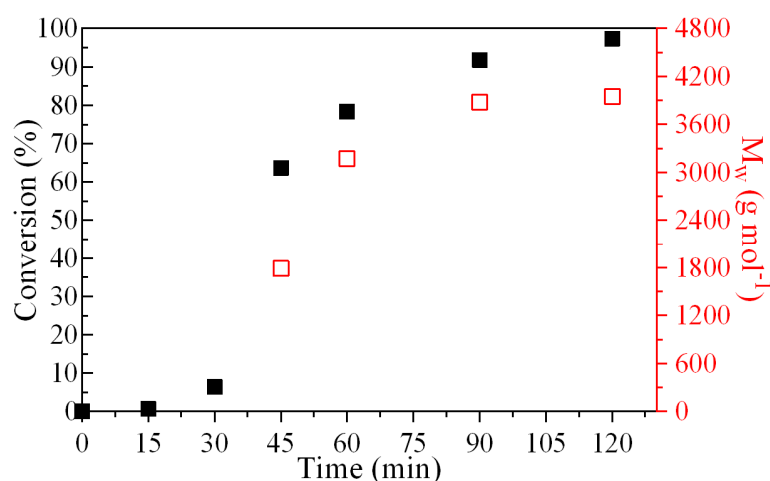
The GMA polymerization was quenched by exposure to air when 60-70% monomer conversion was achieved, in order to avoid monomer-starved conditions and therefore ensure retention of the RAFT end-groups (RODLERT et al., 2000). The kinetics were evaluated to ensure this desired monomer conversion (Figure 47). Samples extracted at different times were also analyzed by GPC solubilized in DMF and using PMMA standards, which confirmed the linear evolution of the weight average molecular weight (M_w) with monomer conversion. The crude macro-CTAs were subsequently purified by dialysis and dried. The reaction was quenched after 45 min for PGMA₃₀-CCCP, 60 min for PGMA₆₀-CCCP, and PGMA₃₀-CPDAB, ^1H NMR studies indicated 57%, 69%, and 71% conversion, respectively. These PGMA macro-CTAs had a M_w of 5325.74 g mol⁻¹, D of 1.43; M_w of 12731.60 g mol⁻¹, D of 1.47; and M_w of 5846.99 g mol⁻¹, D of 1.42, respectively. PGMA macro-CTAs possessed narrow molecular weight distributions ($D \leq 1.47$), indicating that good control was achieved during the RAFT solution polymerization of GMA. Moreover, this synthetic protocol also led to high RAFT end-group fidelity, which is important to enable a relatively high blocking efficiency to be achieved on the addition of the other monomers. This is essential for the synthesis of well-defined diblock copolymers.

Figure 47 – Evolution of monomer conversion and weight average molecular weight with reaction time during the syntheses of three macro-CTAs, PGMA₃₀-CCCP (squares), PGMA₆₀-CCCP (circles) and PGMA₃₀-CPADB (triangles) at 70 °C via RAFT aqueous dispersion polymerization with ACVA as initiator.



Another macro-CTA, the PDMA-CCCP, was synthesized using CCCP as RAFT agent via RAFT polymerization in deionized water at 70 °C with ACVA as the initiator. The DMA polymerization also was quenched by exposure to air when 60-70% monomer conversion was achieved, and the kinetics were utilized to ensure this desired monomer conversion (Figure 48). Again, M_w values presented a linear increase with monomer conversion. The final conversion of DMA was determined by ^1H NMR spectroscopy and denoted as PDMA₃₀-CCCP. The reaction was quenched after 60 min and ^1H NMR studies indicated 60% of conversion. The crude macro-CTAs were subsequently purified by dialysis and dried. This PDMA macro-CTA had an M_w of 3173 g mol^{-1} and D of 1.20 was then chain-extended with NIPAM via RAFT dispersion polymerization in deionized water.

Figure 48 – Evolution of monomer conversion and weight average molecular weight with reaction time curves during the syntheses of macro-CTA, PDMA-CCCP at 70 °C via RAFT aqueous dispersion polymerization with ACVA as initiator.



5.2.2 Thermally initiated aqueous RAFT dispersion polymerization to form diblock copolymers

5.2.2.1 Syntheses of PGMA₃₀-b-HPMA_n and PGMA₃₀-b-PBzMA_n diblock copolymer nanoparticles

The PGMA macro-CTA was subsequently chain-extended with HPMA or BzMA. Then, aqueous PISA of HPMA was performed using PGMA₃₀-CCCP or PGMA₃₀-CPADB as the macro-RAFT as produced by thermal initiation. Table 8 summarizes the various polymers prepared in this study. The polymerizations were conducted from 2.5 to 12.5% w/w solids. A

range of DPs was targeted for the PHPMA block (50 to 400), with DMF or THF GPC molecular weights are shown in the Table. Most polymerizations attained more than 90% conversion as judged by ^1H NMR, which indicated high blocking efficiencies. A high molecular weight shoulder was observed, which becomes more prominent when targeting higher PHPMA DPs. The PGMA-b-PHPMA diblock copolymer molecular weight increased linearly with target DP and the copolymers had relatively high polydispersities (\mathcal{D} of 2.17 for PHPMA target DP of 400). These results are in agreement with the data obtained by Li and Armes (2010) for the syntheses of branched PHPMA involving a similar system.

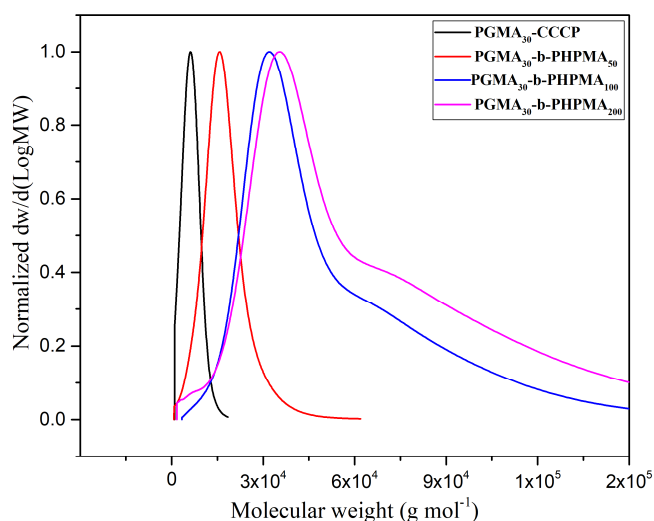
Table 8 - Aqueous RAFT-PISA polymerizations of different systems thermally initiated upon varying solids contents and monomer types and concentrations (DP).

Macro-RAFT agent	Monomer (DP)	Initiator (ratio)	Solids Content (wt. %)	Time (min)	^a Conversion (%)	^b M_w	^b \mathcal{D}	d (nm)
PGMA ₃₀ (CCCP)	HPMA (100)	ACVA (0.2)	10	90	92	40987	1.37	745
PGMA ₃₀ (CCCP)	HPMA (100)	AIPD (0.2)	10	180	97	23881	1.82	288
PGMA ₃₀ (CPADB)	HPMA (100)	ACVA (0.2)	10	120	87	26212	1.59	173
PGMA ₃₀ (CPADB)	HPMA (100)	AIPD (0.2)	10	90	90	33525	1.34	2123
PGMA ₃₀ (CCCP)	HPMA (50)	ACVA (0.2)	10	105	93	14795	1.50	60
PGMA ₃₀ (CCCP)	HPMA (100)	ACVA (0.2)	15	180	95	28536	1.54	4329
PGMA ₃₀ (CCCP)	HPMA (100)	ACVA (0.2)	12.5	180	97	24293	1.39	618
PGMA ₃₀ (CCCP)	HPMA (100)	ACVA (0.2)	2.5	180	91	27846	1.18	276
PGMA ₃₀ (CCCP)	HPMA (200)	ACVA (0.2)	2.5	240	93	55653	1.22	210
PGMA ₃₀ (CCCP)	HPMA (200)	ACVA (0.2)	5	150	96	32626	1.38	202
PGMA ₃₀ (CCCP)	HPMA (200)	ACVA (0.2)	10	60	67	48462	1.9	776
PGMA ₃₀ (CCCP)	HPMA (200)	ACVA (0.2)	12.5	180	97	48621	1.51	2475
PGMA ₃₀ (CCCP)	HPMA (400)	ACVA (0.2)	10	120	69	24376	2.17	617
PGMA ₆₀ (CCCP)	HPMA (100)	ACVA (0.2)	10	1440	90	213360	1.55	102
PGMA ₃₀ (CCCP)	BzMA (100)	ACVA (0.2)	10	240	90	28679	1.74	47
PGMA ₃₀ (CCCP)	BzMA (200)	ACVA (0.2)	10	240	73	52030	1.45	70

^aMonomer conversion determined by ^1H NMR spectroscopy. ^bMolecular weight and polydispersity determined by GPC using PMMA standards.

Figure 49 shows the molecular weight distribution of the same samples analyzed by GPC. The samples synthesized using PGMA-CCCP as macro-CTA and HPMA as monomer showed a narrower molecular weight distribution, while the use DP > 50 generated samples with wider molecular weight distribution. As explained in the literature the high polydispersities resulted due presence of HPMA monomer contaminated with low levels of dimethacrylate impurity that is slowly formed by transesterification during storage. The presence of this bifunctional comonomer in these syntheses means that the PHPMA particles are lightly cross-linked which results in light branching of the PHPMA chains (BLANAZS et al., 2011). Molecular weight distribution indicated a progressive increase in molecular weight during the synthesis of the diblock copolymers (Figure 49). Clearly, the \bar{D} values obtained throughout this study (\bar{D} = 1.34 to 2.17) are generally higher than those normally reported for RAFT aqueous emulsion polymerization syntheses (\bar{D} between 1.05 and 1.3) (PERRIER, 2017). However, there are several literature reports that also report relatively broad molecular weight distributions for such PISA formulations (CHADUC et al., 2013; COCKRAM et al., 2018).

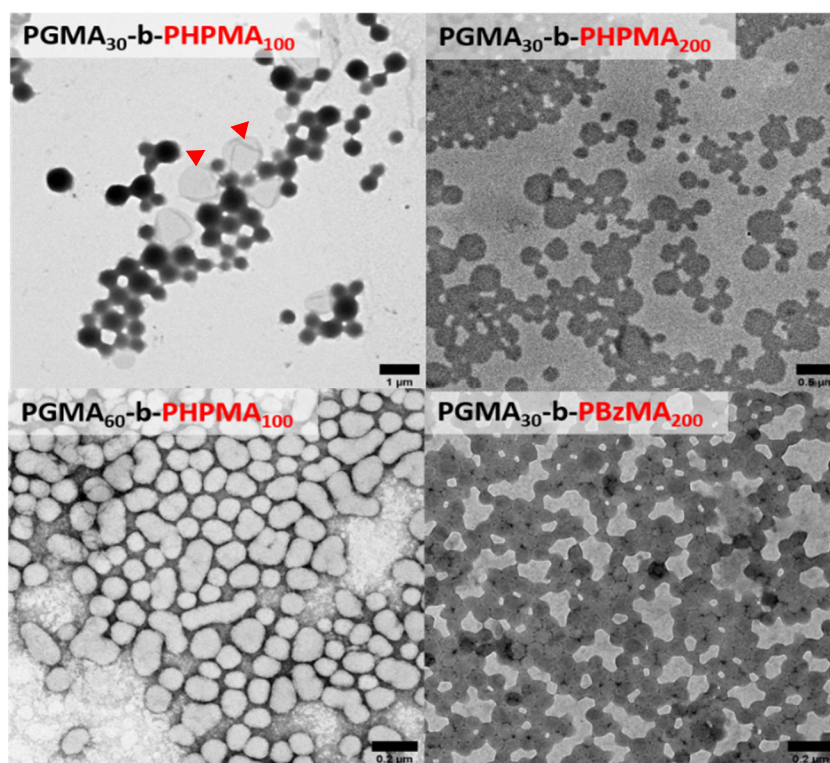
Figure 49 - Molecular weight distribution of a PGMA₃₀-CCCP macro-CTA and a series of PGMA₃₀-b-PHPMA_y diblock copolymers synthesized at 10% w/w solids at 70 °C. A macro-CTA/ACVA molar ratio of 1.0 was used in all cases.



TEM images (Figure 50) suggested that self-assembly occurred in these syntheses. It was concluded that PHPMA and PBzMA are suitable core-forming blocks for successful RAFT aqueous dispersion polymerization. The PGMA₃₀-b-PHPMA₁₀₀ diblock copolymer dispersion was only weakly turbid and exhibited a medley of spherical and vesicle (red arrowheads, Figure 50) morphology. A mixed-phase of spheres and worms was observed for PGMA₆₀-b-

PHPMA₁₀₀, which was also slightly more viscous than the other samples. Images of PGMA₃₀-b-PHMA₂₀₀ and PGMA₃₀-b-PBzMA₂₀₀ displayed spheres.

Figure 50 - TEM images of RAFT-PISA nano-objects of PGMA_n-P(HPMA_n) and PGMA₃₀-P(BzMA₂₀₀) diblock copolymers synthesized at 10% w/w solids at 70 °C. A macro-CTA/ACVA molar ratio of 1.0 was used in all cases.



5.2.2.2 Synthesis of PDMA_n-b-PNIPAM_n diblock copolymer nanoparticles

CCCP was utilized as CTA to mediate RAFT polymerization of DMA monomer, and the synthesized PDMA₃₀-CCCP homopolymers were then applied as macro-CTA to mediate RAFT polymerization of NIPAM monomer using ACVA as the initiator. The experiment was performed to check if it was possible to use PDMA₃₀-CCCP as macro-CTA to obtain PDMA-b-PNIPAM chains with high M_w and low polydispersity, as observed for GMA homopolymer. Kinetics for PDMA-b-PNIPAM block copolymers with a 30/200 monomer molar ratio is shown in Figure 51. The M_w values increase linearly until 80% conversion, reaching 30 000 g mol⁻¹ with $D < 1.20$. Above 80% conversion, M_w values are slightly smaller than the targeted ones, and the polydispersity increases, probably due to the presence of irreversible transfer and termination reactions. Other diblock copolymers with DP 50 to 200 achieved M_w ranging from

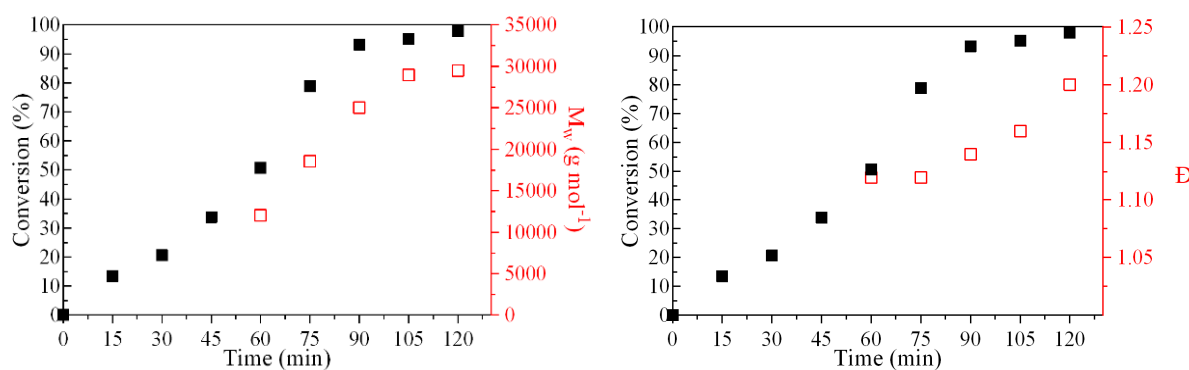
6000 to 32,000 g/mol with low dispersity, as can be seen in Table 9. These results confirm the well-controlled RAFT polymerization.

Table 9 – Aqueous RAFT-PISA polymerizations with PDMA-CCCP as the macro-CTA to mediate polymerization of NIPAM at 70 °C in deionized water using ACVA as initiator and varying NIPAM concentration.

Polymer	Time (min)	^a Conversion (%)	^b M _w	^b D	d (nm)
PDMA ₃₀ -CCCP	60	64	1791	1.28	^c ND
PDMA ₃₀ -b-PNIPAM ₅₀	60	95	6055	1.28	^c ND
PDMA ₃₀ -b-PNIPAM ₁₀₀	60	94	17133	1.57	50
PDMA ₃₀ -b-PNIPAM ₂₀₀	90	96	31190	1.22	228

^aMonomer conversion determined by ¹H NMR spectroscopy. ^bMolecular weight and polydispersity determined by GPC using PMMA standards.

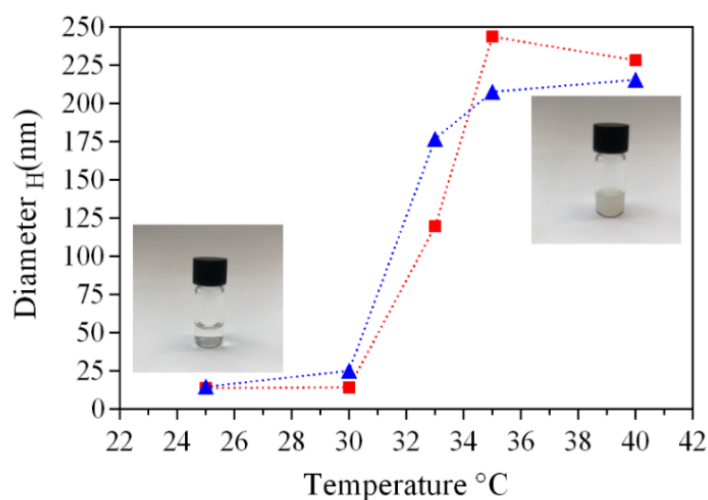
Figure 51 - Evolution of monomer conversion, weight average molecular weight (M_w, left) and polydispersity (D, right) with time during NIPAM block polymerization at 70 °C in deionized water with ACVA as initiator, Monomer DP200.



PNIPAM is a thermoresponsive polymer with a coil-globule transition at ~32 °C (CHEN et al., 2017). Consequently, the PNIPAM-containing block copolymers in solution display temperature-driven self-assembly, being widely studied. The main application is for drug delivery (GUPTA et al., 2014; MA et al., 2017). Regarding an experimental observation of PDMA-b-PNIPAM diblock copolymer synthesized in this research, transparent solutions promptly became turbid when the temperature was switched from room temperature to 40 °C. Figure 52 shows the effect of temperature on the particle size in the range of 25–40 °C. From 25 to 30 °C the particle diameter underwent small changes, but in the 30–35 °C range, the particle size increased dramatically from 19 to 228 nm. In the range of 35–40 °C, the particle size remained stable. These results indicate the temperature sensitive behavior of these nanospheres. PNIPAM segments are in a state of complete dissolution and stretching when the temperature is below 32 °C. As a result, the DLS-based size of the nanospheres is smaller. When the temperature is raised to the lower critical solution temperature (LCST) (~32 °C) of

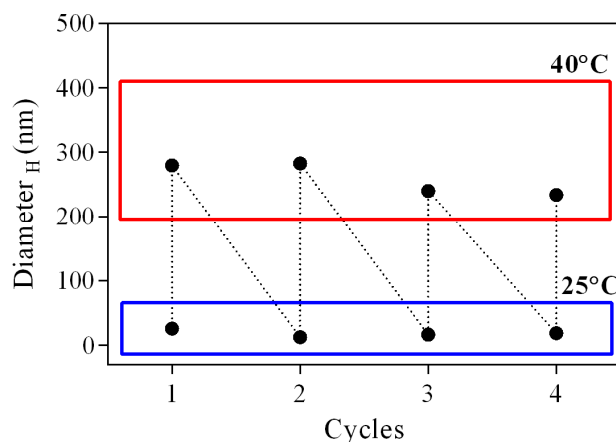
PNIPAM segments aggregate and the population of larger sized aggregates grows. Thus, an important characteristic of a polymeric solution undergoing a volume phase transition. This phenomenon was explained by Zhou et al. (2021) for a similar system, at temperatures above ~ 32 °C, the hydrogen bonds between PNIPAM and water molecules are broken, the hydrophilic chain shrinks and becomes hydrophobic due to the van der Waals forces, hydrogen bond force, and so on, and the polymer changes from the dissolved state to a core-shell structure with PNIPAM as the core, and PDMA as the shell. Therefore, the particle size and light scattering intensity increase, and the dispersion becomes uniform.

Figure 52 - Z-average particle size as a function of temperature for PDMA₃₀-b-PNIPAM₂₀₀ of Mw = 31190 g mol⁻¹ obtained from cumulant fits. Concentration 10 mg mL⁻¹. Heating step (red), Cooling step (blue). The lines connecting the experimental points are only guides for the eyes.



The volume phase transition of PDMA-b-PNIPAM nano-objects is fully reversible and can be switched back and forth between its collapsed and water-swollen states by sequential heating and cooling cycles above and below the LCST. This behavior is summarized in Figure 53 where consecutive heating and cooling cycles between 25 and 45 °C result in the reversibility of the nano-objects between ~ 280 and ~ 234 nm. This reversibility plays a critical role in some applications such as drug delivery, which uses swelling and deswelling as a mechanism to load and release therapeutic agents (TRONGSATITKUL; BUDHLALL, 2013).

Figure 53 - Z-average particle size as a function of the number of heating-cooling cycles, between 25 and 40 °C for PDMA₃₀-b-PNIPAM₂₀₀ of $M_w = 31190 \text{ g mol}^{-1}$ obtained from cumulant fits. Concentration 10 mg mL^{-1} . The lines connecting the experimental points are only guides for the eyes.



5.2.3 PET-RAFT dispersion polymerization to form diblock copolymers

5.2.3.1 Syntheses of PGMA₃₀-b-PHPMA_n and PGMA₃₀-b-PBzMA_n diblock copolymer nanostructures

To investigate the performance of different photocatalysts for PET-RAFT polymerization synthesized by Landfester group from Max-Planck Institute (Figure 45), we used PGMA₃₀-CCCP and PGMA₃₀-CPADB as the macro-CTAs to mediate RAFT polymerization of HPMA. The polymerizations were performed with 10 wt % solids content using deionized water as the solvent, under blue LED irradiation. Table 10 summarizes the various polymers prepared in this study. A range of DPs was targeted for the PHPMA block. Most polymerizations attained more than 90% conversion as judged by ¹H NMR, which indicates high blocking efficiencies. High molecular weights were observed, which becomes more prominent when targeting higher PHPMA DPs. The system with PGMA-b-PHPMA worked better with PGMA-CCCP compared to PGMA-CPADB as macro-CTAs. A visual inspection of the final aqueous dispersions using PGMA-CPADB as macro-CTA revealed precipitated polymer that affected the increase in polydispersity which confirms the low polymerization control.

To increase the reaction rates, it was necessary to add a reducing agent, triethylamine (TEA). Recent work in polymer synthesis (XU et al., 2015; ZAQUEN et al., 2019b) has reported that the addition of TEA improves the reaction yield. For instance, Shanmugam and

co-workers showed that TEA is an excellent reducing agent for the initiation of a free radical polymerization under light (SHANMUGAM; XU; BOYER, 2017). Thus, the effect of the addition of a small amount of TEA in the previous reaction (i.e. [PGMA₃₀ (CCCP) DP100 JB55-61X]) was evaluated. In the presence of TEA, it was evident that the apparent propagation rates increased resulting in higher monomer conversions and molecular weights (Table 10 entries gray lines).

Table 10 - PET-RAFT polymerizations catalyzed by different photocatalysts in deionized water irradiated by blue LED varying Macro-CTAs, monomer concentrations (DP) and with or without reducing agent.

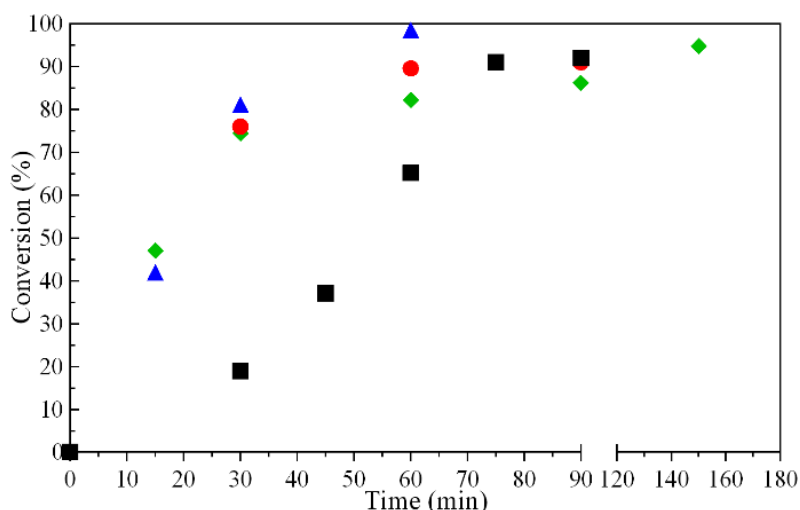
Macro-CTA	DP	Photocatalyst (ratio)	Reducing agent	Time (min)	^a Conversion (%)	^b M _w	^b Đ	d (nm)
PGMA ₃₀ (CCCP)	100	JB55-61X (0.01)	-	120	51	5174	1.66	^c ND
PGMA ₃₀ (CPADB)	100	JB55-61X (0.01)	-	120	40	10082	1.30	73
PGMA ₃₀ (CCCP)	100	JB55-61X (0.05)	-	60	82	3720	1.93	^c ND
PGMA ₃₀ (CPADB)	100	JB55-61X (0.05)	-	1380	60	10681	1.48	^c ND
PGMA ₃₀ (CCCP)	100	JB55-61X (0.01)	TEA	90	93	9903	1.37	298
PGMA ₃₀ (CCCP)	200	JB55-61X (0.01)	TEA	90	91	67619	2.68	1620
PGMA ₃₀ (CPADB)	200	JB55-61X (0.01)	TEA	1380	58	4153	2.18	1319
PGMA ₃₀ (CCCP)	400	JB55-61X (0.01)	TEA	60	84	207094	3.56	^c ND
PGMA ₃₀ (CCCP)	600	JB55-61X (0.01)	TEA	60	90	191954	2.23	158
PGMA ₃₀ (CCCP)	200	CF193 (0.01)	TEA	60	98	66378	1.96	20
PGMA ₃₀ (CCCP)	400	CF193 (0.01)	TEA	120	77	273559	3.32	26
PGMA ₃₀ (CCCP)	600	CF193 (0.01)	TEA	120	84	179951	2.96	33
PGMA ₃₀ (CCCP)	100	NH (0.01)	TEA	150	97	26470	1.48	12
PGMA ₃₀ (CPADB)	200	NH (0.01)	TEA	1440	91	36839	3.71	247
PGMA ₃₀ (CCCP)	200	NH (0.01)	TEA	1440	94	68051	1.81	99
^d PGMA ₃₀ (CCCP)	200	NH (0.01)	TEA	1440	99	464835	2.50	147

Experimental conditions: solvent = water; light source = blue LED light (λ_{\max} = 460 nm, 0.16 mW cm⁻²); [CTA]:[TEA] 1:1. Monomer = HPMA. Solids content 10 wt.%. ^aMonomer conversion determined by ¹H NMR spectroscopy. ^bMolecular weight and polydispersity determined by GPC using PMMA standards. ^cND-not detected. ^d System: water + ethanol 50:50 w/w, monomer: BzMA.

A visual inspection of the final aqueous dispersions using the photocatalyst CF193 indicated a progressive increment in turbidity as the DP of the HPMA core-forming block was increased. It suggests a systematic variation in the size and/or morphology of the colloidal PGMA₃₀-b-PHPMA_n nano-objects prepared under these conditions (WARREN; ARMES, 2014). This was confirmed by DLS analyses (Table 10). For PGMA₃₀-b-PHPMA₆₀₀, an increase in the mean diameter (33 nm) was observed, indicating a possible change in nanoparticle morphology due to the greater volume fraction of the hydrophobic block.

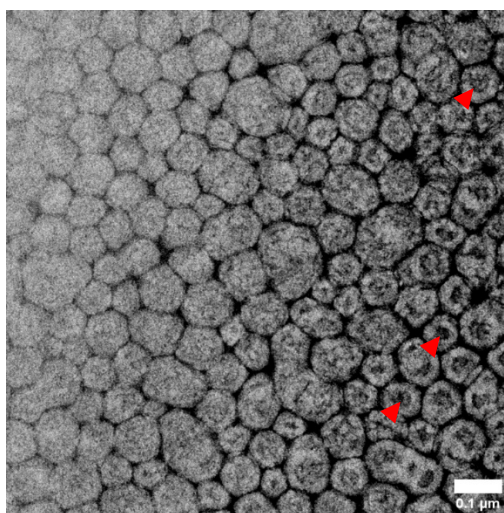
Kinetic plots for aqueous PISA of HPMA at a 10% w/w HPMA concentration using PGMA₃₀-CCCP as the macro-RAFT agent (target degree of polymerization (DP) of 100 and 200) are shown in Figure 54. It is possible to verify that the rate of polymerization of photo-PISA was much higher than that of thermally initiated PISA with $\geq 74\%$ monomer conversion being reached within 15 min under light irradiation. In contrast, 60 min was required to achieve high monomer conversion for the thermally initiated PISA. The fast polymerization behavior of aqueous photo-PISA can be attributed to the rapid initiation of photocatalyst under 460 nm visible light irradiation. Tan et al. (2017) reported that this behavior can be associated with the half-life of ACVA (~ 10 h at 70 °C) which is much longer than that of the photocatalysts tested, even though they are different from those tested in this work. However, UV-vis absorbance spectra of the photocatalysts tested under 460 nm visible light irradiation at different times are necessary to prove this hypothesis.

Figure 54 - Evolution of monomer conversion during thermally initiated (70 °C) and photoinitiated (25 °C) PISA of HPMA in deionized water using PGMA₃₀-CCCP as the macro-RAFT agent at a 10% w/w solids content and the target DP of 100 and 200. Thermally initiated with ACVA, DP 100 (black); Photo-PISA with JB55-61X as photocatalyst, DP 200 (red); CF193 as photocatalyst, DP 200 (blue); NH@SBA15 as photocatalyst, DP 200 (green).



TEM images (Figure 55) suggest that self-assembly occurred in the synthesis of PGMA₃₀-b-PHPMA₂₀₀ using NH as photocatalyst under blue light irradiation. Pure vesicles were only obtained at a monomer concentration of 10% w/w with a DP of 200. For identification of vesicles in TEM images, vesicles usually do not stay spherical but collapse because of the evaporation of water (red arrowheads; Figure 55), then the drying vesicle flattens to a pancake-like shape (MEISTER; BLUME, 2017). The TEM image clearly confirmed the collapsed vesicular structure. Polymer vesicles have been widely investigated because of their stable hollow structure and potential for advanced chemical functionalization and physiological applications (DU; O'REILLY, 2011; IRVINE, 2011). They have been considered as an ideal drug delivery vehicle since both hydrophilic and hydrophobic drugs can be loaded either in the hydrophilic hollow cavity or the hydrophobic membrane in aqueous media (REN et al., 2012). DMF GPC measurement confirmed that diblock copolymers with relatively low polydispersities ($D < 1.81$) and high weight average molecular weight (68051 g mol^{-1}) were produced.

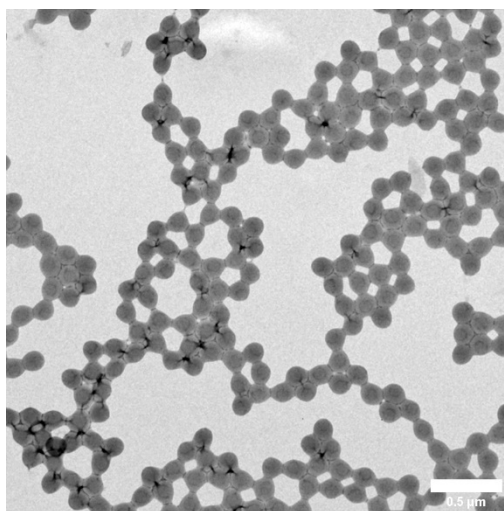
Figure 55 - Transmission electron microscopy (TEM) images of the vesicles observed during the synthesis of PGMA₃₀-b-PHPMA₂₀₀ via photocatalytic polymerization. Solvent: water; light source: blue LED light ($\lambda_{\text{max}} = 460 \text{ nm}$, 0.16 mW cm^{-2}); Photocatalyst: NH; reaction time: 24 hours.



In a similar approach utilizing BzMA as a hydrophobic core segment, PGMA₃₀-b-PBzMA₂₀₀ was synthesized via RAFT dispersion polymerization in alcohol/water mixtures, resulting in pure spheres (Figure 56). Full conversion was achieved with high molecular weight ($464835 \text{ g mol}^{-1}$). After 24 h, stable suspensions were obtained, which was attributed to the

slow polymerization of BzMA favoring nanoparticle rearrangement and, hence, leading to colloidal stability.

Figure 56 - Transmission electron microscopy (TEM) images of the nanoparticles observed during the synthesis of PGMA₃₀-b-PBzMA₂₀₀ via photocatalytic polymerization. Solvent: water:ethanol; light source :blue LED light ($\lambda_{\text{max}} = 460 \text{ nm}$, 0.16 mW cm^{-2}); Photocatalyst : NH; reaction time: 24 hours.



5.3 CONCLUSION

The growth of PGMA_n-b-PHPMA_n, PGMA_n-b-PBzMA_n, and PDMA_n-b-PNIPAM_n diblock copolymer nano-objects prepared by aqueous RAFT dispersion polymerization via photocatalytic or thermal initiation with different macro-RAFT agents has been studied in detail. Kinetic studies indicated that the aqueous photo-PISA was much faster than the thermally initiated PISA, reaching high conversion within only 15 min and with an average molecular weight up to 270000 g mol⁻¹.

We have successfully demonstrated the application of visible light-mediated PET-RAFT polymerization in a PISA dispersion process. Different photocatalysts and monomers were applied to generate nanoparticles of different morphologies, such as spherical and vesicles. We have found that polymerizing at room temperature generated pure vesicles, providing a useful method to produce this morphology. The ability to reproducibly generate exclusively vesicles has important implications for potential applications in drug delivery.

6 FINAL CONCLUSION

This work presents a biotechnological alternative to produce limonene oxide via epoxidation reactions mediated by a new low-cost immobilized lipase preparation from *Candida antarctica* (NS 88011). Yields above 70% were reached in organic solvents, at a low substrate concentration, and under moderate temperature. Results revealed that there are no major differences on the epoxidation reaction when using different support materials of the biocatalyst as Novozym 435 and NS 88011. This work showed for the first time a report of successful limonene oxide production by epoxidation reaction mediated by NS88011, presenting promising results of epoxide yield.

The copolymerization of limonene oxide with phthalic anhydride or maleic anhydride was performed by ring-opening polymerization catalyzed by ionic liquid (IL) BMI·Fe₂Cl₇. Conversions around 80% were reached at a catalyst:limonene oxide molar ratio of 1:100. The resulting polymer presented a perfectly alternating structure; number average molar mass over 1000 g mol⁻¹, and pendant double-bonds that allowed posterior modification of the polymer structure. Regarding their application, such as nanodevices for biological systems, poly(phthalic anhydride-*co*-limonene oxide) (PPALO) nanoparticles (NPs) were also produced and cross-linked with tetrathiol via thiol-ene reaction. The cross-linked PPALO-NPs with a number-weighted mean diameter of 56 nm, spherical morphology, and good colloidal stability were obtained. These NPs were tested for blood compatibility and cell viability, presenting potential for biomedical applications.

The synthesis of nanoparticles directly in water is desirable for a diverse range of applications, such as biomedical. In this Thesis water-soluble poly(glycerol monomethacrylate) (PGMA) and poly(N,N-dimethylacrylamide) (PDMA) macromonomer chain transfer agents (macro-CTAs) have been chain-extended with a range of core-forming monomers *via* Reversible Addition-Fragmentation chain Transfer (RAFT) aqueous polymerization to give diblock copolymers. Copolymers were prepared with a high degree of conversion (> 90%) for each block and the formation of spherical nanoparticles and vesicles was confirmed by transmission electron microscopy (TEM) analysis. Gel Permeation Chromatography (GPC) analysis confirmed that the RAFT polymerizations were well-controlled. These studies provide the basis for further high-throughput screening of RAFT mediated by polymerization induced self-assembly (PISA) formulations which are likely to be required for commercialization of this promising technology.

Based on the results exposed in this thesis, the synthesis of limonene oxide mediated by a new biocatalyst was possible. Moreover, the results of copolymerization via ROP and nanoparticles production were promising, as they increase the application spectrum of these polymers from renewable resources and there are no studies in the literature involving the nanoparticle formation with this polymer. In addition, RAFT polymerization provides a great method to produce nano-objects in an aqueous medium. Allied to this strategy, the photoinduced electron/energy transfer reversible addition-fragmentation chain transfer (PET-RAFT) polymerization has proven to be a powerful tool for synthesizing polymers in environmentally friendly conditions, requires low energy visible light, and opens the door to create several polymer architectures.

6.1 FURTHER WORK

Considering the obtained results in the present thesis, some ideas are presented to complement the work:

1. Study of the copolymerization of LO and PA or MA with different molar ratios of ionic liquid:monomer - 1: 250, 1:500; 1:750, 1:1000, and temperatures in polymerization reactions.
Aim: To find the best molar ratio of catalyst and temperature to achieve high monomer conversion and higher molecular weight.
2. Functionalization of NPs surfaces with protein by thiol-ene reactions.
Aim: To develop nanocarriers that enable the control of protein corona composition in biological fluids, leading to a longer circulation time in the body and consequently acting on specific cells.
3. Evaluate the effect of functionalized and non-functionalized NPs on cell uptake assays and cytotoxicity.
Aim: To examine the application potentials and confirm the modifications performed.
4. Evaluate the effect of *in situ* polymer growth within a synthetic cell.
Aim: To examine the use of light as a natural energy source to induce cellular growth employing PET-RAFT polymerization.

REFERENCES

- ABDULMALEK, E. et al. Chemoenzymatic Epoxidation of Alkenes and Reusability Study of the Phenylacetic Acid. **The Scientific World Journal**, v. 2014, p. 1–7, 2014.
- ADHVARYU, A.; ERHAN, S. Z. Epoxidized soybean oil as a potential source of high-temperature lubricants. **Industrial Crops and Products**, v. 15, n. 3, p. 247–254, 2002.
- AGNER, T. et al. Thermal performance of nanoencapsulated phase change material in high molecular weight polystyrene. **Polímeros**, v. 30, n. 2, p. 1–7, 2020.
- AHLUWALIA, V. K.; KIDWAI, M. **New Trends in Green Chemistry**. Dordrecht: Springer Netherlands, 2004.
- AIKINS, J. A.; WILLIAMS, F. Radiation-Induced Cationic Polymerization of Limonene Oxide, α -Pinene Oxide, and β -Pinene Oxide. In: **American Chemical Society**. p. 335–359, 1985.
- ALBERTSSON, A.-C.; VARMA, I. K. Recent Developments in Ring Opening Polymerization of Lactones for Biomedical Applications. **Biomacromolecules**, v. 4, n. 6, p. 1466–1486, nov. 2003.
- ALLAIN, E. J. et al. Highly enantioselective epoxidation of disubstituted alkenes with hydrogen peroxide catalyzed by chloroperoxidase. **Journal of the American Chemical Society**, v. 115, n. 10, p. 4415–4416, may 1993.
- ALLEGREZZA, M. L.; KONKOLEWICZ, D. PET-RAFT Polymerization: Mechanistic Perspectives for Future Materials. **ACS Macro Letters**, v. 10, n. 4, p. 433–446, 20 abr. 2021.
- ALVES MOREIRA, M.; BERGLER BITENCOURT, T.; DA GRAÇA NASCIMENTO, M. Optimization of Chemo-Enzymatic Epoxidation of Cyclohexene Mediated by Lipases. **Synthetic Communications**, v. 35, n. 15, p. 2107–2114, 2005.
- ALVES, R. C. et al. Cationic miniemulsion polymerization of styrene mediated by imidazolium based ionic liquid. **European Polymer Journal**, v. 104, n. April, p. 51–56, 2018.
- ANDJELKOVIC, D. D. et al. Novel thermosets prepared by cationic copolymerization of various vegetable oils—synthesis and their structure–property relationships. **Polymer**, v. 46, n. 23, p. 9674–9685, nov. 2005.
- ANKUDEY, E. G.; OLIVO, H. F.; PEEPLES, T. L. Lipase-mediated epoxidation utilizing urea–hydrogen peroxide in ethyl acetate. **Green Chem.**, v. 8, n. 10, p. 923–926, 2006.
- ANTON, N.; BENOIT, J.-P.; SAULNIER, P. Design and production of nanoparticles formulated from nano-emulsion templates—A review. **Journal of Controlled Release**, v. 128, n. 3, p. 185–199, jun. 2008.
- AOUF, C. et al. The use of lipases as biocatalysts for the epoxidation of fatty acids and phenolic compounds. **Green Chem.**, v. 16, n. 4, p. 1740–1754, 2014.

ARAMENDÍA, M. A. et al. Epoxidation of limonene over hydrotalcite-like compounds with hydrogen peroxide in the presence of nitriles. **Applied Catalysis A: General**, v. 216, n. 1–2, p. 257–265, 2001.

ARANA-PEÑA, S.; LOKHA, Y.; FERNÁNDEZ-LAFUENTE, R. Immobilization of Eversa Lipase on Octyl Agarose Beads and Preliminary Characterization of Stability and Activity Features. **Catalysts**, v. 8, n. 11, p. 511, 2 nov. 2018.

AURIEMMA, F. et al. Stereocomplexed Poly(Limonene Carbonate): A Unique Example of the Cocrystallization of Amorphous Enantiomeric Polymers. **Angewandte Chemie International Edition**, v. 54, n. 4, p. 1215–1218, 19 jan. 2015a.

AURIEMMA, F. et al. Crystallization of Alternating Limonene Oxide/Carbon Dioxide Copolymers: Determination of the Crystal Structure of Stereocomplex Poly(limonene carbonate). **Macromolecules**, v. 48, n. 8, p. 2534–2550, 28 abr. 2015b.

AWAD, W. H. et al. Thermal degradation studies of alkyl-imidazolium salts and their application in nanocomposites. **Thermochimica Acta**, v. 409, n. 1, p. 3–11, jan. 2004.

BAJWA, A. S. et al. Chemoenzymatic epoxidation of Karanja oil: an alternative to chemical epoxidation? **Asia-Pacific Journal of Chemical Engineering**, v. 11, n. 2, p. 314–322, mar. 2016.

BARRERA ZAPATA, R.; VILLA, A. L.; MONTES DE CORREA, C. Limonene Epoxidation: Diffusion and Reaction over PW-Amberlite in a Triphasic System. **Industrial & Engineering Chemistry Research**, v. 45, n. 13, p. 4589–4596, 1 jun. 2006.

BELLOTTI, V.; SIMONUTTI, R. New Light in Polymer Science: Photoinduced Reversible Addition-Fragmentation Chain Transfer Polymerization (PET-RAFT) as Innovative Strategy for the Synthesis of Advanced Materials. **Polymers**, v. 13, n. 7, p. 1119, 1 abr. 2021.

BENANIBA, M. T.; BELHANECHÉ-BENSEMRA, N.; GELBARD, G. Stabilization of PVC by epoxidized sunflower oil in the presence of zinc and calcium stearates. **Polymer Degradation and Stability**, v. 82, n. 2, p. 245–249, 2003.

BEREZIANKO, I. A.; VASILENKO, I. V.; KOSTJUK, S. V. Acidic imidazole-based ionic liquids in the presence of diisopropyl ether as catalysts for the synthesis of highly reactive polyisobutylene: Effect of ionic liquid nature, catalyst aging, and sonication. **Polymer**, v. 145, p. 382–390, jun. 2018.

BEREZIANKO, I. A.; VASILENKO, I. V.; KOSTJUK, S. V. Cationic polymerization of isobutylene co-initiated by chloroferrate imidazole-based ionic liquid: The advantageous effect of initiator and aromatic compounds. **European Polymer Journal**, v. 121, p. 109307, dez. 2019.

BHATTACHARYA, S. **Solvent-free chemo-enzymatic epoxidation: Experimental and kinetic modelling studies**. 2011. Technischen Universität Berlin, 2011.

BJÖRKLING, F. et al. Lipase catalyzed synthesis of peroxycarboxylic acids and lipase

mediated oxidations. **Tetrahedron**, v. 48, n. 22, p. 4587–4592, 1992.

BJÖRKLING, F.; GODTFREDSSEN, S. E.; KIRK, O. Lipase-mediated formation of peroxy-carboxylic acids used in catalytic epoxidation of alkenes. **Journal of the Chemical Society, Chemical Communications**, n. 19, p. 1301–1303, 1990.

BLANAZS, A. et al. Mechanistic Insights for Block Copolymer Morphologies: How Do Worms Form Vesicles? **Journal of the American Chemical Society**, v. 133, n. 41, p. 16581–16587, 19 out. 2011.

BLANAZS, A.; RYAN, A. J.; ARMES, S. P. Predictive Phase Diagrams for RAFT Aqueous Dispersion Polymerization: Effect of Block Copolymer Composition, Molecular Weight, and Copolymer Concentration. **Macromolecules**, v. 45, n. 12, p. 5099–5107, 26 jun. 2012.

BONON, A. de J. **Obtenção de monômeros naturais através da epoxidação de limoneno**. 2012. Universidade Estadual de Campinas, 2012.

BOOTH, C.; HIGGINSON, W. C. E.; POWELL, E. The polymerization of propylene oxide catalysed by zinc diethyl and water. **Polymer**, v. 5, n. C, p. 479–497, jan. 1964.

BORNSCHEUER, U. T. Immobilizing Enzymes: How to Create More Suitable Biocatalysts. **Angewandte Chemie International Edition**, v. 42, n. 29, p. 3336–3337, 28 jul. 2003.

BRAGA, D. Anuário Hf Brasil 2020-2021. **CEPEA – ESALQ/USP**, p. 54, 2020. Disponível em: <<https://www.hfbrasil.org.br/br/revista/acessar/completo/retrospectiva-2020-perspectivas-2021.aspx>>. Acesso em: 20 jul. 2021.

BRANNIGAN, R. P.; DOVE, A. P. Synthesis, properties and biomedical applications of hydrolytically degradable materials based on aliphatic polyesters and polycarbonates. **Biomaterials Science**, v. 5, n. 1, p. 9–21, 2017.

BYRNE, C. M. et al. Alternating copolymerization of limonene oxide and carbon dioxide. **Journal of the American Chemical Society**, v. 126, n. 37, p. 11404–11405, 2004.

BYUN, J.; LANDFESTER, K.; ZHANG, K. A. I. Conjugated Polymer Hydrogel Photocatalysts with Expandable Photoactive Sites in Water. **Chemistry of Materials**, v. 31, n. 9, p. 3381–3387, 2019.

CAMACHO-CRUZ, L. A.; VELAZCO-MEDEL, M. A.; BUCIO, E. Aqueous polymerizations. In: **Green Sustainable Process for Chemical and Environmental Engineering and Science**. Elsevier, 2020. p. 275–318.

CAMPANELLA, A.; BALTANÁS, M. A. Degradation of the oxirane ring of epoxidized vegetable oils with solvated acetic acid using cation-exchange resins. **European Journal of Lipid Science and Technology**, v. 106, n. 8, p. 524–530, 2004.

CANNING, S. L.; SMITH, G. N.; ARMES, S. P. A Critical Appraisal of RAFT-Mediated Polymerization-Induced Self-Assembly. **Macromolecules**, v. 49, n. 6, p. 1985–2001, 22 mar. 2016.

CAO, M. et al. ICAR ATRP Polymerization-Induced Self-Assembly Using a Mixture of Macroinitiator/Stabilizer with Different Molecular Weights. **Macromolecular Rapid Communications**, v. 40, n. 20, p. 1900296, 14 out. 2019.

CAUSSETTE, M.; MARTY, A.; COMBES, D. Enzymatic Synthesis of Thioesters in Non-conventional Solvents. **Journal of Chemical Technology & Biotechnology**, v. 68, n. 3, p. 257–262, mar. 1997.

CHADUC, I. et al. Effect of the pH on the RAFT Polymerization of Acrylic Acid in Water. Application to the Synthesis of Poly(acrylic acid)-Stabilized Polystyrene Particles by RAFT Emulsion Polymerization. **Macromolecules**, v. 46, n. 15, p. 6013–6023, 13 ago. 2013.

CHAMBON, P. et al. Facile Synthesis of Methacrylic ABC Triblock Copolymer Vesicles by RAFT Aqueous Dispersion Polymerization. **Macromolecules**, v. 45, n. 12, p. 5081–5090, 26 jun. 2012.

CHARLEUX, B. et al. Polymerization-Induced Self-Assembly: From Soluble Macromolecules to Block Copolymer Nano-Objects in One Step. **Macromolecules**, v. 45, n. 17, p. 6753–6765, 11 set. 2012.

CHEABURU-YILMAZ, C. N.; KARASULU, H. Y.; YILMAZ, O. Nanoscaled Dispersed Systems Used in Drug-Delivery Applications. In: **Polymeric Nanomaterials in Nanotherapeutics**. Izmir: Elsevier, 2019. p. 437–468.

CHEN, J. et al. A Multitasking Hydrogel Based on Double Dynamic Network with Quadruple-Stimuli Sensitiveness, Autonomic Self-Healing Property, and Biomimetic Adhesion Ability. **Macromolecular Chemistry and Physics**, v. 218, n. 15, p. 1700166, ago. 2017.

CHIAPPE, C. et al. Pyrazolium- versus Imidazolium-Based Ionic Liquids: Structure, Dynamics and Physicochemical Properties. **The Journal of Physical Chemistry B**, v. 117, n. 2, p. 668–676, 17 jan. 2013.

CHIARADIA, V. **Unsaturated macrolactone polymerization followed by its modification and crosslinking via click chemistry-based reactions**. 2019. Universidade Federal de Santa Catarina, 2019.

CHU, Y. et al. A photocatalyst immobilized on fibrous and porous monolithic cellulose for heterogeneous catalysis of controlled radical polymerization. **Polymer Chemistry**, v. 9, n. 13, p. 1666–1673, 2018.

CINDRIĆ, M. et al. Towards a global greener process: from solvent- less synthesis of molybdenum(VI) ONO Schiff base complexes to catalyzed olefin epoxidation under organic-solvent-free conditions. **New Journal of Chemistry**, v. 41, n. 2, p. 594–602, 2017.

CIRIMINNA, R. et al. Limonene: a versatile chemical of the bioeconomy. **Chem. Commun.**, v. 50, n. 97, p. 15288–15296, 2014.

CIRIMINNA, R. et al. Photocatalytic partial oxidation of limonene to 1,2 limonene oxide. **Chemical Communications**, v. 54, n. 8, p. 1008–1011, 2018.

CLARKE, C. J. et al. Green and Sustainable Solvents in Chemical Processes. **Chemical Reviews**, v. 118, n. 2, p. 747–800, 24 jan. 2018.

COCKRAM, A. A. et al. Optimization of the high-throughput synthesis of multiblock copolymer nanoparticles in aqueous media via polymerization-induced self-assembly. **Reaction Chemistry & Engineering**, v. 3, n. 5, p. 645–657, 2018.

CORMA, A.; IBORRA, S.; VELTY, A. Chemical Routes for the Transformation of Biomass into Chemicals. **Chemical Reviews**, v. 107, n. 6, p. 2411–2502, 1 jun. 2007.

CORNEL, E. J. et al. Principles and Characteristics of Polymerization-Induced Self-Assembly with Various Polymerization Techniques. **CCS Chemistry**, v. 3, n. 4, p. 2104–2125, abr. 2021.

CRIVELLO, J. V et al. The synthesis and cationic polymerization of novel monomers from renewable sources. **Macromolecular Symposia**, v. 107, n. 1, p. 75–83, abr. 1996.

CUNNINGHAM, V. J. et al. Poly(glycerol monomethacrylate)–Poly(benzyl methacrylate) Diblock Copolymer Nanoparticles via RAFT Emulsion Polymerization: Synthesis, Characterization, and Interfacial Activity. **Macromolecules**, v. 47, n. 16, p. 5613–5623, 26 ago. 2014.

CUNNINGHAM, W. B. et al. Sustainable catalytic protocols for the solvent free epoxidation and anti -dihydroxylation of the alkene bonds of biorenewable terpene feedstocks using H₂O₂ as oxidant. **Green Chemistry**, v. 22, n. 2, p. 513–524, 2020.

D'AGOSTO, F.; RIEGER, J.; LANSALOT, M. RAFT-Mediated Polymerization-Induced Self-Assembly. **Angewandte Chemie International Edition**, v. 59, n. 22, p. 8368–8392, 25 maio 2020.

DA SILVA, J. G. et al. Rhodium catalyzed hydroformylation of monoterpenes containing a sterically encumbered trisubstituted endocyclic double bond under mild conditions. **Applied Catalysis A: General**, v. 326, n. 2, p. 219–226, jul. 2007.

DA SILVA, J. M. R.; NASCIMENTO, M. D. G. Chemoenzymatic epoxidation of citronellol catalyzed by lipases. **Process Biochemistry**, v. 47, n. 3, p. 517–522, mar. 2012.

DA SILVEIRA NETO, B. A. et al. Organoindate Room Temperature Ionic Liquid: Synthesis, Physicochemical Properties and Application. **Synthesis**, v. 2004, n. 08, p. 1155–1158, 2004.

DAKE, G. Oxiranes and Oxirenes: Monocyclic. In: **Comprehensive Heterocyclic Chemistry II**. Vancouver: Elsevier, 1996. p. 174–217.

DARENSBOURG, D. J. et al. Copolymerization and cycloaddition products derived from coupling reactions of 1,2-epoxy-4-cyclohexene and carbon dioxide. Postpolymerization functionalization via thiol-ene click reactions. **Macromolecules**, v. 47, n. 21, p. 7347–7353, 2014.

DATTA, S.; CHRISTENA, L. R.; RAJARAM, Y. R. S. Enzyme immobilization: an overview on techniques and support materials. **Biotech**, v. 3, n. 1, p. 1–9, 6 fev. 2013.

DAVIES, D. I.; PARROTT, M. J. **Free Radicals in Organic Synthesis**. Berlin, Heidelberg: Springer Berlin Heidelberg, 1978. v. 7

DAVIS, J. H. Working Salts: Syntheses and Uses of Ionic Liquids Containing Functionalized Ions. In: Tuscaloosa: American Chemical Society, 2002. p. 247–258.

DEL RIO, E. et al. Polymerization of epoxidized vegetable oil derivatives: Ionic-coordinative polymerization of methylepoxyoleate. **Journal of Polymer Science Part A: Polymer Chemistry**, v. 48, n. 22, p. 4995–5008, 15 nov. 2010.

DELMAS, T. et al. How To Prepare and Stabilize Very Small Nanoemulsions. **Langmuir**, v. 27, n. 5, p. 1683–1692, mar. 2011.

DERRY, M. J.; FIELDING, L. A.; ARMES, S. P. Polymerization-induced self-assembly of block copolymer nanoparticles via RAFT non-aqueous dispersion polymerization. **Progress in Polymer Science**, v. 52, p. 1–18, jan. 2016.

DING, S.; RADOSZ, M.; SHEN, Y. Ionic Liquid Catalyst for Biphasic Atom Transfer Radical Polymerization of Methyl Methacrylate. **Macromolecules**, v. 38, n. 14, p. 5921–5928, jul. 2005.

DOBROVOLSKAIA, M. A.; MCNEIL, S. E. Understanding the correlation between in vitro and in vivo immunotoxicity tests for nanomedicines. **Journal of Controlled Release**, v. 172, n. 2, p. 456–466, dez. 2013.

DOCHERTY, P. J.; DERRY, M. J.; ARMES, S. P. RAFT dispersion polymerization of glycidyl methacrylate for the synthesis of epoxy-functional block copolymer nanoparticles in mineral oil. **Polymer Chemistry**, v. 10, n. 5, p. 603–611, 2019.

DOMÍNGUEZ DE MARÍA, P. et al. Biotechnological applications of *Candida antarctica* lipase A: State-of-the-art. **Journal of Molecular Catalysis B: Enzymatic**, v. 37, n. 1–6, p. 36–46, dez. 2005.

DONDONI, A. The Emergence of Thiol-Ene Coupling as a Click Process for Materials and Bioorganic Chemistry. **Angewandte Chemie International Edition**, v. 47, n. 47, p. 8995–8997, 2008.

DU, J.; O'REILLY, R. K. Anisotropic particles with patchy, multicompartiment and Janus architectures: preparation and application. **Chemical Society Reviews**, v. 40, n. 5, p. 2402, 2011.

EDRIS, A. E. Pharmaceutical and therapeutic Potentials of essential oils and their individual volatile constituents: a review. **Phytotherapy Research**, v. 21, n. 4, p. 308–323, abr. 2007.

FABER, K. **Biotransformations in Organic Chemistry**. 6. ed. Berlin, Heidelberg: Springer Berlin Heidelberg, 2011.

FACIN, B. R. et al. Driving Immobilized Lipases as Biocatalysts: 10 Years State of the Art and Future Prospects. **Industrial & Engineering Chemistry Research**, v. 58, n. 14, p. 5358–5378, 10 abr. 2019.

FELIPE, L. O.; BICAS, J. L. Terpenos: compostos majoritários de óleos essenciais. **Química e Sociedade**, v. 39, n. 2, p. 120–130, 2017.

FERGUSON, C. J. et al. Effective ab Initio Emulsion Polymerization under RAFT Control. **Macromolecules**, v. 35, n. 25, p. 9243–9245, 3 dez. 2002.

FERGUSON, C. J. et al. Ab Initio Emulsion Polymerization by RAFT-Controlled Self-Assembly. **Macromolecules**, v. 38, n. 6, p. 2191–2204, 1 mar. 2005.

FERGUSON, C. T. J. et al. Dispersible porous classical polymer photocatalysts for visible light-mediated production of pharmaceutically relevant compounds in multiple solvents. **Journal of Materials Chemistry A**, v. 8, n. 3, p. 1072–1076, 2020.

FERRANDI, E. E. et al. Efficient Epoxide Hydrolase Catalyzed Resolutions of (+)- and (-)-cis / trans -Limonene Oxides. **ChemCatChem**, v. 7, n. 19, p. 3171–3178, out. 2015.

FEUSER, P. E. et al. Superparamagnetic poly(methyl methacrylate) nanoparticles surface modified with folic acid presenting cell uptake mediated by endocytosis. **Journal of Nanoparticle Research**, v. 18, n. 4, p. 104, 12 abr. 2016.

FIELDING, L. A. et al. RAFT dispersion polymerization in non-polar solvents: facile production of block copolymer spheres, worms and vesicles in n-alkanes. **Chemical Science**, v. 4, n. 5, p. 2081, 2013.

FINDLEY, T. W.; SWERN, D.; SCANLAN, J. T. Epoxidation of Unsaturated Fatty Materials with Peracetic Acid in Glacial Acetic Acid Solution. **Journal of the American Chemical Society**, v. 67, n. 3, p. 412–414, mar. 1945.

FIRDAUS, M.; MEIER, M. A. R. Renewable polyamides and polyurethanes derived from limonene. **Green Chemistry**, v. 15, n. 2, p. 370–380, 2013.

G. JACOB, R. et al. Essential Oils as a Sustainable Raw Material for the Preparation of Products with Higher Value-Added. **Revista Virtual de Química**, v. 9, n. 1, p. 294–316, 2017.

GHADERI, S.; GHANBARZADEH, S.; HAMISHEHKAR, H. Evaluation of Different Methods for Preparing Nanoparticle Containing Gammaoryzanol for Potential Use in Food Fortification. **Pharmaceutical Sciences**, v. 20, n. March, p. 130–134, 2015.

GU, Y.; JÉRÔME, F. Bio-based solvents: an emerging generation of fluids for the design of eco-efficient processes in catalysis and organic chemistry. **Chemical Society Reviews**, v. 42, n. 24, p. 9550, 2013.

GUIDOTTI, M. et al. Heterogeneous Catalytic Epoxidation: High Limonene Oxide Yields by Surface Silylation of Ti-MCM-41. **Chemical Engineering & Technology**, v. 34, n. 11, p. 1924–1927, nov. 2011.

GUIDOTTI, M.; PALUMBO, C. Catalytic Epoxidation of Organics from Vegetable Sources. In: **Encyclopedia of Inorganic and Bioinorganic Chemistry**. Chichester, UK: John Wiley & Sons, Ltd, 2016. p. 1–11.

GUIMARÃES, T. R. et al. Polymerization-induced self-assembly via RAFT in emulsion: effect of Z-group on the nucleation step. **Polymer Chemistry**, v. 12, n. 1, p. 122–133, 2021.

GUINDANI, C. et al. Covalently Binding of Bovine Serum Albumin to Unsaturated Poly(Globalide-Co- ϵ -Caprolactone) Nanoparticles by Thiol-Ene Reactions. **Macromolecular Bioscience**, v. 19, n. 10, p. 1900145, 6 out. 2019.

GUNAM RESUL, M. F. M. et al. Development of a selective, solvent-free epoxidation of limonene using hydrogen peroxide and a tungsten-based catalyst. **Reaction Chemistry & Engineering**, v. 3, n. 5, p. 747–756, 2018.

GUNSTONE, F. D. **Fatty Acid and Lipid Chemistry**. Boston, MA: Springer US, 1996.

GUPTA, M. K. et al. Cell Protective, ABC Triblock Polymer-Based Thermoresponsive Hydrogels with ROS-Triggered Degradation and Drug Release. **Journal of the American Chemical Society**, v. 136, n. 42, p. 14896–14902, 22 out. 2014.

GURBANOV, M. S.; MAMEDOV, B. A. Epoxidation of flax oil with hydrogen peroxide in a conjugate system in the presence of acetic acid and chlorinated cation exchanger KU-2 \times 8 as catalyst. **Russian Journal of Applied Chemistry**, v. 82, n. 8, p. 1483–1487, 24 ago. 2009.

HASE, Y. et al. The vibrational spectra of phthalic anhydride. **Journal of Molecular Structure**, v. 30, n. 1, p. 37–44, jan. 1976.

HATAZAWA, M. et al. Cationic Co–Salphen Complexes Bisligated by DMAP as Catalysts for the Copolymerization of Cyclohexene Oxide with Phthalic Anhydride or Carbon Dioxide. **Macromolecules**, v. 50, n. 20, p. 7895–7900, 24 out. 2017.

HATTON, F. L. et al. Aqueous one-pot synthesis of epoxy-functional diblock copolymer worms from a single monomer: new anisotropic scaffolds for potential charge storage applications. **Polymer Chemistry**, v. 10, n. 2, p. 194–200, 2019.

HAUENSTEIN, O. et al. Bio-based polycarbonate from limonene oxide and CO₂ with high molecular weight, excellent thermal resistance, hardness and transparency. **Green Chemistry**, v. 18, n. 3, p. 760–770, 2016.

HAUENSTEIN, O.; AGARWAL, S.; GREINER, A. Bio-based polycarbonate as synthetic toolbox. **Nature Communications**, v. 7, n. 1, p. 11862, 15 dez. 2016.

HAUSMANN, S.; JAEGER, K.-E. Lipolytic Enzymes from Bacteria. In: TIMMIS, K. N. (Ed.). **Handbook of Hydrocarbon and Lipid Microbiology**. Berlin, Heidelberg: Springer Berlin Heidelberg, 2010. p. 1099–1126.

HE, J. et al. Sodium Bis(acyl)phosphane oxide (SBAPO): An efficient photoinitiator for blue light initiated aqueous RAFT dispersion polymerization. **Polymer**, v. 145, p. 70–79, jun. 2018.

HERRERO, E. et al. Catalytic Epoxidation of Limonene. **Molecules**, v. 5, n. 12, p. 336–337, 22 mar. 2000.

HORNUNG, C. H. et al. Synthesis of RAFT Block Copolymers in a Multi-Stage Continuous Flow Process Inside a Tubular Reactor. **Australian Journal of Chemistry**, v. 66, n. 2, p. 192,

2013.

HOYLE, C. E.; LEE, T. A. I. Y.; ROPER, T. Thiol – Enes : Chemistry of the Past with Promise for the Future. v. 42, p. 5301–5338, 2004.

HU, S.; HAGER, L. P. Asymmetric epoxidation of functionalized cis-olefins catalyzed by chloroperoxidase. **Tetrahedron Letters**, v. 40, n. 9, p. 1641–1644, fev. 1999.

HUANG, W. et al. Hollow nanoporous covalent triazine frameworks via acid vapor-assisted solid phase synthesis for enhanced visible light photoactivity. **Journal of Materials Chemistry A**, v. 4, n. 20, p. 7555–7559, 2016.

HUANG, W. et al. Visible-Light-Promoted Selective Oxidation of Alcohols Using a Covalent Triazine Framework. **ACS Catalysis**, v. 7, n. 8, p. 5438–5442, 4 ago. 2017.

HUDAYA, T. et al. Synthesis of Biokerosene through Electrochemical Hydrogenation of Terpene Hydrocarbons from Turpentine Oil. **Journal of Engineering and Technological Sciences**, v. 48, n. 6, p. 655–664, 30 dez. 2016.

HUSSAIN, H. et al. meta-Chloroperbenzoic acid (mCPBA): a versatile reagent in organic synthesis. **RSC Adv.**, v. 4, n. 25, p. 12882–12917, 2014.

IRVINE, D. J. One nanoparticle, one kill. **Nature Materials**, v. 10, n. 5, p. 342–343, 17 maio 2011.

ISNARD, F. et al. Ring-Opening Copolymerization of Epoxides with Cyclic Anhydrides Promoted by Bimetallic and Monometallic Phenoxy-Imine Aluminum complexes. **ChemCatChem**, v. 9, n. 15, p. 2972–2979, 9 ago. 2017.

ISNARD, F. et al. Tetracoordinate aluminum complexes bearing phenoxy-based ligands as catalysts for epoxide/anhydride copolymerization: some mechanistic insights. **Catalysis Science & Technology**, v. 9, n. 12, p. 3090–3098, 2019.

JEONG, H. et al. In vitro blood cell viability profiling of polymers used in molecular assembly. **Scientific Reports**, v. 7, n. 1, p. 9481, 25 dez. 2017.

JESKE, R. C.; DICICCIO, A. M.; COATES, G. W. Alternating copolymerization of epoxides and cyclic anhydrides: An improved route to aliphatic polyesters. **Journal of the American Chemical Society**, v. 129, n. 37, p. 11330–11331, set. 2007.

JONES, E. R. et al. Efficient Synthesis of Amine-Functional Diblock Copolymer Nanoparticles via RAFT Dispersion Polymerization of Benzyl Methacrylate in Alcoholic Media. **Macromolecules**, v. 45, n. 12, p. 5091–5098, 26 jun. 2012.

KAHVECI, M. U. et al. Photoinitiated Cationic Polymerization of Mono and Divinyl Ethers in Aqueous Medium Using Ytterbium Triflate as Lewis Acid. **Macromolecular Chemistry and Physics**, v. 209, n. 18, p. 1881–1886, 22 set. 2008.

KARAGOZ, B. et al. Polymerization-Induced Self-Assembly (PISA) – control over the morphology of nanoparticles for drug delivery applications. **Polym. Chem.**, v. 5, n. 2, p. 350–

355, 2014.

KEDDIE, D. J. et al. RAFT Agent Design and Synthesis. **Macromolecules**, v. 45, n. 13, p. 5321–5342, 10 jul. 2012.

KEDDIE, D. J. A guide to the synthesis of block copolymers using reversible-addition fragmentation chain transfer (RAFT) polymerization. **Chem. Soc. Rev.**, v. 43, n. 2, p. 496–505, 2014.

KERN, M. R.; BOYES, S. G. RAFT polymerization kinetics and polymer characterization of P3HT rod-coil block copolymers. **Journal of Polymer Science Part A: Polymer Chemistry**, v. 52, n. 24, p. 3575–3585, out. 2014.

KHOLKHOEV, B. C.; BURDUKOVSKII, V. F.; MOGNONOV, D. M. Preparation of aromatic polyamidines and their transformation in polybenzimidazoles. **Express Polymer Letters**, v. 8, n. 9, p. 635–646, 2014.

KIRT, B. B. Anuário brasileiro de Horti&Fruti 2021. **Brazilian Yearbook**, p. 104, 2021.

KRISTENSEN, J. B.; XU, X.; MU, H. Process optimization using response surface design and pilot plant production of dietary diacylglycerols by lipase-catalyzed glycerolysis. **Journal of Agricultural and Food Chemistry**, v. 53, n. 18, p. 7059–7066, 2005.

KRSTINA, J. et al. Narrow Polydispersity Block Copolymers by Free-Radical Polymerization in the Presence of Macromonomers. **Macromolecules**, v. 28, n. 15, p. 5381–5385, 1 jul. 1995.

KUBO, T. et al. Enantioselective Epoxidation of Terminal Alkenes to (R)- and (S)-Epoxides by Engineered Cytochromes P450 BM-3. **Chemistry - A European Journal**, v. 12, n. 4, p. 1216–1220, 23 jan. 2006.

KUKHTA, N. A.; VASILENKO, I. V.; KOSTJUK, S. V. Room temperature cationic polymerization of β -pinene using modified $AlCl_3$ catalyst: toward sustainable plastics from renewable biomass resources. **Green Chemistry**, v. 13, n. 9, p. 2362, 2011.

LANDFESTER, K.; EISENBLÄTTER, J.; ROTHE, R. Preparation of polymerizable miniemulsions by ultrasonication. **Journal of Coatings Technology and Research**, v. 1, n. 1, p. 65–68, jan. 2004.

LATOURETTE, H. K. et al. A novel continuous countercurrent epoxidation process. **Journal of the American Oil Chemists Society**, v. 37, n. 11, p. 559–563, 1960.

LEI, Z. et al. Clean and selective Baeyer–Villiger oxidation of ketones with hydrogen peroxide catalyzed by Sn-palygorskite. **Journal of Organometallic Chemistry**, v. 691, n. 26, p. 5767–5773, dez. 2006.

LEIMANN, F. V. et al. Poly(3-hydroxybutyrate-co-3-hydroxyvalerate) nanoparticles prepared by a miniemulsion/solvent evaporation technique: effect of phbv molar mass and concentration. **Brazilian Journal of Chemical Engineering**, v. 30, n. 2, p. 369–377, jun. 2013.

LEITE, M. J. L. **Polimerização por abertura de anel mediada por líquido iônico**

BMIFe₂Cl₇. 2018. Universidade Federal de Santa Catarina, 2018.

LEMOULT, S. C.; RICHARDSON, P. F.; ROBERTS, S. M. Lipase-catalysed Baeyer-Villiger Reactions. **Journal of the Chemical Society, Perkin Transactions 1**, v. 1, p. 89–91, 1995.

LI, L. et al. Reactions of turpentine using Zr-MCM-41 family mesoporous molecular sieves. **Catalysis Letters**, v. 100, n. 3–4, p. 227–233, abr. 2005.

LI, S.; HAN, G.; ZHANG, W. Photoregulated reversible addition–fragmentation chain transfer (RAFT) polymerization. **Polymer Chemistry**, v. 11, n. 11, p. 1830–1844, 2020.

LI, Y.; ARMES, S. P. RAFT Synthesis of Sterically Stabilized Methacrylic Nanolatexes and Vesicles by Aqueous Dispersion Polymerization. **Angewandte Chemie International Edition**, v. 49, n. 24, p. 4042–4046, 1 jun. 2010.

LIAW, H.-J. et al. Relationship between flash point of ionic liquids and their thermal decomposition. **Green Chemistry**, v. 14, n. 7, p. 2001, 2012.

LIN, H. et al. Biocatalytic Epoxidation for Green Synthesis. In: **Green Biocatalysis**. Hoboken, NJ, NJ: John Wiley & Sons, Inc, 2016. p. 351–372.

LIN, Z.; IERAPETRITOU, M.; NIKOLAKIS, V. Phthalic anhydride production from hemicellulose solutions: Technoeconomic analysis and life cycle assessment. **AIChE Journal**, v. 61, n. 11, p. 3708–3718, nov. 2015.

LIU, S. et al. Polymerization of α -pinene using Lewis acidic ionic liquid as catalyst for production of terpene resin. **Biomass and Bioenergy**, v. 57, n. 53, p. 238–242, out. 2013.

LONGO, J. M.; SANFORD, M. J.; COATES, G. W. Ring-Opening Copolymerization of Epoxides and Cyclic Anhydrides with Discrete Metal Complexes: Structure-Property Relationships. **Chemical Reviews**, v. 116, n. 24, p. 15167–15197, 2016.

LOOSLI, F.; STOLL, S. Effect of surfactants, pH and water hardness on the surface properties and agglomeration behavior of engineered TiO₂ nanoparticles. **Environmental Science: Nano**, v. 4, n. 1, p. 203–211, 2017.

LOUMOUMOU, A. N. et al. Optimization of the extraction of the p -menthadienol isomers and aristolone contained in the essential oil from *Elyonurus hensii* using a 2³ full factorial design. **Food Science & Nutrition**, v. 5, n. 3, p. 784–792, maio 2017.

LOWE, A. B. Thiol-ene “click” reactions and recent applications in polymer and materials synthesis. **Polym. Chem.**, v. 1, n. 1, p. 17–36, 2010.

LU, S. et al. Efficacy of Simple Short-Term in Vitro Assays for Predicting the Potential of Metal Oxide Nanoparticles to Cause Pulmonary Inflammation. **Environmental Health Perspectives**, v. 117, n. 2, p. 241–247, fev. 2009.

LUDWICZUK, A.; SKALICKA-WOŹNIAK, K.; GEORGIEV, M. I. **Terpenoids**. Plovdiv: Elsevier, 2017.

- LUO, X. et al. Switching between Thermal Initiation and Photoinitiation Redirects RAFT-Mediated Polymerization-Induced Self-Assembly. **Macromolecules**, v. 54, n. 6, p. 2948–2959, 23 mar. 2021.
- MA, J. et al. Preparation of Thermo-Responsive and Cross-Linked Fluorinated Nanoparticles via RAFT-Mediated Aqueous Polymerization in Nanoreactors. **Molecules**, v. 22, n. 2, p. 152, 25 jan. 2017.
- MACHADO, T. O.; SAYER, C.; ARAUJO, P. H. H. Thiol-ene polymerisation: A promising technique to obtain novel biomaterials. **European Polymer Journal**, v. 86, p. 200–215, jan. 2017.
- MAHMOUD, E.; WATSON, D. A.; LOBO, R. F. Renewable production of phthalic anhydride from biomass-derived furan and maleic anhydride. **Green Chem.**, v. 16, n. 1, p. 167–175, 2014.
- MALKO, M. W.; WRÓBLEWSKA, A. The importance of R-(+)-limonene as the raw material for organic syntheses and for organic industry. **Chemik**, v. 70, n. 4, p. 198–202, 2016.
- MANDELLI, D. et al. Alumina-catalyzed alkene epoxidation with hydrogen peroxide. **Applied Catalysis A: General**, v. 219, n. 1–2, p. 209–213, out. 2001.
- MANE, S. R. Trending methods employed for polymerization induced self-assembly. **New Journal of Chemistry**, v. 44, n. 17, p. 6690–6698, 2020.
- MANOEL, E. A. et al. Accurel MP 1000 as a support for the immobilization of lipase from *Burkholderia cepacia*: Application to the kinetic resolution of myo -inositol derivatives. **Process Biochemistry**, v. 50, n. 10, p. 1557–1564, out. 2015.
- MATTOS DOS SANTOS, P. C. et al. Evaluation of in vitro cytotoxicity of superparamagnetic poly(thioether-ester) nanoparticles on erythrocytes, non-tumor (NIH3T3), tumor (HeLa) cells and hyperthermia studies. **Journal of Biomaterials Science, Polymer Edition**, v. 29, n. 16, p. 1935–1948, 2 nov. 2018.
- MC, Á.; MI, P. Hydration of α -Pinene over Heteropoly Acid H₃PW₁₂O₄₀ and H₃PMo₁₂O₄₀ **Journal of Chromatography & Separation Techniques**, v. 06, n. 07, 2015.
- MCCLAY, K.; FOX, B. G.; STEFFAN, R. J. Toluene Monooxygenase-Catalyzed Epoxidation of Alkenes. **Applied and Environmental Microbiology**, v. 66, n. 5, p. 1877–1882, 2000.
- MEISTER, A.; BLUME, A. (Cryo)Transmission Electron Microscopy of Phospholipid Model Membranes Interacting with Amphiphilic and Polyphilic Molecules. **Polymers**, v. 9, n. 12, p. 521, 2017.
- MELCHORS, M. S. et al. Epoxidation of (R)-(+)-Limonene to 1,2-Limonene Oxide Mediated by Low-Cost Immobilized *Candida antarctica* Lipase Fraction B. **Industrial & Engineering Chemistry Research**, v. 58, n. 31, p. 13918–13925, 2019.
- MÉNDEZ-SÁNCHEZ, D. et al. Chemoenzymatic epoxidation of alkenes based on peracid formation by a *Rhizomucor miehei* lipase-catalyzed perhydrolysis reaction. **Tetrahedron**, v. 70, n. 6, p. 1144–1148, 2014.

MENDOZA-MUÑOZ, N.; ALCALÁ-ALCALÁ, S.; QUINTANAR-GUERRERO, D. Preparation of Polymer Nanoparticles by the Emulsification-Solvent Evaporation Method: From Vanderhoff's Pioneer Approach to Recent Adaptations. In: VAUTHIER, C.; PONCHEL, G. (Ed.). **Polymer Nanoparticles for Nanomedicines**. Cham: Springer International Publishing, 2016. p. 87–121.

MERYAM SARDAR, R. A. Enzyme Immobilization: An Overview on Nanoparticles as Immobilization Matrix. **Biochemistry & Analytical Biochemistry**, v. 04, n. 02, 2015.

MIAO, S. et al. Vegetable-oil-based polymers as future polymeric biomaterials. **Acta Biomaterialia**, v. 10, n. 4, p. 1692–1704, abr. 2014.

MICHEL, T. **Epoxidation of Terpenes with Molecular Catalysts in Homogeneous Phase**. 2012. Technische Universität München, 2012.

MICHEL, T. et al. Selective epoxidation of (+)-limonene employing methyltrioxorhenium as catalyst. **Journal of Molecular Catalysis A: Chemical**, v. 358, p. 159–165, jun. 2012.

MIGUEZ, T. A. **Polimerização catiônica em solução e miemulsão mediada por líquidos iônicos imidazólicos**. 2018. Universidade Federal de Santa Catarina, 2018.

MILCHERT, E.; MALARCZYK, K.; KŁOS, M. Technological Aspects of Chemoenzymatic Epoxidation of Fatty Acids, Fatty Acid Esters and Vegetable Oils: A Review. **Molecules**, v. 20, n. 12, p. 21481–21493, 2 dez. 2015.

MISHRA, V.; KUMAR, R. Living Radical Polymerization: a Review. **Journal of Scientific Research Banaras Hindu University**, v. 56, p. 141–176, 2012.

MOAD, G. A Critical Assessment of the Kinetics and Mechanism of Initiation of Radical Polymerization with Commercially Available Dialkyldiazene Initiators. **Progress in Polymer Science**, v. 88, p. 130–188, jan. 2019a.

MOAD, G. A Critical Survey of Dithiocarbamate Reversible Addition-Fragmentation Chain Transfer (RAFT) Agents in Radical Polymerization. **Journal of Polymer Science Part A: Polymer Chemistry**, v. 57, n. 3, p. 216–227, 14 fev. 2019b.

MOAD, G.; RIZZARDO, E.; THANG, S. H. Living Radical Polymerization by the RAFT Process. **Australian Journal of Chemistry**, v. 58, n. 6, p. 379, 27 mar. 2005.

MOAD, G.; RIZZARDO, E.; THANG, S. H. Radical addition–fragmentation chemistry in polymer synthesis. **Polymer**, v. 49, n. 5, p. 1079–1131, mar. 2008.

MOAD, G.; RIZZARDO, E.; THANG, S. H. End-functional polymers, thiocarbonylthio group removal/transformation and reversible addition–fragmentation–chain transfer (RAFT) polymerization. **Polymer International**, v. 60, n. 1, p. 9–25, jan. 2011.

MOHAMAD, N. R. et al. An overview of technologies for immobilization of enzymes and surface analysis techniques for immobilized enzymes. **Biotechnology & Biotechnological Equipment**, v. 29, n. 2, p. 205–220, 4 mar. 2015.

MOREIRA, M. A. **Produção enzimática de peróxi-ácidos e sua utilização na epoxidação de terpenos**. 2008. Universidade Federal de Santa Catarina, 2008.

MOREIRA, M. A.; NASCIMENTO, M. G. Chemo-enzymatic epoxidation of (+)-3-carene. **Catalysis Communications**, v. 8, n. 12, p. 2043–2047, dez. 2007.

MUNDIL, R. et al. Alternating ring-opening copolymerization of cyclohexene oxide with phthalic anhydride catalyzed by iron(III) salen complexes. **Macromolecular Research**, v. 23, n. 2, p. 161–166, 12 fev. 2015.

MUSYANOVYCH, A.; LANDFESTER, K. Polymer Micro- and Nanocapsules as Biological Carriers with Multifunctional Properties. **Macromolecular Bioscience**, v. 14, n. 4, p. 458–477, abr. 2014.

MUTZEL, A. et al. Monoterpene SOA – Contribution of first-generation oxidation products to formation and chemical composition. **Atmospheric Environment**, v. 130, p. 136–144, abr. 2016.

NAGAO, M.; HOSHINO, Y.; MIURA, Y. Quantitative preparation of multiblock glycopolymers bearing glycountits at the terminal segments by aqueous reversible addition-fragmentation chain transfer polymerization of acrylamide monomers. **Journal of Polymer Science Part A: Polymer Chemistry**, v. 57, n. 8, p. 857–861, 15 abr. 2019.

NAGAVARMA, B. V. N. et al. Different techniques for preparation of polymeric nanoparticles- A review. **Asian Journal of Pharmaceutical and Clinical Research**, v. 5, n. SUPPL. 3, p. 16–23, 2012.

NAKANO, K.; NOZAKI, K. Polymerization of Epoxides. In: **Comprehensive Organometallic Chemistry III**. Tokyo: Elsevier, 2007. p. 595–621.

NARDINI, M.; DIJKSTRA, B. W. α/β Hydrolase fold enzymes: the family keeps growing. **Current Opinion in Structural Biology**, v. 9, n. 6, p. 732–737, dez. 1999.

NEJAD, E. H. et al. Catalytic Ring-Opening Copolymerization of Limonene Oxide and Phthalic Anhydride: Toward Partially Renewable Polyesters. **Macromolecules**, v. 46, n. 3, p. 631–637, 12 fev. 2013.

NISHIDA, H.; TOKIWA, Y. Effects of higher-order structure of poly(3-hydroxybutyrate) on its biodegradation. II. Effects of crystal structure on microbial degradation. **Journal of Environmental Polymer Degradation**, v. 1, n. 1, p. 65–80, 1993.

NORSTRÖM, E. **Terpenes as renewable monomers for biobased materials**. 2011. KTH Vetenskap Dem Konst, 2011.

NOTHLING, M. D. et al. Progress and Perspectives Beyond Traditional RAFT Polymerization. **Advanced Science**, v. 7, n. 20, p. 2001656, 26 out. 2020.

OKADA, M. Chemical syntheses of biodegradable polymers. **Progress in Polymer Science (Oxford)**, v. 27, n. 1, p. 87–133, 2002.

OLIVEIRA, F. F. D. et al. Charge-Tagged Acetate Ligands As Mass Spectrometry Probes for Metal Complexes Investigations: Applications in Suzuki and Heck Phosphine-Free Reactions. **The Journal of Organic Chemistry**, v. 76, n. 24, p. 10140–10147, 16 dez. 2011.

ORELLANA-COCA, C. et al. Chemo-enzymatic epoxidation of linoleic acid: Parameters influencing the reaction. **European Journal of Lipid Science and Technology**, v. 107, n. 12, p. 864–870, dez. 2005.

OUELLETTE, R. J.; RAWN, J. D. Alkenes and Alkynes. In: **Principles of Organic Chemistry**. Elsevier, 2015. p. 95–132.

PÄIVIÖ, M.; PERKIÖ, P.; KANERVA, L. T. Solvent-free kinetic resolution of primary amines catalyzed by *Candida antarctica* lipase B: effect of immobilization and recycling stability. **Tetrahedron: Asymmetry**, v. 23, n. 3–4, p. 230–236, fev. 2012.

PARRINO, F. et al. Polymers of Limonene Oxide and Carbon Dioxide: Polycarbonates of the Solar Economy. **ACS Omega**, v. 3, n. 5, p. 4884–4890, 31 maio 2018.

PATROCINIO, V. M. B. et al. High Molecular Weight Polystyrene Obtained by Cationic Emulsion Polymerization Catalyzed by Imidazolium-Based Ionic Liquid. **Macromolecular Reaction Engineering**, v. 13, n. 2, p. 1800061, 30 abr. 2019.

PAUL, S. et al. Ring-opening copolymerization (ROCOP): synthesis and properties of polyesters and polycarbonates. **Chemical Communications**, v. 51, n. 30, p. 6459–6479, 2015.

PEÑA CARRODEGUAS, L. et al. Al III -Catalysed Formation of Poly(limonene)carbonate: DFT Analysis of the Origin of Stereoregularity. **Chemistry - A European Journal**, v. 21, n. 16, p. 6115–6122, 13 abr. 2015.

PENFOLD, N. J. W. et al. Emerging Trends in Polymerization-Induced Self-Assembly. **ACS Macro Letters**, v. 8, n. 8, p. 1029–1054, 2019.

PERES, L. B. L. B. et al. PLLA/PMMA blend in polymer nanoparticles: influence of processing methods. **Colloid and Polymer Science**, v. 295, n. 9, p. 1621–1633, 4 set. 2017.

PERRIER, S. 50th Anniversary Perspective: RAFT Polymerization—A User Guide. **Macromolecules**, v. 50, n. 19, p. 7433–7447, 10 out. 2017.

PETKAR, M. et al. Immobilization of lipases for non-aqueous synthesis. **Journal of Molecular Catalysis B: Enzymatic**, v. 39, n. 1–4, p. 83–90, 2006.

PHILLIPS, R. S. Temperature modulation of the stereochemistry of enzymatic catalysis: Prospects for exploitation. **Trends in Biotechnology**, v. 14, n. 1, p. 13–16, jan. 1996.

PHOMMALYSACK-LOVAN, J. et al. PET-RAFT polymerisation: towards green and precision polymer manufacturing. **Chemical Communications**, v. 54, n. 50, p. 6591–6606, 2018.

PIANTINI, U. et al. A biocatalytic route towards rose oxide using chloroperoxidase. **Food Chemistry**, v. 129, n. 3, p. 1025–1029, dez. 2011.

PINTO REIS, C. et al. Nanoencapsulation I. Methods for preparation of drug-loaded polymeric nanoparticles. **Nanomedicine: Nanotechnology, Biology and Medicine**, v. 2, n. 1, p. 8–21, mar. 2006.

POLAND, S. J.; DARENSBOURG, D. J. A quest for polycarbonates provided via sustainable epoxide/CO₂ copolymerization processes. **Green Chem.**, v. 19, n. 21, p. 4990–5011, 2017.

POLLONI, A. E. et al. Polyesters from Macrolactones Using Commercial Lipase NS 88011 and Novozym 435 as Biocatalysts. **Applied Biochemistry and Biotechnology**, v. 184, n. 2, p. 659–672, 23 fev. 2018.

PUBCHEM. **D-Limonene.** Disponível em: <https://pubchem.ncbi.nlm.nih.gov/compound/___-Limonene#section=Top>. Acesso em: 19 mar. 2019a.

PUBCHEM. **Limonene-1,2-Epoxide.** Disponível em: <https://pubchem.ncbi.nlm.nih.gov/compound/Limonene-1_2-epoxide>. Acesso em: 9 mar. 2019b.

RAFIEE-MOGHADDAM, R. et al. Lipase epoxidation optimizing of Jatropha Curcas Oil using perlauric acid. **Digest Journal of Nanomaterials and Biostructures**, v. 9, n. 3, p. 1159–1169, 2014.

RALIYA, R. et al. Perspective on Nanoparticle Technology for Biomedical Use. **Current Pharmaceutical Design**, v. 22, n. 17, p. 2481–2490, 27 abr. 2016.

RAMAIAH, M. Radical reactions in organic synthesis. **Tetrahedron**, v. 43, n. 16, p. 3541–3676, jan. 1987.

RANGANATHAN, S. et al. A one pot reaction cascade of in situ hydrogen peroxide production and lipase mediated in situ production of peracids for the epoxidation of monoterpenes. **Journal of Molecular Catalysis B: Enzymatic**, v. 114, p. 72–76, 2015.

RANGANATHAN, S. et al. Optimization of the lipase mediated epoxidation of monoterpenes using the design of experiments—Taguchi method. **Process Biochemistry**, v. 51, n. 10, p. 1479–1485, 2016.

RANGANATHAN, S. **Development of Sustainable Chemo-enzymatic Processes for the Epoxidation of Terpenes.** 2018. Technische Universität München, 2018.

RANGANATHAN, S.; ZEITLHOFER, S.; SIEBER, V. Development of a lipase-mediated epoxidation process for monoterpenes in choline chloride-based deep eutectic solvents. **Green Chemistry**, v. 19, n. 11, p. 2576–2586, 2017.

RATCLIFFE, L. P. D.; RYAN, A. J.; ARMES, S. P. From a Water-Immiscible Monomer to Block Copolymer Nano-Objects via a One-Pot RAFT Aqueous Dispersion Polymerization Formulation. **Macromolecules**, v. 46, n. 3, p. 769–777, 12 fev. 2013.

REETZ, M. T. Lipases as practical biocatalysts. **Current Opinion in Chemical Biology**, v. 6, n. 2, p. 145–150, abr. 2002.

REN, S. **d-Limonene, a Renewable Component for Polymer Synthesis**. 2017. University of Ottawa, 2017.

REN, T. et al. Multifunctional polymer vesicles for ultrasensitive magnetic resonance imaging and drug delivery. **Journal of Materials Chemistry**, v. 22, n. 24, p. 12329, 2012.

RIOS, N. S. et al. Biotechnological potential of lipases from *Pseudomonas*: Sources, properties and applications. **Process Biochemistry**, v. 75, n. August, p. 99–120, dez. 2018.

ROBERT, C.; DE MONTIGNY, F.; THOMAS, C. M. Tandem synthesis of alternating polyesters from renewable resources. **Nature Communications**, v. 2, n. 1, p. 586, 13 set. 2011.

ROBINSON, P. K. Enzymes: principles and biotechnological applications. **Essays In Biochemistry**, v. 59, n. 0, p. 1–41, 15 nov. 2015.

RODLERT, M. et al. End-Group Fidelity in Nitroxide-Mediated Living Free-Radical Polymerizations. n. September, p. 4749–4763, 2000.

RODRIGUES, T. S. **Estudos sobre Carbenos N-Heterocíclicos e Reações de Polimerizações com Derivados Imidazólios**. 2013. Universidade de Brasília, 2013.

RODRIGUES, T. S. et al. Styrene polymerization efficiently catalyzed by iron-containing imidazolium-based ionic liquids: Reaction mechanism and enhanced ionic liquid effect. **Catalysis Communications**, v. 63, p. 66–73, 2015.

ROWE-KONOPACKI, M. D.; BOYES, S. G. Synthesis of Surface Initiated Diblock Copolymer Brushes from Flat Silicon Substrates Utilizing the RAFT Polymerization Technique. **Macromolecules**, v. 40, n. 4, p. 879–888, fev. 2007.

ROYALS, E. E.; LEFFINGWELL, J. C. Reactions of the Limonene 1,2-Oxides. I. The Stereospecific Reactions of the (+)-cis- and (+)-trans-Limonene 1,2-Oxides. **The Journal of Organic Chemistry**, v. 31, n. 6, p. 1937–1944, jun. 1966.

RUEDA, N. et al. Chemical Modification in the Design of Immobilized Enzyme Biocatalysts: Drawbacks and Opportunities. **The Chemical Record**, v. 16, n. 3, p. 1436–1455, jun. 2016.

RÜSCH GEN. KLAAS, M.; WARWEL, S. Complete and partial epoxidation of plant oils by lipase-catalyzed perhydrolysis. **Industrial Crops and Products**, v. 9, n. 2, p. 125–132, jan. 1999.

RYU, H. K. et al. Ring-opening copolymerization of cyclic epoxide and anhydride using a five-coordinate chromium complex with a sterically demanding amino triphenolate ligand. **Polymer Chemistry**, v. 11, n. 22, p. 3756–3761, 2020.

SÁ, A. G. A. et al. Biocatalysis of aromatic benzyl-propionate ester by different immobilized lipases. **Bioprocess and Biosystems Engineering**, v. 41, n. 5, p. 585–591, 2018.

SALVI, H. M.; YADAV, G. D. Chemoenzymatic Epoxidation of Limonene Using a Novel Surface-Functionalized Silica Catalyst Derived from Agricultural Waste. **ACS Omega**, v. 5, n.

36, p. 22940–22950, 15 set. 2020.

SAURABH, T. et al. Epoxidation of vegetable oils: A Review. **Int. J. Adv. Eng. Technol**, v. 2, n. Iv, p. 491–501, 2011.

SCHNEIDER, R. de C. S. et al. Chemo-enzymatic epoxidation of sunflower oil methyl esters. **Journal of the Brazilian Chemical Society**, v. 20, n. 8, p. 1473–1477, 2009.

ŠEBESTA, R.; KMENTOVÁ, I.; TOMA, Š. Catalysts with ionic tag and their use in ionic liquids. **Green Chemistry**, v. 10, n. 5, p. 484, 2008.

SECUNDO, F. et al. The lid is a structural and functional determinant of lipase activity and selectivity. **Journal of Molecular Catalysis B: Enzymatic**, v. 39, n. 1–4, p. 166–170, maio 2006.

SELL, C. Perfumery materials of natural origin. In: **The Chemistry of Fragrances**. Cambridge: Royal Society of Chemistry, 1999. 1p. 24–51.

SEMSARILAR, M.; ABETZ, V. Polymerizations by RAFT: Developments of the Technique and Its Application in the Synthesis of Tailored (Co)polymers. **Macromolecular Chemistry and Physics**, v. 222, n. 1, p. 2000311, 6 jan. 2021.

SHANMUGAM, S. et al. Heterogeneous Photocatalysis as a Means for Improving Recyclability of Organocatalyst in “Living” Radical Polymerization. **Macromolecules**, v. 51, n. 3, p. 779–790, 13 fev. 2018.

SHANMUGAM, S.; XU, J.; BOYER, C. Exploiting Metalloporphyrins for Selective Living Radical Polymerization Tunable over Visible Wavelengths. **Journal of the American Chemical Society**, v. 137, n. 28, p. 9174–9185, 22 jul. 2015.

SHANMUGAM, S.; XU, J.; BOYER, C. Photocontrolled Living Polymerization Systems with Reversible Deactivations through Electron and Energy Transfer. **Macromolecular Rapid Communications**, v. 38, n. 13, p. 1700143, jul. 2017.

SHI, B. et al. Development of ICAR ATRP–Based Polymerization-Induced Self-Assembly and Its Application in the Preparation of Organic–Inorganic Nanoparticles. **Macromolecular Rapid Communications**, v. 40, n. 24, p. 1900547, 28 dez. 2019.

SIENEL, G.; RIETH, R.; ROWBOTTOM, K. T. Epoxides. In: **Ullmann’s Encyclopedia of Industrial Chemistry**. Weinheim, Germany, Germany: Wiley-VCH Verlag GmbH & Co. KGaA, 2000. p. 2–4.

SILVA, T. S. et al. Polimerização em miniemulsão inversa da ϵ -caprolactona mediada por líquido iônico. In: Bento Gonçalves. **Anais... Bento Gonçalves: Anais do 15º Congresso Brasileiro de Polímeros (15 CBPOL)**, 2019.

SILVESTRE, A. J. D.; GANDINI, A. Terpenes: Major sources, properties and applications. **Monomers, Polymers and Composites from Renewable Resources**, p. 17–38, 2008.

SKOURIDOU, V.; STAMATIS, H.; KOLISIS, F. N. Lipase-mediated epoxidation of α -pinene.

Journal of Molecular Catalysis B: Enzymatic, v. 21, n. 1–2, p. 67–69, 2003a.

SKOURIDOU, V.; STAMATIS, H.; KOLISIS, F. N. A Study on the Process of Lipase-catalyzed Synthesis of α -pinene Oxide in Organic Solvents. **Biocatalysis and Biotransformation**, v. 21, n. 6, p. 285–290, 11 dez. 2003b.

SOLANS, C. et al. Nano-emulsions. **Current Opinion in Colloid & Interface Science**, v. 10, n. 3–4, p. 102–110, out. 2005.

SONG, P. F. et al. Synthesis and properties of aliphatic polycarbonates derived from carbon dioxide, propylene oxide and maleic anhydride. **Journal of Applied Polymer Science**, v. 109, n. 6, p. 4121–4129, 15 set. 2008.

STOLLE, A.; ONDRUSCHKA, B.; HOPF, H. Thermal Rearrangements of Monoterpenes and Monoterpenoids. **Helvetica Chimica Acta**, v. 92, n. 9, p. 1673–1719, set. 2009.

SUGIHARA, S. et al. Non-spherical morphologies from cross-linked biomimetic diblock copolymers using RAFT aqueous dispersion polymerization. **Soft Matter**, v. 7, n. 22, p. 10787, 2011.

SUGIHARA, S. Polymerization-Induced Self-assembly of Block Copolymer Nano-objects via Green RAFT Polymerization. In: **Molecular Technology**. Weinheim, Germany: Wiley-VCH Verlag GmbH & Co. KGaA, 2019. 4p. 1–29.

SUN, S. et al. Enzymatic Epoxidation of Corn Oil by Perstearic Acid. **Journal of the American Oil Chemists' Society**, v. 88, n. 10, p. 1567–1571, 6 out. 2011.

SVEDENDAHL, M. et al. Direct epoxidation in *Candida antarctica* lipase B studied by experiment and theory. **ChemBioChem**, v. 9, n. 15, p. 2443–2451, 2008.

TAHERIMEHR, M.; PESCARMONA, P. P. Green polycarbonates prepared by the copolymerization of CO₂ with epoxides. **Journal of Applied Polymer Science**, v. 131, n. 21, p. 1–17, 5 nov. 2014.

TAN, J. et al. Photo-PISA: Shedding Light on Polymerization-Induced Self-Assembly. **ACS Macro Letters**, v. 4, n. 11, p. 1249–1253, 17 nov. 2015.

TAN, J. et al. An insight into aqueous photoinitiated polymerization-induced self-assembly (photo-PISA) for the preparation of diblock copolymer nano-objects. **Polymer Chemistry**, v. 8, n. 8, p. 1315–1327, 2017.

TAN, S. G.; CHOW, W. S. Biobased epoxidized vegetable oils and its greener epoxy blends: A review. **Polymer - Plastics Technology and Engineering**, v. 49, n. 15, p. 1581–1590, 2010.

TANGESTANINEJAD, S. et al. Efficient epoxidation of alkenes with sodium periodate catalyzed by reusable manganese(III) salophen supported on multi-wall carbon nanotubes. **Applied Catalysis A: General**, v. 381, n. 1–2, p. 233–241, jun. 2010.

TIAN, X. et al. Recent Advances in RAFT Polymerization: Novel Initiation Mechanisms and Optoelectronic Applications. **Polymers**, v. 10, n. 3, p. 318, 14 mar. 2018.

TIRAN, C. et al. Chemo-enzymatic epoxidation of fatty compounds – Focus on processes involving a lipase-catalyzed perhydrolysis step. **Molecular Biology and Evolution**, v. 15, p. 12–16, 2012.

TOMKE, P. D.; RATHOD, V. K. Ultrasound assisted lipase catalyzed synthesis of cinnamyl acetate via transesterification reaction in a solvent free medium. **Ultrasonics Sonochemistry**, v. 27, p. 241–246, 2015.

TÖRNVALL, U. et al. Stability of immobilized *Candida antarctica* lipase B during chemo-enzymatic epoxidation of fatty acids. **Enzyme and Microbial Technology**, v. 40, n. 3, p. 447–451, 2007.

TRIPATHI, A. K. et al. Effect of d-Limonene on Three Stored-Product Beetles. **Journal of Economic Entomology**, v. 96, n. 3, p. 990–995, 1 jun. 2003.

TRONGSATITKUL, T.; BUDHLALL, B. M. Temperature dependence of serum protein adsorption in PEGylated PNIPAm microgels. **Colloids and Surfaces B: Biointerfaces**, v. 103, p. 244–252, mar. 2013.

TROTT, G.; GARDEN, J. A.; WILLIAMS, C. K. Heterodinuclear zinc and magnesium catalysts for epoxide/CO₂ ring opening copolymerizations. **Chemical Science**, v. 10, n. 17, p. 4618–4627, 2019.

TZIALLA, A. A. et al. Effective immobilization of *Candida antarctica* lipase B in organic-modified clays: Application for the epoxidation of terpenes. **Materials Science and Engineering B: Solid-State Materials for Advanced Technology**, v. 165, n. 3, p. 173–177, 2009.

VANDENBERG, E. J. Epoxide polymers: Synthesis, stereochemistry, structure, and mechanism. **Journal of Polymer Science Part A-1: Polymer Chemistry**, v. 7, n. 2, p. 525–567, fev. 1969.

VARLAS, S. et al. Predicting Monomers for Use in Aqueous Ring-Opening Metathesis Polymerization-Induced Self-Assembly. **ACS Macro Letters**, v. 8, n. 4, p. 466–472, 16 abr. 2019.

VIJAYARAGHAVAN, R.; MACFARLANE, D. R. Novel acid initiators for the rapid cationic polymerization of styrene in room temperature ionic liquids. **Science China Chemistry**, v. 55, n. 8, p. 1671–1676, 25 ago. 2012.

VLČEK, T.; PETROVIĆ, Z. S. Optimization of the chemoenzymatic epoxidation of soybean oil. **Journal of the American Oil Chemists' Society**, v. 83, n. 3, p. 247–252, mar. 2006.

WANG, G. et al. Polymerization-induced self-assembly of acrylonitrile via ICAR ATRP. **Polymer**, v. 129, p. 57–67, out. 2017.

WANG, Z. et al. Preparation and Characterization of Micro/Nano-emulsions Containing Functional Food Components. **Japan Journal of Food Engineering**, v. 16, n. 4, p. 263–276, 2015.

WARREN, N. J.; ARMES, S. P. Polymerization-Induced Self-Assembly of Block Copolymer Nano-objects via RAFT Aqueous Dispersion Polymerization. **Journal of the American Chemical Society**, v. 136, n. 29, p. 10174–10185, 23 jul. 2014.

WARWEL, S. et al. Polymers and surfactants on the basis of renewable resources. **Chemosphere**, v. 43, n. 1, p. 39–48, 2001.

WELTON, T. Room-Temperature Ionic Liquids. Solvents for Synthesis and Catalysis. **Chemical Reviews**, v. 99, n. 8, p. 2071–2084, 11 ago. 1999.

WHITAKER, J. R.; DEKKER, M. Principles of Enzymology for the Food Sciences. **Journal of Food Safety**, v. 15, p. 365–366, 1995.

WIEMANN, L. O.; FALTL, C.; SIEBER, V. Lipase-mediated epoxidation of the cyclic monoterpene limonene to limonene oxide and limonene dioxide. **Zeitschrift für Naturforschung - Section B Journal of Chemical Sciences**, v. 67, n. 10, p. 1056–1060, 2012.

WILBON, P. A.; CHU, F.; TANG, C. Progress in Renewable Polymers from Natural. **Macromolecular Rapid Communications**, v. 34, p. 32–43, 2013.

WINKLER, M. et al. Renewable polycarbonates and polyesters from 1,4-cyclohexadiene. **Green Chemistry**, v. 17, n. 1, p. 300–306, 2015.

WRIGHT, D. B. et al. ROMPISA: Ring-Opening Metathesis Polymerization-Induced Self-Assembly. **ACS Macro Letters**, v. 6, n. 9, p. 925–929, 19 set. 2017.

WRÓBLEWSKA, A. The Epoxidation of Limonene over the TS-1 and Ti-SBA-15 Catalysts. **Molecules**, v. 19, n. 12, p. 19907–19922, 28 nov. 2014.

WRÓBLEWSKA, A.; MALKO, M.; WALASEK, M. Environmental friendly method of the epoxidation of limonene with hydrogen peroxide over the Ti-SBA-15 catalyst. **Polish Journal of Chemical Technology**, v. 20, n. 4, p. 6–12, 1 dez. 2018.

XIE, W.; ZANG, X. Lipase immobilized on ionic liquid-functionalized magnetic silica composites as a magnetic biocatalyst for production of trans -free plastic fats. **Food Chemistry**, v. 257, n. October 2017, p. 15–22, ago. 2018.

XU, J. et al. A Robust and Versatile Photoinduced Living Polymerization of Conjugated and Unconjugated Monomers and Its Oxygen Tolerance. **Journal of the American Chemical Society**, v. 136, n. 14, p. 5508–5519, 9 abr. 2014.

XU, J. et al. Organo-photocatalysts for photoinduced electron transfer-reversible addition–fragmentation chain transfer (PET-RAFT) polymerization. **Polymer Chemistry**, v. 6, n. 31, p. 5615–5624, 2015.

XU, J. et al. Selective Photoactivation: From a Single Unit Monomer Insertion Reaction to Controlled Polymer Architectures. **Journal of the American Chemical Society**, v. 138, n. 9, p. 3094–3106, 9 mar. 2016.

YADAV, G. D.; DEVI, K. M. Enzymatic synthesis of perlauric acid using Novozym 435. **Biochemical Engineering Journal**, v. 10, n. 2, p. 93–101, mar. 2002.

YADAV, N.; YADAV, R.; GOYAL, A. Chemistry of Terpenoids. **International Journal of Pharmaceutical Sciences Review and Research**, v. 27, n. 45, p. 272–278, 2014.

YAN, N.; XIAO, C.; KOU, Y. Transition metal nanoparticle catalysis in green solvents. **Coordination Chemistry Reviews**, v. 254, n. 9–10, p. 1179–1218, maio 2010.

YE, Y.-S.; RICK, J.; HWANG, B.-J. Ionic liquid polymer electrolytes. **J. Mater. Chem. A**, v. 1, n. 8, p. 2719–2743, 2013.

ZAQUEN, N. et al. Scalable Aqueous Reversible Addition–Fragmentation Chain Transfer Photopolymerization-Induced Self-Assembly of Acrylamides for Direct Synthesis of Polymer Nanoparticles for Potential Drug Delivery Applications. **ACS Applied Polymer Materials**, v. 1, n. 6, p. 1251–1256, 2019a.

ZAQUEN, N. et al. Rapid Oxygen Tolerant Aqueous RAFT Photopolymerization in Continuous Flow Reactors. **Macromolecules**, v. 52, n. 4, p. 1609–1619, 26 fev. 2019b.

ZEHM, D.; RATCLIFFE, L. P. D.; ARMES, S. P. Synthesis of Diblock Copolymer Nanoparticles via RAFT Alcoholic Dispersion Polymerization: Effect of Block Copolymer Composition, Molecular Weight, Copolymer Concentration, and Solvent Type on the Final Particle Morphology. **Macromolecules**, v. 46, n. 1, p. 128–139, 8 jan. 2013.

ZENEVICZ, M. C. P. et al. Enzymatic hydrolysis of soybean and waste cooking oils under ultrasound system. **Industrial Crops and Products**, v. 80, p. 235–241, 2016.

ZHANG, Q. et al. Terpene Cyclizations inside a Supramolecular Catalyst: Leaving-Group-Controlled Product Selectivity and Mechanistic Studies. **Journal of the American Chemical Society**, v. 139, n. 33, p. 11482–11492, 23 ago. 2017.

ZHAO, W. et al. Optimization of the RAFT polymerization conditions for the in situ formation of nano-objects via dispersion polymerization in alcoholic medium. **Polym. Chem.**, v. 5, n. 24, p. 6990–7003, 28 ago. 2014.

ZHOU, C. et al. A new type of dual temperature sensitive triblock polymer (P(AM- co -AN)- b -PDMA- b -PNIPAM) and its self-assembly and gel behavior. **New Journal of Chemistry**, v. 45, n. 13, p. 5925–5932, 2021.

ZHU, Y. et al. Lead Halide Perovskite Nanocrystals as Photocatalysts for PET-RAFT Polymerization under Visible and Near-Infrared Irradiation. **ACS Macro Letters**, v. 9, n. 5, p. 725–730, 19 maio 2020.

ZUO, Y.; CAO, J.; FENG, S. Sunlight-induced cross-linked luminescent films based on polysiloxanes and d -limonene via thiol-ene “click” chemistry. **Advanced Functional Materials**, v. 25, n. 18, p. 2754–2762, 2015.

ZWENGER, S.; BASU, C. Plant terpenoids: Applications and future potentials. **Molecular Biology**, v. 3, n. February, p. 1–7, 2008.